



Terms and Conditions of Use of Digitised Theses from Trinity College Library Dublin

Copyright statement

All material supplied by Trinity College Library is protected by copyright (under the Copyright and Related Rights Act, 2000 as amended) and other relevant Intellectual Property Rights. By accessing and using a Digitised Thesis from Trinity College Library you acknowledge that all Intellectual Property Rights in any Works supplied are the sole and exclusive property of the copyright and/or other IPR holder. Specific copyright holders may not be explicitly identified. Use of materials from other sources within a thesis should not be construed as a claim over them.

A non-exclusive, non-transferable licence is hereby granted to those using or reproducing, in whole or in part, the material for valid purposes, providing the copyright owners are acknowledged using the normal conventions. Where specific permission to use material is required, this is identified and such permission must be sought from the copyright holder or agency cited.

Liability statement

By using a Digitised Thesis, I accept that Trinity College Dublin bears no legal responsibility for the accuracy, legality or comprehensiveness of materials contained within the thesis, and that Trinity College Dublin accepts no liability for indirect, consequential, or incidental, damages or losses arising from use of the thesis for whatever reason. Information located in a thesis may be subject to specific use constraints, details of which may not be explicitly described. It is the responsibility of potential and actual users to be aware of such constraints and to abide by them. By making use of material from a digitised thesis, you accept these copyright and disclaimer provisions. Where it is brought to the attention of Trinity College Library that there may be a breach of copyright or other restraint, it is the policy to withdraw or take down access to a thesis while the issue is being resolved.

Access Agreement

By using a Digitised Thesis from Trinity College Library you are bound by the following Terms & Conditions. Please read them carefully.

I have read and I understand the following statement: All material supplied via a Digitised Thesis from Trinity College Library is protected by copyright and other intellectual property rights, and duplication or sale of all or part of any of a thesis is not permitted, except that material may be duplicated by you for your research use or for educational purposes in electronic or print form providing the copyright owners are acknowledged using the normal conventions. You must obtain permission for any other use. Electronic or print copies may not be offered, whether for sale or otherwise to anyone. This copy has been supplied on the understanding that it is copyright material and that no quotation from the thesis may be published without proper acknowledgement.

Visualisation and Simulation of Myocardial Infarctions from 12-Lead ECG



A Thesis

Submitted to the Office of Graduate Studies

of

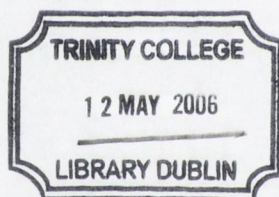
Trinity College Dublin

in Candidacy for the Degree of

Doctor of Philosophy

August, 2005

by **John T Ryan**



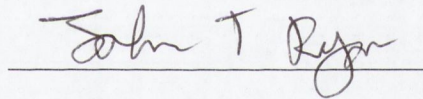
THESIS
7875

© Copyright by John T Ryan 2005

All Rights Reserved

Declaration

This thesis has not been submitted as an exercise for a degree at any other University. Except where otherwise stated, the work described herein has been carried out by the author alone. This thesis may be borrowed or copied upon request with the permission of the Librarian, Trinity College, University of Dublin. The copyright belongs jointly to the University of Dublin and John T Ryan.

A handwritten signature in cursive script, reading "John T Ryan", is written over a horizontal line.

Signature of Author

Acknowledgements

For her invaluable help, guidance, constant support and general tolerance for a “very applied” project, I would like to extend my sincerest gratitude to my supervisor, Carol O'Sullivan. Amid the chaos of hosting the Eurographics conference Carol has found time to thoroughly examine my thesis. The ISG has been a great place over the last three years to learn and live. I would like to thank all the members, both past and present, for putting up with me!

Without the help of my clinical collaborators this thesis would not have been written. I would like to thank Dr Niall Mulvihill for his excellent insight into all things “cardiology”. His pro-active approach and efficiency were exactly what this project needed in the last two years. I would like to thank Professor Chris Bell for his exceptional input throughout the duration of the project, even on his busiest days. Also, thanks to his secretary Ann, for always fitting me in. There are many staff members in St James' hospital that need to be thanked. Thank you to Dr Geraldine McMahon and all the staff in the coronary care unit for allowing me to access to the patients and their trust in my medical abilities. Thank you to the cardiology department staff for training me in the *art of electrocardiography*. Thanks to Dr Peter Crean for initially organising the collaborations.

Finally, thank you to my friends and family, and, of course, to my band for delaying our European and Russian tours!

Abstract

Myocardial Infarction (MI) is one of the main causes of death throughout the world. More commonly known as *heart attack*, it is caused by the occlusion of one or more of the arteries that supply the heart. Cardiac enzymes found through blood analysis are frequently used to estimate infarct size. The peak creatine kinase (CK) enzyme or troponin (Tn) protein are widely used to determine prognosis and treatment. Non-invasive imaging techniques are also frequently used in clinical practice to determine infarct size and location. These techniques all rely on skilled operators to interpret the images generated. In this thesis, we describe a simple technique for non-invasive assessment of myocardial infarct size and location by generating a 3 dimensional representation of the infarct location from the surface electrocardiograph (ECG).

We borrow techniques from the fields of direct volume rendering, realtime-rendering, virtual reality, physiological simulation, volume animation and slice-based texturing. From an initial polygonal mesh model, we produced a hybrid volumetric and mesh model for the mapping of the automatically interpreted results from 12 lead ECG. Myocardial infarctions are represented within our system as areas around central voxels that correspond to the lead vectors. We introduced voxels within our model by aligning them to axes representing the lead vectors. The voxels are inputted into the volume where the axes intersect with the model. The electrical propagation animation recognizes the infarcted cells and cannot pass these cells, thus spreading around them. The MI detection system measures the parameters as found by either the automatic or manual markers system. Currently the system measures the difference between the ST segment and the iso-electric line for each lead, thus giving the extent, if any, of infarction. These measurements are then used as references for the radius around that specific lead's model-representation voxel. The T waves are also checked for inversion. The animation of the electrical propagation is automatically choreographed with markers that are selected by the user or automatically selected using the automatic wave classifier. We offer a new metric that is a cumulative indicator of ST segment deviation. ECG measurements are established to be more accurate than blood-chemical markers, so such metric is very useful for the credibility of this tool.

We worked alongside collaborators in various clinical and medical education settings. Our software was tested by monitoring patients, over a period of 3 months, in the Coronary Care Unit (CCU) in St James' Hospital, Dublin. All abnormal ECGs were detected correctly. We also monitored patients during angioplasty procedures. During this procedure a balloon catheter is used and, on inflation, ST segment elevation occurs on the corresponding leads, which is used as a definitive validation of the localiser algorithm. This is definitive proof that the software is successful because real-time video fluoroscopy is used to show that the location of the catheter is at the same location as the simulated stress area on the model. The software was demonstrated to cardiology clinicians and it was seen as very beneficial for several reasons. Firstly, as a potential diagnostic tool, it could save the clinician time on measuring the extent of STEMIs (ST Elevation MIs). It was also recognised as an invaluable teaching tool, giving the student a greater spatial awareness of these kinds of conditions. There is also potential in the area of patient awareness. The software allows a patient to see that an MI is not just visible on graph-paper.

Related Publications

"A Virtual Reality Toolkit for the Diagnosis and Monitoring of Myocardial Infarctions."

J. Ryan, C. O'Sullivan, C. Bell, N. Mulvihill.

Proceedings of Volume Graphics Conference 2005, StoneyBrook New York, USA.
IEEE, p55-62 (2005)

"Real-time Interactive Volumetric Animation of the Heart's Electrical Cycle from Automatically Synchronized ECG."

J. Ryan, C. O'Sullivan, C. Bell.

Computer Animation and Virtual Worlds Journal (Wiley, 2004); 15: 353-360. Also presented at CASA, (Computer Animation and Social Agents) conference in Geneva July 2004.

"A Virtual Reality Electrocardiography Teaching Tool."

J. Ryan, C. O'Sullivan, C. Bell, R. Mooney.

Proceedings of the Second International Conference,
Biomedical Engineering. p250-253 (2004).

"The Construction of a Volumetric Cardiac Model for Real-Time ECG Simulation."

John Ryan, Robert Mooney, Dr. Carol O' Sullivan and Prof. Chris Bell. WSCG Conference on Computer Graphics Plzen, Czech Republic (2003).

Contents

1	Introduction	1
1.1	Motivation	1
1.2	System Overview	2
1.3	Methodologies	3
1.4	Scope	4
1.5	Hypotheses	6
1.6	Summary of Chapters	7
2	Medical Principles	10
2.1	The Heart.	10
2.1.1	Anatomy	10
2.1.2	Physiology	11
2.1.3	Pathology	12
2.2	Electrocardiography	13
2.2.1	A Brief History of Electrocardiography	13
2.2.2	Electrocardiographic Principles	14
2.3	Myocardial Infarction (MI)	16
2.4	Diagnosis and Monitoring of Myocardial Infarction	18
2.4.1	Signs and Symptoms	18

2.4.2	Predisposing Factors	18
2.4.3	Bio-chemical Markers	19
2.4.4	ECG	20
2.4.4.1	Early Raised T Waves	20
2.4.4.2	ST Segment Elevation and Depression	21
2.4.4.3	Inverted T Waves	21
2.4.4.4	Pathological Q Waves	22
2.4.4.5	Localisation of MI	23
2.5	Treatment of Myocardial Infarction	23
2.5.1	Drugs	23
2.5.2	Defibrillation	24
2.5.3	Thrombolysis	25
2.5.4	Angiography	25
2.5.5	Percutaneous Transluminal Coronary Angioplasty (PTCA) and Stenting	26
2.5.6	Financial Implications of MI Treatment	28
2.6	Interpreting the ECG	30
2.6.1	Automatic Interpretation of ECG Data	30
2.6.2	Automatic ST Segment Detection	31
2.6.3	Limitations of Automatic ECG Interpretation Algorithms .	33
2.6.4	Human-guided Interpretation Algorithms	33
2.7	SCP and Other ECG File Formats	34
3	Graphics in Medicine and Medical Education	36
3.1	Basic Principles of Computer Graphics	36
3.1.1	Graphics Libraries	38

3.2	Volume Visualization	39
3.2.1	Image Order Traversal	40
3.2.2	Object Order Traversal	40
3.2.3	Texture-based Volume Rendering	41
3.2.4	Hybrid Rendering	43
3.3	Real-time Volumetric Animation	43
3.4	Cellular Automata (CA) in Biomedical Simulations	44
3.5	Virtual Surgery and Endoscopic Techniques	44
3.5.1	Augmented Reality Applications	45
3.6	The Previous Version of the ECG Teaching Tool	46
3.7	Simulation of Heart Electro-physiology	48
3.8	Libraries for Interaction and Graphical User Interfaces	50
3.9	Increased Immersion Techniques	50
3.9.1	Stereoscopic Viewing Conditions	50
4	Implementation	53
4.1	The Heart Model	53
4.1.1	Model Acquisition	53
4.1.2	Model Development	55
4.1.3	Voxelisation	57
4.1.4	Volume Artefacts	58
4.1.5	Classification of Cells	60
4.2	The Display Environment and the Graphical User Interface	62
4.2.1	Languages and Libraries	62
4.2.2	GUI Design and Layout	62
4.2.3	Model Interaction	63

4.3	Data-structures	64
4.3.1	Model Structure	64
4.3.2	Cell Data-structures	65
4.3.3	Animation Structures for Speed Optimization	66
4.3.4	ECG Handling - The SCP File Format and Huffman Decoding	67
4.4	The ECG Window	71
4.5	The Animation System	72
4.6	The ECG Classification and Interpretation System	75
4.6.1	Automatic Representation of Myocardial Infarctions	76
4.6.1.1	Wave Abnormalities	77
4.6.1.2	MI Location	78
4.6.1.3	MI Extent	80
4.6.1.4	The MI Sensitivity Slider	81
4.6.1.5	The Voxel-Count as a Metric	81
4.6.1.6	The ST Accumulator as a Metric	82
4.6.1.7	The MI Report Dialogue Window	82
4.7	The Surface Representation Experiment	83
4.8	Enhancing the VR Environment	84
4.8.1	Stereoscopic Viewing Conditions	84
5	Clinical Trials and Evaluation Methodologies	86
5.1	Evaluating Diagnostic and Teaching Tools	87
5.1.1	Case Studies	87
5.1.2	Quantitative Validation	87
5.1.3	Experimental Techniques	88
5.1.4	Qualitative Validation	88

5.1.5	Combined Evaluation	89
5.2	Initial Considerations for ECG Retrieval	89
5.3	Recording the Electrocardiogram	90
5.4	Ethical Considerations and Proposals	91
5.5	The Training Period	92
5.6	The Coronary Care Unit	92
5.6.1	Patient Selection	93
5.6.2	Recorded Information	93
5.6.3	General Findings in the CCU	96
5.7	The Angioplasty Limb	98
5.7.1	Experiment Design	98
5.7.2	Lead Placement and Displacement	98
5.7.3	Acquisition of ECGs and Video Fluoroscopy Footage	99
6	Results	101
6.1	The CCU Findings	101
6.1.1	Refining the Patient List	101
6.2	CCU - Case Studies	102
6.2.1	Patient 1: Lateral MI	103
6.2.2	Patient 2: Antero-Septal MI	104
6.2.3	Patient 3: Antero-Lateral MI	105
6.2.4	Patient 4: Infero-Lateral MI	106
6.2.5	Patient 5: Inferior MI	107
6.2.6	Patient 6: LBBB	108
6.2.7	The Metrics - A Comparison	109
6.3	Validating the System in the Catheter Laboratory	110

6.3.1	Patients with Minor ST Elevation	111
6.3.2	Patients with More Extensive ST Elevation	112
6.3.3	The Standard Progression	113
6.3.4	Patients with Initial ECG Abnormalities	113
6.3.5	Summary of the Angioplasty Phase Findings	115
6.4	Clinical Feedback	117
6.4.1	An Interview with a Consultant Cardiologist	119
6.5	Other Results	124
6.5.1	Graphical Issues	124
6.5.2	The “Human in the Loop” Approach	125
6.5.3	T Wave Inversion	126
7	Conclusions and Future Work	128
7.1	Future Directions	131
A	The SCP File Format	134
B	The OBJ File Format	136
C	Sample ECGs	139
D	Glossary	143
	References	165

List of Figures

2.1	Diagram of the Heart.	12
2.2	Diagram of the Heart Muscle Tissue.	13
2.3	Sketch of Luigi Galvanis Laboratory.	14
2.4	Example of Typical ECG Waveform.	15
2.5	Diagram of Einthovens Triangle.	15
2.6	Different Views from Different Leads.	16
2.7	Diagram of the MI Process.	18
2.8	Heart with Blockage causing MI.	19
2.9	Tall T Wave.	21
2.10	ST Elevation.	21
2.11	Inverted T Wave.	22
2.12	Pathological Q Wave.	22
2.13	Evidence of Infarction.	23
2.14	12 Lead ECG Axes.	24
2.15	Frames of an angiogram.	26
2.16	Angiogram with Inflated Balloon Catheter.	28
2.17	Angiogram with Catheter and Stent.	29
3.1	Gaussian splat kernel.	41

LIST OF FIGURES

3.2	Texture-based Volume Representation.	42
3.3	Previous Heart Model.	47
3.4	Electrical Network Construction.	49
3.5	3D Stereoscopic Shutter-Mechanism Glasses.	51
3.6	Head Mounted Display - Inside View.	51
4.1	Initial heart model.	54
4.2	The final polygonal model.	55
4.3	Screenshots of the initial representation of the bundle-branch network.	56
4.4	Initial volume represented with points.	58
4.5	Slice Retrieval - location of viewing field.	59
4.6	Slice Retrieval - slice as viewed in opengl window.	59
4.7	Slice Retrieval - slice with dual colour representation.	60
4.8	Reconstructed volume model - without and with inner mesh.	60
4.9	Artefact produced when camera was parallel to slice-stack.	61
4.10	Classification of cell-types.	61
4.11	A screenshot of the visualisation toolkit at work with the final layout.	63
4.12	Screenshot of a model that is clipped along the frontal plane.	65
4.13	Screenshot of a model displayed with frontal slice-view during animation sequence.	66
4.14	Datastructure for the handling of different model objects.	67
4.15	Structure of the cell object.	68
4.16	SCP object structure.	70
4.17	ECG window structure.	72
4.18	Initial propagation shape.	73

4.19 Final propagation shape.	74
4.20 Diagram of different cell types.	75
4.21 ECG window with classified wave markers.	76
4.22 ECG window with average ST segment marker.	76
4.23 ECG lead axes in relation to the model.	79
4.24 Measuring the ST segment.	80
4.25 Two different extents.	80
4.26 Screenshot of a sample MI report dialogue window.	83
4.27 Direct surface representation of lead voltages.	84
4.28 Stereoscopic apparatus.	85
5.1 Our 12 lead ECG console connected via serial cable to a laptop. . .	91
5.2 Age Distribution.	96
5.3 Gender Distribution.	97
5.4 Smoking Status Distribution.	97
5.5 Angiography Sequence of Coronary Arteries.	98
6.1 Patient 1 - Lateral MI (Green represents area of infarcted tissue). Clinically, lateral refers to the left side of the heart, thus our soft- ware's interpretation is correct.	103
6.2 Patient 2 - Antero-Septal MI. A stress area in the anterior region or the septal wall. Our software's interpretation is anatomically correct.	104
6.3 Patient 3 - Antero-Lateral MI. Again, our software's interpretation is correct.	105
6.4 Patient 4 - Infero-Lateral MI. Green region on inferior and lateral aspects of the heart model. This verifies the softwares interpretation.	106

LIST OF FIGURES

6.5	Patient 5 - Inferior MI. Green region on the inferior aspect of the heart. Our software's interpretation is correct.	107
6.6	Patient 6 - with left bundle-branch block. The software picks up on the region of stress.	108
6.7	Comparison of metrics, with the ST accumulator ascending.	109
6.8	Initial Angiograms	110
6.9	Angiograms After vessels were re-opened	111
6.10	The software's interpretation and corresponding ECG	112
6.11	Patient 8's interpretation and ECG	113
6.12	Comparison of ECGs, leads II and III.	114
6.13	Patient 1: Inferior stress-area.	115
6.14	Patient 7: Inferior and anterior stress-areas.	116
6.15	Standard Progression of Angioplasty ECGs.	116
6.16	Angiogram demonstrating initial views of the occluded artery.	117
6.17	Angiogram demonstrating the same artery with inflated balloon.	118
6.18	Angiogram post-reperfusion.	119
6.19	Progression for Patient 9.	119
6.20	Animation Strip of Cardiac Electrical Cycle.	126
6.21	Example of conflict between T wave inversion and ST change, blue represents T wave inversion and green ST change.	127
A.1	SCP Section Header Structure.	135
A.2	Default Huffman Table.	135
C.1	ECG taken during the CCU evaluation phase. There is noticeable ST segment elevation on leads III and aVF. There is also ST depression in I, aVL, v2, v3 and v4	140

C.2 ECG taken during the CCU evaluation phase. There is noticeable
ST segment elevation on leads II, III and aVF. **141**

C.3 ECG taken during the angioplasty evaluation phase. There is no-
ticeable ST segment elevation on leads III, aVF, v1 and v2. **142**

List of Tables

2.1	ECG Lead Locations	17
4.1	Structure of SCP File	69
4.2	MI Changes	78
B.1	OBJ Instructions	137

Chapter 1

Introduction

The electrocardiograph (ECG) has been used in medicine for over 100 years as a crucial diagnostic tool for heart abnormalities. Even though the advent of imaging modalities such as computed tomography (CT), magnetic resonance imaging (MRI), positron emission tomography (PET) and ultrasound have revolutionised medical diagnoses, the humble ECG remains one of the key diagnostic tools used in the field of cardiology. From the ECG, very specific information about heart-rate and heart-rhythm as well as locations and extents of abnormalities can be derived. The use of computer graphics in medicine and medical education is becoming more wide-spread as techniques and technologies improve. This thesis describes the visualisation of ECG information by the use of computer graphics.

1.1 Motivation

Currently the cardiologist uses bio-chemical markers found through blood analysis to monitor patients suffering with myocardial infarction (MI). An MI is more commonly known as a “heart attack” and is one of the major causes of *morbid-*

*ity*¹ and *mortality* (FBC⁺02). This condition is caused by a blockage in one or more coronary arteries, resulting in dead or dying sections of the heart muscle. Even though bio-chemical markers are used in the monitoring of MI, the ECG is far more useful in providing evidence of the extent and location of infarction. One of the main aims of this project is to provide a VR tool that a cardiologist or cardiology worker can use to speed up and enhance this diagnosis and monitoring process, converting real ECG data to a virtual interpretation on a volumetric heart model. Another aim was to use the same system as a teaching tool including simulations of the cardiac electrical cycle as well as abnormalities such as MI. This thesis is an investigation of representing MIs in 3D space from standard ECG input and describes the development of such a tool.

1.2 System Overview

From an initial heart structural model (New York University heart model), we produced an improved volume model for use within our system. For the handling of ECGs, we chose to mainly use the common SCP (Standard Communication Protocol) file format. This file format is currently the format of choice for most ECG consoles. Our ECG recording equipment is capable of exporting ECGs in this format. Myocardial infarctions are represented within our system as regions around central points (voxels) that correspond to the lead vectors. These points were introduced into our model by aligning them to relevant ECG axes. Our software also produces an animation of the hearts electrical cycle. This electrical cycle animation recognizes the infarcted or dead cells as non-conductive, thus spreading around them. The MI detection system measures the parameters as

¹Throughout the thesis, italicised terms like this are explained in the glossary (Appendix D)

found by either the automatic or manual marker classification system. Currently the system measures the difference between the *ST segment*¹ and the normal (iso-electric) line for each lead, thus giving an extent, if any, of abnormality. These measurements are then used as references for the radius around that specific lead's model-representation point. The animation of the electrical propagation is automatically choreographed with markers that are selected by the user or automatically selected using the automatic wave classifier. This wave classifier uses the So and Chan (SC97) QRS² detection algorithm, which was the most suitable detection algorithm because of its suitability to real-time systems. Once the QRS complex is found, the other waveforms are found by traversing backwards and forwards from that point. This is not always accurate, so a manual human-guided wave classification tool is incorporated into the software. We incorporated a standard metric for the extent of MI into our system. The purpose of a metric like this would be to see if the bio-chemical measurements correlate with the measurements within our system. There are two types of metrics available in the toolkit. We use a voxel counter that counts the number of dead voxels or cells once the interpretation process is complete. The second metric, is a cumulative value of *ST segment* deviation.

1.3 Methodologies

Throughout the duration of the project, we worked alongside collaborators in various clinical and medical education settings. Our software was tested by monitoring patients in the Coronary Care Unit (CCU) in St James' Hospital, Dublin over a period of 3 months. All abnormal ECGs were detected correctly. We

¹Section of ECG wave, See Glossary

²One of the key waveforms within the ECG

also monitored patients during angioplasty procedures. During this procedure a balloon catheter is used and, on inflation, ST segment elevation occurs on the corresponding leads, which is used as a definitive validation of the localiser algorithm. This is definitive proof that the software works because real-time video fluoroscopy is used to show that the location of the catheter is the same location as the simulated stress area on the model. The software was demonstrated to cardiology clinicians and it was seen as very beneficial for several reasons. Firstly, as a potential diagnostic tool, it could save the clinician time on measuring the extent of STEMIs (ST Elevation MIs). It was also recognised as an invaluable teaching tool, giving the student a greater spatial awareness of these kinds of conditions. There is also potential in the area of patient awareness. The software allows a patient to see that an MI is not just readable on graph-paper. We took some control ECGs on patients that had no MI or had recovered from MIs and interestingly, these ECGs showed the correct results, no pathologies.

1.4 Scope

Traditionally, due to the vast and complex nature of the hearts physiology, simulations of the hearts electrical cycle require hugely detailed models and enormous amounts of computing power. To add such detailed volumetric animations of the cardiac electrical cycle to our system would have been outside the scope of this project. Therefore, it was decided that, although not *ideal*, a simpler version of such an animation system was incorporated into our software. The main justification for this feature was to provide a teaching tool that allows the user to view the cardiac cycle as well as myocardial infarctions from loaded ECGs. One of the main requirements was that it would be easily accessible and implementable

on a number of platforms. For this reason, we chose to program our software with cross-platform libraries (FLTK, OpenGL) and prepare the system so that it could be used on a standard PC¹. These specifications allowed the software to be easily demonstrated on a laptop with enough capabilities for interacting in real-time with a volume of $256 \times 256 \times 100$ resolution.

In identifying locations of myocardial infarctions from ECG, a vest with multiple arrays of electrodes (224) (RGJR04) would be very helpful. However, this configuration is very rarely seen in clinical practice. For this reason, we chose the most standard configuration: the 12 lead ECG. A multi-electrode vest would also have been beyond the scope of the project because of the costs involved. It was decided to incorporate one ECG file format, apart from our initial ASCII file format. We chose the SCP file format for one crucial reason: it was the only open-source file format that our ECG equipment was capable of exporting.

Although some automatic ECG recognition and detection algorithms were experimented with, it was not within the scope of this thesis to perform significant new research in this domain. We incorporated a *human in the loop* approach to lead classification. This area of research is gaining interest because, not only are some of these algorithm more effective, clinicians generally have more faith in their own expertise than that of computer-based algorithms that may have a high mis-diagnosis rate.

The validation phase of our system mainly comprised of clinical trials and evaluations. A thorough user feedback study of our toolkit was not performed because, during the project, we received constant feedback from consultant cardiologists and other medical staff. Also, by the time we had finished all the clinical trials and evaluations, it was considered that these results provided sufficient

¹By standard PC, we mean approximately 2GHz processor, 1GHz RAM, 256MB Graphics Card

proof that our software worked. Our software was demonstrated at a medical forum within the hospital and feedback was attained.

At the beginning of the project, after some initial meetings with our clinical collaborators, it became apparent that, without our own equipment and personnel for the acquisition of the digital ECGs, the project would be impossible. This was for two reasons. Firstly, the hospital at which we were mainly based only recorded ECGs as paper-printouts and digital exportation from the ECG consoles was not achievable. Also, because of an already understaffed cardiology department, ECG technologists were not available for extra work. After some initial consultations, an opportunity arose. With our previous medical experience, it would be possible to gain access to patients after an ECG training period. Then, after the acquisition of an ECG console capable of exporting SCP files via serial-cable to a laptop, we could begin our ECG monitoring.

1.5 Hypotheses

There were multiple hypotheses within this project. These comprised mainly of the following:

- In the field of cardiology, there is an inherent absence of visual feedback tools, especially in the domain of electrocardiography. It was predicted that a **novel approach to the diagnosis and monitoring** of the common pathology of **myocardial infarction** using conventional **3D and volumetric computer graphics** techniques could be developed.
- We hypothesised that we could evaluate the interpreter's localisation algorithm using our unique method. This evaluation technique involves the

recording of a patient's ECG on the inflation of a balloon catheter during an *angioplasty* procedure. The *video fluoroscopy* angiography recordings were used to confirm the locations of the interpreter's detected MI locations.

- We predicted that the electrical depolarisation and repolarisation of cardiac cells could be represented effectively using **real-time volumetric animation techniques**. The visual representation coincides with automatically synchronized electrocardiogram (ECG) input. Whilst other projects in similar fields use super-computers or vastly complex cellular structures (SFE⁺03), one of the aims of this project is to simplify the process for real-time optimization.
- In the domain of medical education, it was hypothesised that this tool would provide the student with a valuable representation of the cardiac electrical cycle and myocardial infarctions. When learning electrocardiography, the abstract concept of 3D localisation is difficult to visualise. This tool allows the student to see both the relevant ECG and the corresponding visualisation, which provides the student with a greater sense of spatial awareness.
- In the realm of volume graphics, we predicted that by using hardware-based texturing techniques we could accurately portray the associated pathologies and physiological processes.

1.6 Summary of Chapters

Chapter 2 - Medical Principles provides a detailed background of the medical principles relevant to this thesis. After an initial overview of the

anatomical, physiological and pathological issues surrounding the heart, an in-depth discussion of the causes, diagnosis, monitoring and treatment of myocardial infarction follows. Then there will be a comprehensive discussion of electrocardiography and its role in the monitoring and diagnosis of MI as well as related subjects including the SCP file, automatic recognition and detection algorithms and angioplasty.

Chapter 3 - Graphics in Medicine and Medical Education investigates the area of computer graphics with a leaning towards the applications within the field of medicine and medical education. A detailed description of the relevant graphical techniques including basic graphics, volume graphics, virtual/augmented reality, virtual surgery and animation will be given.

Chapter 4 - Implementation describes all the aspects relating to the development of our toolkit. The acquisition and development of the cardiac model will firstly be described along with the volumisation techniques used. Then, the system design will be described including information about the particular datastructures that were used. The electrical propagation animation system will then be described. The handling of ECG information as well as the development of SCP file format readers and writers will be discussed. A description of the classification and interpretation system will be followed by the MI simulation and representation techniques. Finally, increased immersion techniques and the development the graphical user interface will be explained.

Chapter 5 - Clinical Trials and Evaluation Methodologies discusses the process of evaluating the software in different phases. The ECG recording process is firstly described along with the relevant ethical and training

issues. Then, the two main phases of clinical evaluations are discussed. These include the evaluation of the system with ECGs from the coronary care unit in St James Hospital, Dublin and also the evaluation of the localisation techniques using real-time ECGs recorded during percutaneous transluminal coronary angioplasty (PTCA¹) procedures.

Chapter 6 - Results and Discussion provides the results of our various evaluations and discusses each phase's findings.

Chapter 7 - Future Work and Conclusions discusses the potential future applications and improvements as well as finalising the findings of this thesis.

¹A common type of angioplasty, defined in glossary

Chapter 2

Medical Principles

This chapter is mainly concerned with exploring and identifying the issues surrounding heart abnormalities such as myocardial infarction. Firstly, there will be a short background of the anatomical, physiological and pathological principles involved as well as an in-depth discussion about myocardial infarction and its causes, treatments and methods of diagnosis. A comprehensive discussion of electrocardiography and its role in the diagnosis and monitoring of this condition is also included. Related subjects such as angioplasty, the SCP file format and automatic recognition and detection algorithms for electrocardiography are also discussed. This chapters contains some terms with which non-medical readers may not be familiar. A glossary is included for this reason (Appendix D).

2.1 The Heart.

2.1.1 Anatomy

The heart is located centrally in the chest in a cavity called the *mediastinum*, and is responsible for pumping blood around the body. It is generally made up of

muscle, which is known as the *myocardium*. The average adult heart weighs approximately 0.5kg and it beats on average around 100,000 times a day. The heart has four chambers (two atria and two ventricles). The right atrium along with the venous system sucks deoxidised blood from most of the body and passes it to the right ventricle. The right ventricle then passes it to the lungs where oxidisation occurs and the blood is returned via the pulmonary vein to the left atrium. This blood is passed to the left ventricle, which outputs the regenerated blood to the body again via the *aorta*. The heart lies within a fibrous sac called the pericardium, which is lined internally by the serous pericardium. This consists of a parietal lining layer and a visceral layer that adheres the heart and adjacent large vessels to each other. The electrical conduction system of the heart is quite complex and has an electrical presence greater than most other anatomical phenomena. An electrical impulse begins at the SA (Sino-Atrial) node, which is an area of specialised cardiac muscle at the top right of the heart. This electrical impulse then conducts through the atria until it reaches the AV (Atrio-Ventricular) node. This node is also a specialised area of cardiac muscle and continues into the AV bundle branch, which conducts the electrical impulse into a network of muscle fibre branches in each ventricle (MHL98). Figure 2.1 demonstrates the main internal structures of the heart.

2.1.2 Physiology

The word *physiology* refers to the branch of biology that deals with activities and functions of living matter (ie. tissues and cells). Heart physiology is a much studied area because of the intricate nervous/electrical system along with the heart's unique muscle structure. Figure 2.2 demonstrates a section of heart muscle. The myocardium's specialised cardiac muscle tissue is unique to the

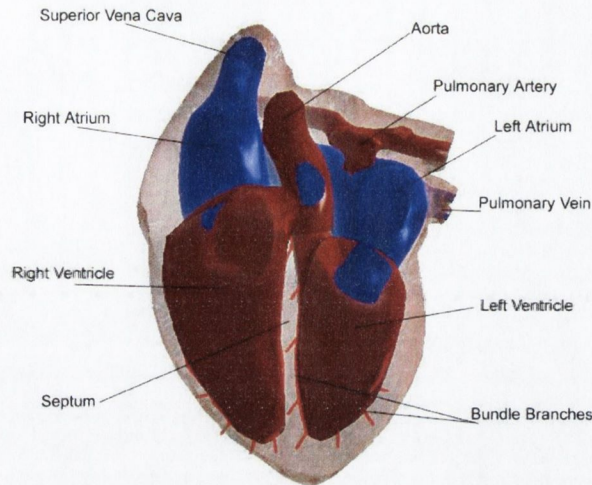


Figure 2.1: Diagram of the Heart.

heart and consists of cells/fibres that are in very close contact with the ends of adjacent cells. This makes the cardiac cells resemble a sheet of muscle. Rather than having a separate nerve supply to each fibre, an electrical impulse from key nerve supplies spreads through this “sheet” of muscle causing a contraction in the area of depolarisation. These contractions are the basis of blood flow within the heart. The electrical propagation generally travels in the same direction as the fibre orientation.

2.1.3 Pathology

A *pathology* is a manifestation of functional or anatomical abnormality or disease. Many heart pathologies relate to its blood or nerve supply or sometimes a combined abnormality. *Cardiac Failure* is a term used when there is a failure of the cardiac output to meet the needs of the body (WW96). Cardiac failure is normally caused by a lower level abnormality with the blood or nerve supply to the tissue concerned. The heart’s valves may become damaged and cause a

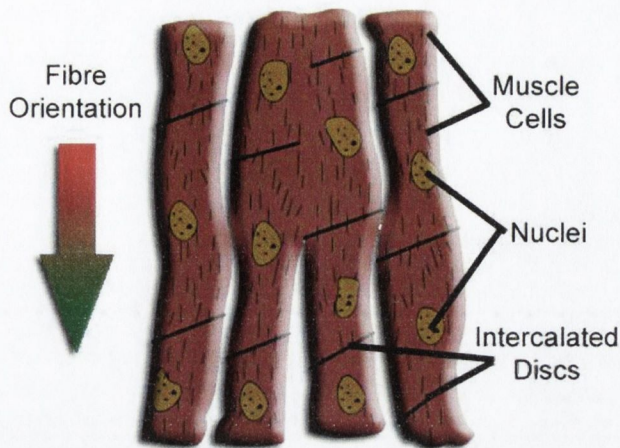


Figure 2.2: Diagram of the Heart Muscle Tissue.

blood-flow disturbance which is sometimes called *regurgitation*. *Ischemia* refers to the lack of oxygen at cellular level to a certain area of tissue (Pha96). There are two main pathologies as a result of this phenomenon: *Angina Pectoris* and *Myocardial Infarction*. Both of these conditions are caused by a restricted blood flow, which, in turn, causes ischemic conditions. *Angina Pectoris* is sometimes resolved in the same way as myocardial infarction (LCP02), but in general is a less severe condition. Since it is the key focus of this thesis, myocardial infarction will be explained and discussed in detail later in this chapter.

2.2 Electrocardiography

2.2.1 A Brief History of Electrocardiography

In 1787 Luigi Galvani discovered that attaching a metal instrument to the lumbar nerve of a frog and applying an electrical charge caused violent muscular contractions (Gal91). This phenomenon became known as galvanism. After this discovery, bio-electricity became a richly researched area. Between 1893 and 1896

George Burch and Willem Einthoven developed methods for calibrating and correcting the data produced by a device called the capillary electrometer. Finally a shape was predicted that was very close to the “true” ECG shape (Zyw05). These denominations of electrocardiographic waveforms are still in use today. Below there is a sketch of Luigi Galvani’s laboratory with the frogs lower half and galvanometer (Figure 2.3¹).

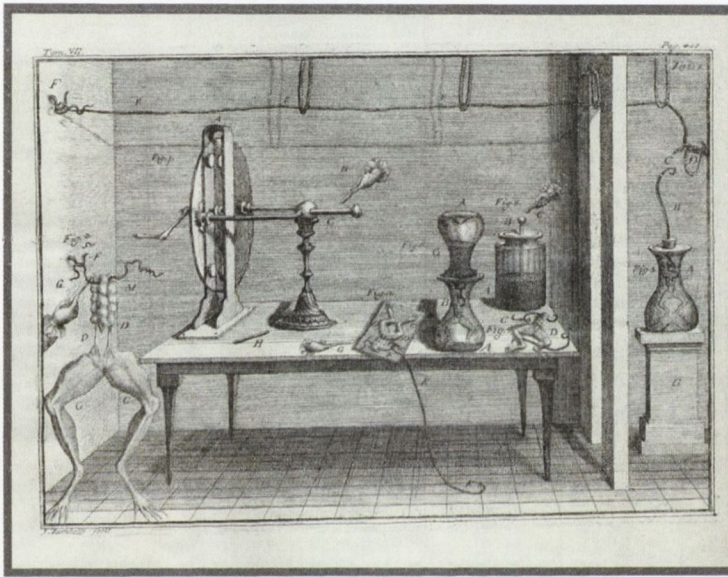


Figure 2.3: Sketch of Luigi Galvanis Laboratory.

2.2.2 Electrocardiographic Principles

The body’s tissue and fluids are good conductors of electricity, so the heart can be monitored from the outside by attaching electrodes to various parts of the body. The recorded ECG displays a waveform in 2D. The voltage is represented vertically and time is represented horizontally. Sections of the wave coincide with physiological occurrences within the heart. Figure 2.4 demonstrates a typical

¹Courtesy of Archives and Special Collections, Columbia University Health Sciences Library

ECG from lead II in a standard three lead configuration.

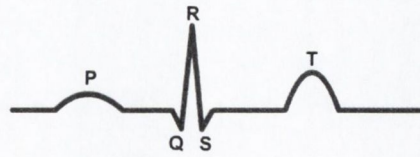


Figure 2.4: Example of Typical ECG Waveform.

The different sections of the wave are also shown from P to T. The P wave corresponds to the electrical propagation through the atria, i.e. when the impulse travels from the SA node to the AV node. The QRS complex occurs when the electrical propagation rushes through the bundle-branches and the ventricles depolarise. This QRS complex is the most prominent waveform within the ECG and is most commonly used to measure heart-rate. There are normally 12 leads in a standard clinical configuration. Within this configuration there are 3 standard leads, 3 augmented leads and 6 precordial leads. An electrical current travelling from the negative node to the positive node of a bipolar electrode is the basis of electrocardiography. This causes a positive deflection around the isoelectric line by the lead. The original three-lead bipolar electrode pair setup was first used by the inventor of ECG, Einthoven. It is still referred to as Einthoven's Triangle. (See Figure 2.5)

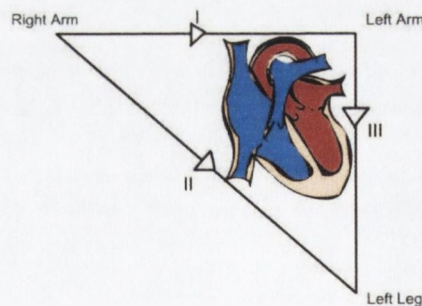


Figure 2.5: Diagram of Einthovens Triangle.

Figure 2.6 demonstrates the wave of depolarisation. The shape of the QRS complex in any lead depends on the orientation of the corresponding lead to the vector of depolarisation.

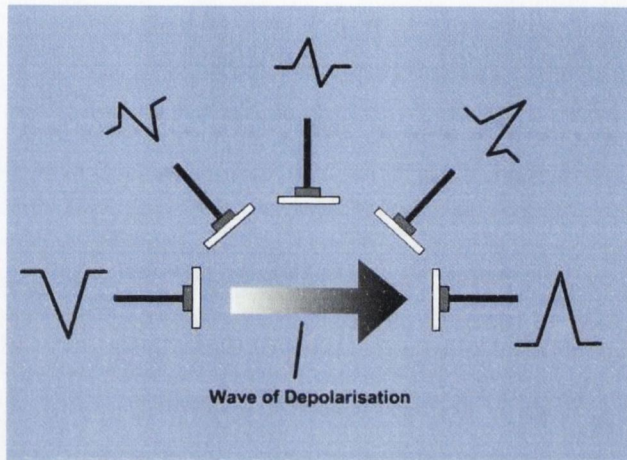


Figure 2.6: Different Views from Different Leads.

Table 2.1 shows the locations of the standard leads in a 12 lead configuration. Note that some of the leads are missing, because they are computed afterwards.

2.3 Myocardial Infarction (MI)

An MI is an area of myocardial tissue that has died due to a lack of oxygen to that particular part. This occurs when there is a thrombosis in one or more of the supplying coronary arteries. Thrombosis occurs when there is an intra-vascular blood-clot. The commonest cause of this phenomenon is when an atheromatous plaque lodges within the artery and causes a blockage or thrombosis. (WW96) The extent and location of the MI depends on the location and size of the offending arteries. Once heart cells die, they cannot regenerate. Instead, they form a section of fibrous tissue that has no role within the heart. This tissue becomes non-conductive to the electrical propagation which then becomes evident on the

2.3 Myocardial Infarction (MI)

Table 2.1: ECG Lead Locations

Lead No.	External Lead Location
v1	Chest lead, 4th intercostal space, just to the right of the sternum
v2	Chest lead, 4th intercostal space, just to the left of the sternum
v3	Chest lead, between v2 and v4
v4	Chest lead, 5th intercostal space, the mid-clavicular line
v5	Chest lead, between v4 and v6
v6	Chest lead, on the same level as v4, on the mid axillary line
AVL	Left arm or upper left torso
AVR	Right arm or upper right torso
AVF	Right lower leg

diagnostic ECG. Although myocardial infarction refers to dead cells within the myocardium, cardiology practitioners refer to MI more as a process. This process has three main steps: ischemia, injury and infarction. Ischemia is basically a lack of oxygen to the tissue normally supplied by a certain blood vessel. Through time, this ischemia turns to injury of the tissue and finally, the last step is infarction where the cells actually die. Figure 2.7 shows this process. An infarction like this is called an antero-lateral infarction and is caused by an occlusion to the left circumflex. Regarding incidence related to age and gender, Foley et al found that more men than women (66% v's 34%) suffered infarction with a mean age of 71 and 72 respectively (FBC⁺02).

Figure 2.8 demonstrates an occlusion in the left anterior descending coronary artery.

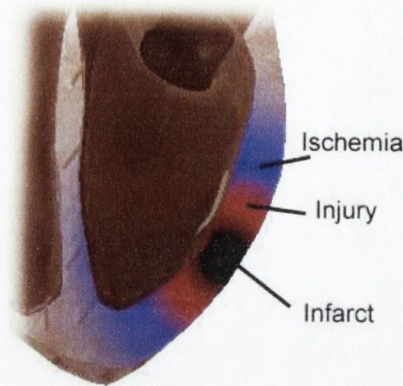


Figure 2.7: Diagram of the MI Process.

2.4 Diagnosis and Monitoring of Myocardial Infarction

2.4.1 Signs and Symptoms

The signs and symptoms of MI are gender-specific. Men experience the following signs of a heart attack: Chest pain, dizziness, dyspnoea (shortness of breath), radiating pains in the chest and arms, intense sweating and nausea (Ger00). With women, although chest pain may be experienced, often pain may be experienced elsewhere (ie. in the back, neck, shoulder and/or throat). Also, women experience more of the non-chest-pain related symptoms including: nausea, vomiting, fatigue and dyspnoea.

2.4.2 Predisposing Factors

There are many factors that make a patient more susceptible to coronary diseases and syndromes. Smoking is well established as causing various heart diseases, which in turn increase the risk of myocardial infarction. One study showed that

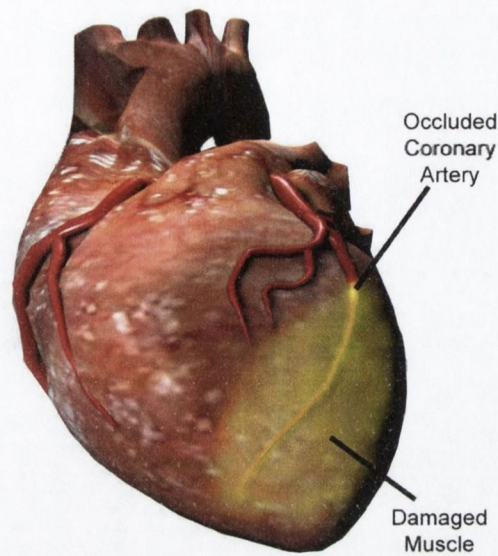


Figure 2.8: Heart with Blockage causing MI.

women may be more sensitive than men to some of the harmful effects of smoking on the heart (PHS⁺98). Abnormal blood pressure is also a pre-disposing factor of MI and, although high blood pressure or *hypertension* is commonly associated with MI, low blood pressure may also be a risk (CCW94). Diabetes is well established as a predisposing factor for cardiac disorders (EWM02). Also, depression carries some risks of MI, more so with men than with women (HCFP98).

2.4.3 Bio-chemical Markers

Cardiac *Troponin* is a regulatory protein of the thin actin filaments of the cardiac muscle. The troponin T and I proteins are highly sensitive and specific markers of myocardial injury (APFR04). In 2000, the joint European Society of Cardiology and American College of Cardiology Committee accepted their measurement in serum as the standard bio-chemical marker in the diagnosis and management of

acute myocardial infarction (TA00). As Amman et al noted, though, because a lot of patients with raised troponin levels have conditions other than MI, these assumptions could lead to unjustified and potentially harmful diagnoses as well as increased medical costs (APFR04). CK or Creatine Kinase is also a bio-chemical marker useful in the monitoring of MI. However, CK MB can be raised and not necessarily be an indication of myocardial damage (Tho97). Some studies have found troponin T and I proteins to be more sensitive and specific than creatine kinase levels (GR03). One of the major disadvantages of using this technique in the diagnosis and monitoring of MI that it takes a long time, due to the requirement of lab analysis of blood. For this reason, ECG is a very helpful tool.

2.4.4 ECG

The electrocardiogram has been used for over a hundred years in the diagnosis and monitoring of myocardial infarctions. Although the ECG is primarily used in the assessment of heart rate and rhythm, the ST segment, QRS complex, T and Q wave act as a new set of criteria in the measurement of MI (Pha96).

2.4.4.1 Early Raised T Waves

A tall T wave is the first change that would be noticed on the ECG if a patient has just had an MI. This is called the *hyperacute* phase of MI. As well as being taller, the T waves may become more symmetrical and more pointed. Unless this *hyperacute* phase is recorded on ECG, it can be discounted since most patients on average delay about 1 hour before they seek medical assistance (Lei03). Figure 2.9 demonstrates this waveform.

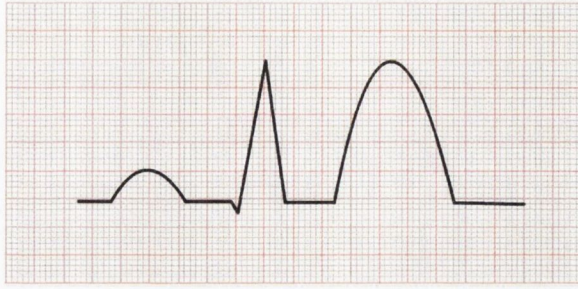


Figure 2.9: Tall T Wave.

2.4.4.2 ST Segment Elevation and Depression

As time progresses, the initial ischemia turns into myocardial injury and the ST segment provides the primary evidence of this phenomenon. ST segment elevation in two or more contiguous leads is the most frequently used indicator in the diagnosis of MI (MB02b). ST segment elevation normally occurs in the first few hours in what is called the *acute* phase of infarction (Pha96). Figure 2.10 demonstrates this waveform.

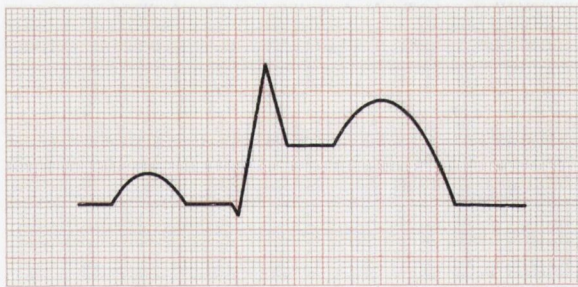


Figure 2.10: ST Elevation.

2.4.4.3 Inverted T Waves

The T wave may become inverted also in the acute phase of infarction. Inverted T waves, however, do not have to occur after ST segment elevation. In fact, it

may precede ST segment elevation or they may occur simultaneously (Pha96).

Figure 2.11 demonstrates this waveform.

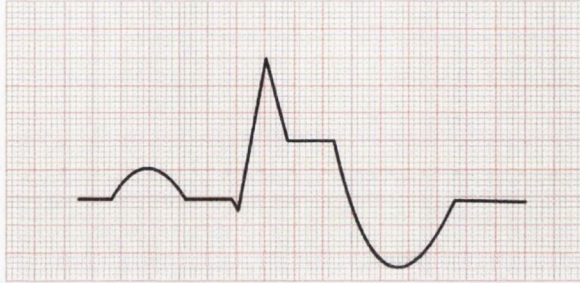


Figure 2.11: Inverted T Wave.

2.4.4.4 Pathological Q Waves

After all of these changes, the Q wave may develop abnormal characteristics, namely being 40ms or more wide (Pha96). This is suggestive of infarction and is represented in Figure 2.12. Once all the initial changes fade, the pathological Q wave remains as evidence that the infarction occurred (Figure 2.13). When developing an ECG diagnostic tool it is important to consider that there are a lot of different units and ways of representing time. Therefore, the “40ms or more wide” should be carefully considered.

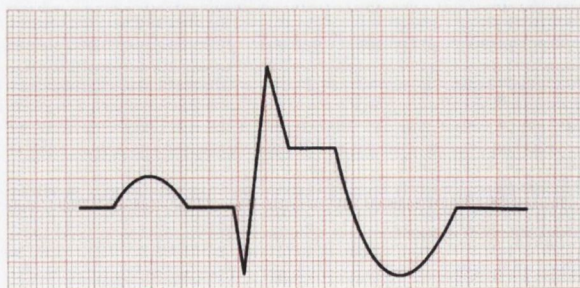


Figure 2.12: Pathological Q Wave.

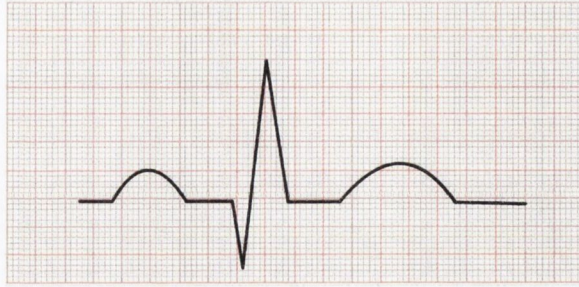


Figure 2.13: Evidence of Infarction.

2.4.4.5 Localisation of MI

In the localisation of MI, we view the ECG leads as cameras aimed at different parts of the heart. If a certain lead demonstrates abnormalities, as seen in the previous section, it is likely that the area of the heart at which this lead is aimed has some abnormality. For example leads, II, III and aVF view the inferior surface of the heart, so, if these leads show indicative changes, it is likely that there is an inferior infarction (MM02). Figure 2.14 demonstrates the ECG lead axes.

2.5 Treatment of Myocardial Infarction

2.5.1 Drugs

The most common drugs that are used in the treatment of myocardial infarction include aspirin, cephalosporins, oral steroids, H2 antagonists, paracetamol and glyceryl trinitrate (GTN) (O'S01). Although ibuprofen is commonly used as an anti-inflammatory for MI patients, there is some evidence that it inhibits the anti-platelet effects of aspirin, which could be harmful (KS03). The analysis of this claim is very difficult because ibuprofen is available over the counter and it is difficult to get information about its use after discharge (CWP+03).

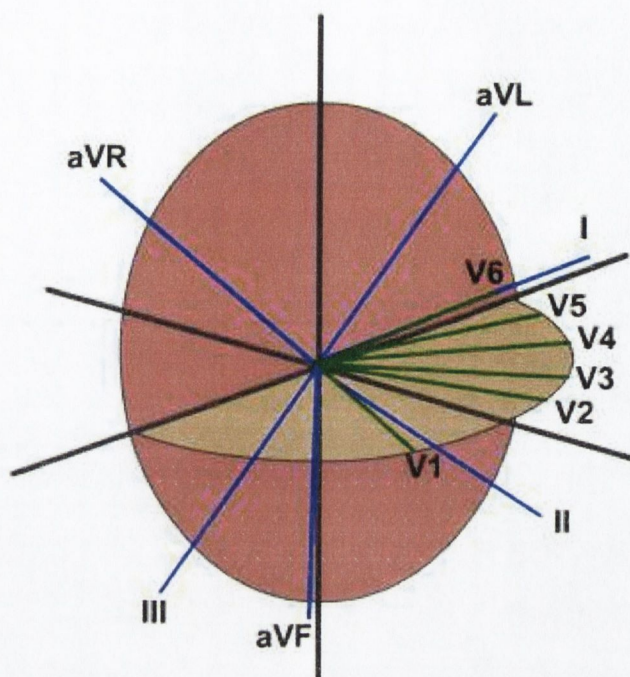


Figure 2.14: 12 Lead ECG Axes.

2.5.2 Defibrillation

Fibrillation is the abnormal, uncoordinated and sometimes rapid movements of the heart in replacement of the normal rhythms of the myocardium. *Defibrillation* is the act of restoring a fibrillating heart either by using drugs or electric shock. Defibrillation has been estimated to save six times more lives than thrombolysis (see next sub-section). However, the patient has to reach medical assistance before he/she can be defibrillated (JN02). It is also known that an hour normally elapses before a patient with acute myocardial infarction will seek medical assistance (KKPW03), which is too late for defibrillation. Public access defibrillators are becoming more and more commonplace, with defibrillators situated in shopping centres and airports. However, because a lot of patients have heart attacks in their homes, this remains a problematic area.

2.5.3 Thrombolysis

Thrombolysis is the process of dissolving or breaking up a blood-clot. In a previous study performed in St James' hospital Dublin, 67% of all acute myocardial infarction patients were treated with thrombolysis (FBC⁺02). Thrombolysis involves the administering a drug containing a thrombolytic pharmacological agent capable of lysing or dissolving a blood clot. Although percutaneous transluminal coronary angioplasties (PTCAs) are very effective, they are quite expensive and dependent on whether the hospital has an angiography suite or not. PTCAs have been around for nearly two decades but the relatively recent introduction of thrombolysis has meant that even the smallest GP surgery is capable of treating acute myocardial infarction (Pha96). It has been shown that pre-hospital thrombolysis has reduced mortality by about 20% (Lei03).

2.5.4 Angiography

Angiography is the imaging of blood vessels by passing a contrast agent into the offending artery. Although ultrasound and magnetic resonance imaging (MRI) are sometimes used in this process, the most common branch is x-ray angiography. In this case, a radio-opaque contrast agent is administered into the vessel concerned and x-ray examination follows the highlighted vessels. Figure 2.15 shows an angiogram taken during this project. It consists of two frames captured during a multiple angioplasty procedure. Generally, the images seen on angiography monitors are inverted versions of conventional x-ray images (*i.e.*, higher densities are darker than lower densities). The ECG leads can be seen in the second frame. The cardiologist altered the x-ray views in order that the ECGs could be acquired at the same time as the procedure. The coronary arteries that

are being worked on appear darker than the surrounding tissue as well as the catheter tube. This is because they are filled with a contrast agent that has a greater density than the surrounding material, thus being more radio-opaque under x-ray monitoring.

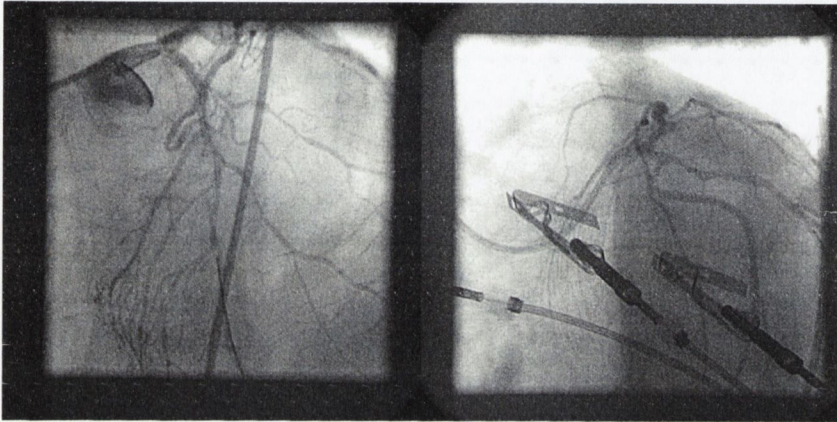


Figure 2.15: Frames of an angiogram.

2.5.5 Percutaneous Transluminal Coronary Angioplasty (PTCA) and Stenting

When a coronary artery is blocked or narrowed, an angioplasty or PTCA procedure is often performed. This procedure involves the passing of a balloon catheter up the aorta from the puncture entry point (normally the femoral artery in the groin area). A balloon catheter, as its name suggests, has an inflatable section towards the top of the tube. Once the specially designed catheter enters the specific area of the diseased coronary artery, the balloon is inflated. This inflation normally causes a widening of the constricted area and sometimes a wire-mesh tube called a *stent* is used to reinforce the vessel. This procedure is performed under an x-ray fluoroscopy angiography unit. A contrast agent is normally used to find

the specific artery and position the catheter. Figure 2.16 shows an angiogram with an inflated balloon catheter.

On inflation of the balloon catheter, the balloon causes a temporary cessation of blood flow. This in turn leads to temporary ischemia of the tissue normally supplied by this blood vessel. As a result of this temporary ischemia, if the patient is being monitored by 12 lead ECG, the ST segment of the ECG leads corresponding to this part of the heart becomes elevated, thus producing a definitive correlation between the recorded ECG and the actual procedure. Angioplasty has a more successful outcome than thrombolysis. *Patency rate* is a metric for a vessel remaining unblocked. Gershlick and More compared the 95% patency rate of angioplasty with the overall patency rates of 80% with thrombolysis (GM98). Furthermore, studies have shown a better outcome and lower early mortality rates where angioplasty had a lower enzyme rise, less reinfarction and also a lower 31 month mortality rate (SGB+95). However, an angioplasty should ideally be performed within the first 90 minutes after the first medical contact (dWAB+03). Townsend recently suggested that another method that might deliver equivalent or even better results than primary angioplasty, while avoiding the associated problems, would be pre-hospital thrombolysis prior to an angioplasty (TD05).

A *stent* is a device that keeps an artery open after being forced open with a balloon catheter. It is a wire mesh tube that fits neatly onto the end of the catheter and, once the lumen of the artery is opened, the stent is expanded to fit the artery and the balloon and catheter are removed. A stent is used to combat a very common problem, namely arterial restenosis. This phenomenon occurs normally within three months when there is a proliferation of smooth muscle as a reaction to vessel injury and happens in over 30% of patients, but with

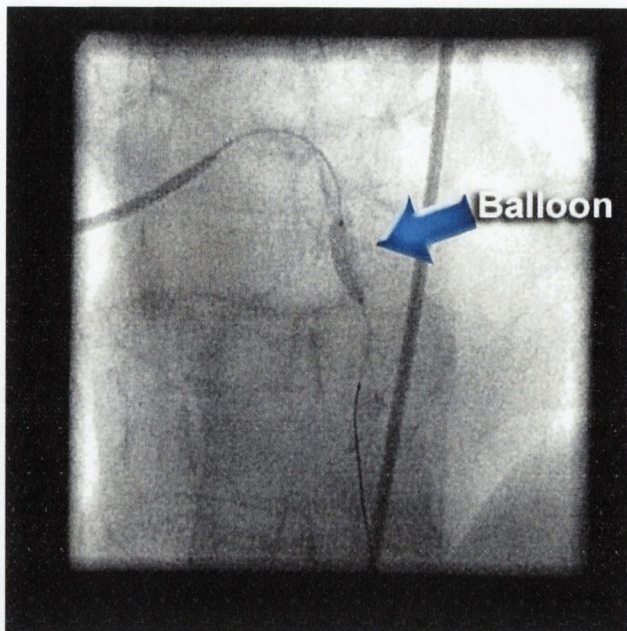


Figure 2.16: Angiogram with Inflated Balloon Catheter.

the advent of these stenting techniques the rates of restenosis lie between 10% and 20% (MB02a). Figure 2.17 demonstrates an angiogram with a catheter, guide-wire and stent. A stent can also be seen in figure 2.16 below the inflated balloon.

2.5.6 Financial Implications of MI Treatment

Because MI treatment is quite costly, there are many implications for health services and patients. There is constantly a balancing act between cost-effectiveness and clinical effectiveness. A recent study in the UK by Hartwell et al has suggested that immediate angioplasty is both clinically more effective and financially more effective than thrombolysis (HCL+05). This incorporates many factors, including the fact that thrombolysis has a higher MI recurrence rate. Also, within this suggestion, it is assumed that both these interventions are routinely avail-

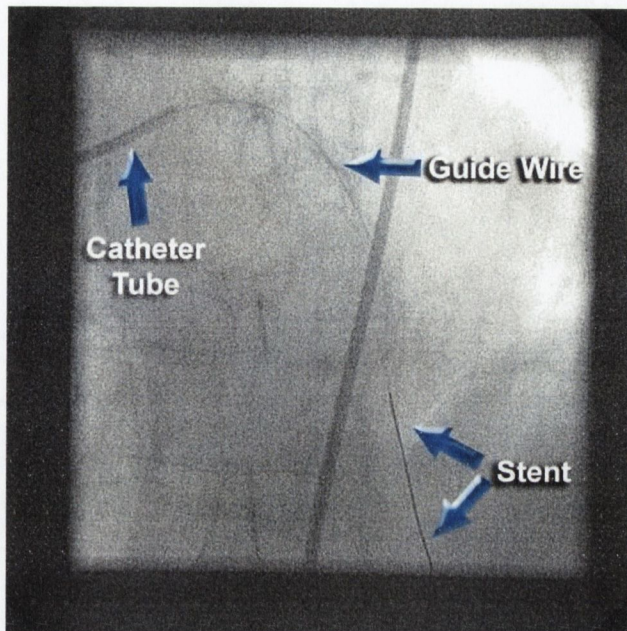


Figure 2.17: Angiogram with Catheter and Stent.

able. This, of course, may be relatively true in the US, but in the UK, Ireland and most of Europe, immediate angioplasties would require a colossal health service upgrade. Hartwell et al noticed that an upgrade like this would not only require a huge amount of initial capital and revenue for catheter laboratory provision and running costs, but also a mass recruitment of cardiologists, radiographers, cardiac technologists and nurses. Of course, staffing would be the biggest problem with already a chronic shortage of these staff in most European countries. So, for these reasons, thrombolysis remains a short-term answer to a long-term problem. In Ireland, the vast majority of revascularisation cases undergo thrombolysis rather than PTCA (67% v's 5%, respectively) (FBC⁺02).

2.6 Interpreting the ECG

2.6.1 Automatic Interpretation of ECG Data

Research has been conducted in the field of automatic ECG interpretation and pattern recognition for about 50 years (TS90). However, it is still considered to be a very complex area of research. One main approach in this field involves the use of pattern recognition and parameter measurement. With the results of these processes, the ECG can be interpreted and abnormalities can be detected. The first task of pattern recognition is unfortunately the most problematic. The QRS complex is a waveform that correlates with the excitation of the bundle-branches and ventricles. The most common application of this parameter is the measurement of heart rate. However, more importantly to our system, the other waveforms within the ECG can be found using this complex as a starting point for the detection of the other waveforms. Kohler et al (KHO02) found it difficult to select an “ideal” QRS detection algorithm, since all were designed for different purposes. Algorithms were identified from many different fields including artificial neural networks (XHT92), genetic algorithms (PCV95), wavelet transforms (KMBB99) and syntactic pattern recognition (TS90). Tatara and Cinar (TC02) discuss a method of interpreting ECG data by integrating statistical and artificial intelligence tools. More recently, Fernandez et al developed a combined algorithm in the detection of the R-peak (FHM05). They combined several established wavelet algorithms with the Pan Tompkins (PT85) QRS detection algorithm and obtained substantial improvements. This combined algorithm ran both methods in parallel and, when either of the methods disagreed, a suitable decision strategy was applied. In some of these cases, the Pan Tompkins algorithm would be re-run with a different threshold. However, as always with ECG algorithms, they

found that noisy data hindered this process. Macek described an incremental machine learning algorithm that used online *bagging* and *boosting* techniques, which proved superior to standard batch machine learning algorithms (Mac05). Bagging and boosting are well established classification techniques in the field of machine learning.

The So and Chan (SC97) QRS detection algorithm seems to be the most appropriate for our purposes because it was aimed at real-time systems. This QRS detection algorithm operates on the premise that the QRS-onset is found when two consecutive ECG data points satisfy the condition:

$$\text{slope}(n) > \text{slope-threshold}$$

The relevant parameters are derived this way:

$$\text{slope}(n) = -2X(n-2) - X(n-1) + X(n+1) + 2X(n+2)$$

$$\text{slope-threshold} = \text{threshold-parameter}/16 * \text{maxi}$$

$$\text{maxi} = (\text{first-max} \text{ maxi})\text{filter-parameter} + \text{maxi}$$

$$\text{first-max} = \text{height of R point} \text{ height of QRS onset}$$

The filter-parameter is set to either 2,4,8 or 16. From the QRS-onset marker, the Q, R and S waves can be found easily by traversing backwards and forwards.

2.6.2 Automatic ST Segment Detection

Since the automatic detection of the ST segment has many clinical and commercial applications, it is an area rich with research. Silipo et al found that, by borrowing concepts from the areas of principal component analysis and artificial neural networks, an ST-T level change detection algorithm could be developed. From a database of 97000 normal and abnormal ST-T segments, they found that

their algorithm obtained a sensitivity of 77% and a positive predictive accuracy of 86% (SLMM95). Martinez et al found that a complex demodulation approach was suitable in ambulatory recordings (MOL00). Joo et al suggested that one of the disadvantages of conventional detectors based on local morphologic features is that global yet subtle changes, such as that from the start of the QRS complex to the end of the T-wave, go undetected (JSH⁺98). They described an algorithm based on local and global signal morphology that obtained a sensitivity of 55% and a specificity of 98%. Although a lot of the automatic ischemia/MI detection algorithms cater for ST segment changes, few cater for the entire ST-T complex. Garcia et al developed an algorithm that does just this. Their algorithm is applied to the *root mean square* (rms) series of differences between the beat segment and an average pattern segment. After making a few improvements at a post-processing stage, they obtained a sensitivity of approximately 90% (GSOL00). One of the most established ST segment detection algorithms, which a lot of the literature refers to, is that of Jager et al. They developed a Karhunen-Loeve transform (KLT) based algorithm which incorporates a single-scan trajectory recognition algorithm using the Mahalanobis distance function between the feature vectors (JMM98). They used the KLT approach to reject any noise, thus leaving the resulting wave-form in a more readable state. They recorded a sensitivity of approximately of 85%. The KLT, which is also called principal components analysis (PCA) is a technique to simplify a dataset and is based on the statistics of the data, therefore this technique is data dependent. A Mahalanobis distance function is a function based on the distance of a case from a centroid. A *centroid* is the mean point within a set of independent variables within a multidimensional space. Therefore, Mahalanobis distance can be thought of as a measure providing an indication of whether or not an observation

is an outlier compared to the independent variable.

In general, there is a myriad of detection algorithms, all of which are not 100% accurate considering the changeable nature of ECG.

2.6.3 Limitations of Automatic ECG Interpretation Algorithms

Throughout the literature, the sensitivities and specificities of algorithms are quite low for clinical diagnosis. A conventional algorithm that uses localized ST-elevation and a rule-based classifier has a sensitivity of 35% and a specificity of 98% (JSH⁺98). This, to a cardiologist or clinician, would not be good enough when dealing with “real” patients who have critical conditions. Several detection algorithms incorporate some kind of noise filter. This is an area that needs to be carefully considered, since a noise filter has the capability of deleting or distorting important wave information that could be critical.

2.6.4 Human-guided Interpretation Algorithms

Even with some of the best algorithms in the computer diagnosis of myocardial infarction, the sensitivity is still only less than 85% (AGM⁺02). However, a well trained cardiology practitioner can have 100% sensitivity. There is a new train of thought that proposes the incorporation of human input into the detection process. Anderson et al incorporated human input into a vehicle routing algorithm. Vehicle routing algorithms have been researched for many years. They found that their results compared favorably with previous purely computer-based algorithms (AAL⁺00). Throughout the duration of this project, while working in the cardiology setting, we found that most cardiologists and clinicians shared

the opinion that commercially available software for automatic detection and interpretation of ECG was overly sensitive to changes that would be considered *normal* and had a high mis-diagnosis rate. Because of this attitude, these kinds of software applications are rarely used in a clinical setting. There is a definite opening for semi-automatic tools that consider the user's expertise in the diagnosis process. This branch of interactive optimization has a key role within this project.

2.7 SCP and Other ECG File Formats

Once digital ECG was born, the various manufacturers developed their own specific file formats to store ECG and patient information. However, as time went on, it became apparent that, due to the multi-manufacturer nature of most health-care settings, it was important to develop a common file format. DICOM is a file format originally designed as a protocol for medical image data exchange. This file format is already in use for magnetic resonance, computed tomography, ultrasound and general x-ray imaging, as well as being the accepted standard in cardiology settings such as cathlabs in most US and European hospitals (BS05). The DICOM standard now incorporates its own ECG handling features as well as catering for the ECG specific SCP (Standard Communications Protocol) file format.

SCP (Standard Communications Protocol) is a file format for digitised ECGs. The basis for SCP was developed in 1989-1991 during a European AIM R and D project. During this project, a quality assured ECG signal compression algorithm was developed, which is now used within the SCP file format (Zyw05). The original SCP documentation had many ambiguities and therefore resulted in

2.7 SCP and Other ECG File Formats

many of the manufacturers misinterpreting the standard. For this reason it was reviewed in 2000 and became the AAMI Standard EC71 (Eur00).

Within the scope of this project, the existing ECG acquisition equipment could only export the ECG data as SCP files. Therefore, it was necessary to use this file format. Appendix A holds more in-depth information about the SCP file format.

Chapter 3

Graphics in Medicine and Medical Education

The omnipresence of graphics technology has extended into medicine and medical education since its inception. The development of multi-planar medical imaging modalities such as MRI and CT paved the way for 3D reconstruction and various visualisation techniques. Once image acquisition and image processing takes place, computer graphics allows us to visualize medical image data in many different ways. This chapter outlines the graphical principles relevant to our project. For readers without a background in computer graphics, this chapter will contain terms that may not be understood. These terms are explained in the glossary (Appendix D).

3.1 Basic Principles of Computer Graphics

In the field of 3D computer graphics a *scene* is normally made up of a camera or view-plane, lighting and the model. The model is normally made up of

smaller objects or *primitives* including lines, points and polygons. A *polygon* is a closed set of lines that make up one of the most common primitives for model representation. A polygonal mesh is normally made up of quadrilateral, or more commonly, triangular polygons. These primitives are then coloured, textured, illuminated and shaded according to various parameters. A polygon may be textured if needed by applying a *texture mapping* technique. This technique involves mapping pixels of a texture (texels) to the confines of the polygon or mesh. Texture mapping allows a model to look more realistic by applying a real texture, but, also this technique is used in texture-based volumes (discussed later in this chapter) to represent volumetric attributes rather than just superficial skin meshes. *Shading* is the process of simulating how the face of a polygon would look when the lighting model is applied. Flat-shading shades the polygon according to the polygon's *normal* vector. Other shading models use a smoothing algorithm that uses vertex normals to create a blending / smoothing effect. There are two view-plane projections that are relevant to this project: the perspective projection and orthographic projection. The perspective projection is a method of converting a 3D scene to a 2D image plane, but preserving the scene's three-dimensionality. The orthographic projection, on the other hand takes a straight-on view of the scene and is particularly useful when retrieving slice-information.

In the field of electro-physiological visualisation, realistic models and simulations are becoming commonplace in medical education and practice due to the rapidly developing field of 3D graphics and virtual reality. This is aided by ever-increasing computer specifications and decreasing costs. VR training in medicine provides the student/practitioner with a greater sense of spatial awareness as well as eliminating the possibility of jeopardising the patient's safety (DPO⁺03). Volume representation, 3D animation and interactivity are obvious advantages

over 2D images.

3.1.1 Graphics Libraries

OpenGL (Open Graphics Library) is a cross-language, cross-platform library of functions for the production of 3D computer graphics. It is mainly used in computer games, CAD, virtual reality, medical and scientific visualisation. Its main competitor is Direct3D. OpenGL's main advantage over Direct3D is portability, with Direct3D mainly being tied to one platform: Microsoft Windows. In the fields of medical visualisation and simulation, OpenGL seems more suitable because of its cross-platform capabilities, whereas Direct3D was mainly developed for computer games. OpenGL is widely accepted for its merits in representation and manipulation of volumetric medical data (LDB95). Java3D is a java-based API that normally runs on top of either OpenGL or Direct3D. Although Java is an ideal cross-platform environment, its inherent speed problems are often a deterrent compared with optimised languages like C++ for many medical visualisation and simulation applications (HBAN04). However, Java does have excellent networking, internet and encryption capabilities which are becoming more important in medicine as more and more hospitals are using facilities such as telemedicine. Therefore, it should not be completely disregarded as a viable option. Another option for this toolkit would be to use VRML (Virtual Reality Modelling Language). VRML is especially useful for world wide web applications and it interfaces very well with Java and Javascript. John et al. (JPVP99) described such an application that was used in the training of surgeons for ventricular catheterisation procedures. The web and multi-user extension features of VRML make it ideal for the field of teleradiology (JRSB00). X3D is a successor to VRML which has added web functionality. It features the ability to encode a

scene using the syntax of XML (GBKA04). For volume applications, the sizes of datasets would raise a bandwidth issue. Although, SGI's OpenGL VizServer is an option that caters for large datasets (SCC⁺04)

3.2 Volume Visualization

Within the discipline of computer graphics, the polygon was one of the first rendering primitives. The framebuffer contained the pixel information of the polygons that were rasterised. Multi-dimensions then became interesting, especially among the scientific and medical communities, where the display of information attained from modalities such as computed tomography (CT) was gaining in importance. A *voxel* is box shaped representation of the smallest part of a three-dimensional space, basically the 3D equivalent of a *pixel*. There are various different volume renderers available. Some renderers work behind the scenes and turn a volume dataset into a set of isosurfaces using algorithms such as that of Lorensen and Cline's "Marching Cubes Algorithm" (LC87). Although this can produce very effective results and is used in many medical applications such as virtual endoscopy, it only gives a surface representation. This may be of no use in applications where varying densities are an integral part of the visualization process. A typical example of this would be an MRI volume of soft-tissue. This type of application is called a *direct volume rendering* and it seeks to capture an impression of the entire 3D dataset by accounting for emission and absorption effects of all the elements (MMC99) (Lev88) (JESMM⁺97). Fire, gas, smoke and fluid simulation commonly use the latter form of volume visualization as well as the simulation of physiological phenomena such as blood-flow and the simulation of various electro-physiological processes. In volume graphics, the rendering

phase is viewpoint independent and insensitive to the complexity of the object or scene, as well as allowing Boolean and block operations and constructive solid modelling (CKY00).

3.2.1 Image Order Traversal

Two of the most common image order algorithms are ray-tracing and ray-casting. Ray-tracing involves the tracing of the ray from the camera/observer through the scene and computing all the lighting factors, such as reflection, absorption and refraction. Ray-casting, which is commonly used in games, is a more simplified version of ray-tracing. It does not consider the new directions a ray of light takes after bouncing off a surface. The simplest of all the direct volume rendering algorithms is the use of OpenGL points to represent each voxel of the volume data-set. The alpha and colour attributes of the OpenGL points would be altered accordingly. A previous version of our ECG simulation software used this method of volume visualisation (MORB03). Although this method represented each voxel accurately, the processing time was prohibitively slow at a rate as slow as 2 frames per second after precomputations (ROBM04). As well as this performance deficit, the resulting images were blocky. A better way to represent a volume by points is *splatting*.

3.2.2 Object Order Traversal

Unlike image order traversal, i.e., working from the view-plane backwards, object order traversal works from the objects forward towards the viewplane. *Splatting* is an object-order common direct volume rendering technique and was first described by Westover (Wes89). It involves voxels being represented by Gaussian kernels,

whose pre-integrated footprints are accumulated to form the image (NM05). Splatting yields a similar look to that of ray-casting, except at a greater speed because the projection footprint that the interpolation kernel leaves on the image is precomputed (MY96). Figure 3.1 shows the typical form of the splat kernel.

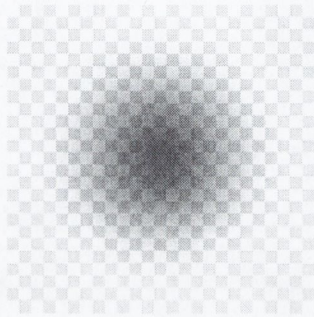


Figure 3.1: Gaussian splat kernel.

3.2.3 Texture-based Volume Rendering

Texture-based volume representation offers an excellent method for achieving interactive rates for reasonably sized datasets (CCF94) (KMM⁺01). However, current graphics hardware is not suitable for larger datasets since there is an upper bound of 256-512Mbytes on commercially available graphics cards. Guthe et al developed a method of handling large volume datasets on standard PCs by using a wavelet based system that decompresses on the fly and uses hardware texture mapping (GWGS02).

One problem associated with texture-based volume rendering is that, if the volume is only stacked along one axis, an artefact can be caused when the camera becomes parallel with the slices. This artefact can be minimised and sometimes eradicated by creating a lattice of slices along each axis, or also using certain techniques with 3D-textures as supported by many graphics cards and OpenGL (WWE04). Depending on the application of texture-based volume rendering,



Figure 3.2: Texture-based Volume Representation.

shading may need to be applied. Volume shading involves the application of an illumination model to the outer voxels of the volume. Further considerations need to be made if an interactive clipping function is available. In this case, illumination should not only be based on the properties of the scalar field, but also represent the orientation of the clipping surface concerned (WEE03). Volume clipping techniques have huge potential in the area of clinical practice, where a clinician can interactively cut slices and shapes to get to what he/she is interested in. By using OpenGL and a standard graphics card, texture-based volume rendering offers the easiest way to represent a volume of an acceptable resolution at an interactive and real-time speed. Figure 3.2 demonstrates this process. Firstly, slices are acquired and represented on texture-mapped quadrilateral polygons. These slices are then stacked and finally a blending algorithm is used and irrelevant voxels are not displayed.

3.2.4 Hybrid Rendering

Sometimes it is very useful to represent medical phenomena with both iso-surfaces and volumetrics. This is especially useful for applications such as virtual surgery, where a virtual scalpel may be used on a polygonal mesh representing the skin, with a volume underneath representing the underlying tissue. This kind of rendering can help achieve interactive rates on what otherwise would be very large datasets (MGS97). Wilson et al. proposed a method of hybrid rendering for large data-sets ranging from gigabytes to petabytes (WKL02). This method involved the use of hardware texture mapping and point-based rendering, instead of conventional direct volume visualization, and they found that interactive speeds were achievable on a single PC.

3.3 Real-time Volumetric Animation

One of the challenges with volumetric animation is the sheer magnitude of data involved. Even with a relatively small volume of $64 \times 64 \times 64$, to display an animation in real-time requires significant amounts of processor power, whether the animation is pre-computed or not. For animations that are computed “on the fly”, the restrictions are even further amplified. Chen et al showed that a volume model of size $140 \times 220 \times 71$ could be animated in real-time (approx 22 frames per second) using some simple physically-based elasticity rules (CQHKM98). This animation was a simulation depicting a muscle segment from the visible human project. Real time volumetric animation has several applications in medicine and especially surgery simulations (BNC96). When animating the electrical propagation through the heart it may be necessary to precompute the frames. Instead of saving the entire resolution of the volume for each frame, there is a technique

called *differential volume rendering* (SGJ94). This technique involves changing only those voxels that differ from the previous time-step within the animation. This achieves considerable disk-space savings as well as inexpensive processing times and real-time rendering of the 3D flow.

3.4 Cellular Automata (CA) in Biomedical Simulations

A cellular automaton (CA) is a cell in a lattice structure that has a finite number of states and rules, and can be used to illustrate a wide variety of phenomena from physics, chemistry, biology, economics, physiology *etc.* (CZG04). This model structure is especially suitable for the representation of the heart's electrical cycle (SGJ94), thus, being of relevance to this project. Biological cells, like cellular automata, generally follow a set of certain rules and have a finite set of states, thus CAs are very suitable for biomedical simulations. Peirce and Skalak found cellular automata to be very useful in examining pattern changes in subcutaneous microvascular networks induced by focal applications of exogenous vascular endothelial growth responses (PS03). Some of the cellular states they considered include proliferation, differentiation, migration and apoptosis. In cardiac simulation some of the cellular states would include depolarisation state, ionic states, fibre orientations *etc.*

3.5 Virtual Surgery and Endoscopic Techniques

Virtual reality graphics and haptics allow ample scope in the area of virtual surgery. There are two main branches in this field: surgical simulation and "real-

world” surgical applications. With surgical simulation, the surgeon or trainee can practice on a virtual phantom before entering the operating theatre (SHS⁺00). The second branch involves the visualisation of complex datasets in surgical environments (Joh03) and the use of robotics for minimally invasive surgery (MNK⁺04). Surgical simulation for training makes the process more intuitive and informative while reducing the cost and duration (CM98).

With the advent of multi-slice CT, a reconstruction technique that connected the colon segments in all slices was developed (HMK⁺97). This technique was called virtual colonoscopy and the main motivation was to be less invasive and possibly less expensive than the alternatives: barium enema or virtual colonoscopy. Since then there have been many similar virtual endoscopic techniques including virtual bronchoscopy (BMF⁺03), virtual endoscopy of the joints (arthroscopy) and even virtual endoscopy of the coronary arteries (BL05). This field is a richly researched area and has yielded many successful outcomes. However, there is a huge mountain to pass before these techniques would be routinely used in a clinical setting: *i.e.*, who does the manual segmentation? This is a very time-consuming job and qualified personnel in this area are limited. The staff needed would have to have a large enough knowledge-base that any abnormalities would not be omitted in the process. Perhaps there is room for a specialist job in this field within our health settings. In 1993, a directive was introduced within the European Union that outlined legislation for working time (THE93). This reinforces the need for these new specialist positions.

3.5.1 Augmented Reality Applications

The term *augmented reality* is often misunderstood and erroneously considered to be the same as *virtual reality* (VR). In the field of medical and surgical sim-

ulations, augmented reality normally means a combination of VR and the “real-world” (Azu97). A head mounted display (HMD) can be used to superimpose virtual reality objects over real-world objects. There are many potential applications for this kind of superimposition. One of these is augmented reality ultrasound imaging. For example, State et al. developed a real-time stereoscopic video-see-through for ultrasound-guided needle biopsy of the breast and a physician successfully guided a needle into an artificial tumour within a phantom of a human breast (SLG⁺96).

3.6 The Previous Version of the ECG Teaching Tool

In the first year of this project, Mooney et al experimented with various graphical techniques (MORB03). Using a model that comprised of an inner and outer heart wall meshes, the volumetric data was originally acquired using a ray-casting algorithm. Volumes were created, in the first instance, by creating an octree for each mesh. The depth of the octree also represented the resolution of the volume buffer. Random rays were cast from the centre of each node and the number of triangular crossings were recorded. With this algorithm, any node that was inside the surface resulted in an odd number of crossings, whereas any nodes outside yielded an even number of crossings. To eliminate the possibility of error due to rays that were cast at vertices or edges, multiple rays were cast from each node. In order to produce the volume between the inner and outer meshes, boolean operations were applied to the voxel classifications of the mesh-set and the voxels representing the myocardium were extracted. Figure 3.3 shows the resulting myocardial volume model. The volume was represented graphically

3.6 The Previous Version of the ECG Teaching Tool

using an OpenGL point per group of cells. Although intuitively attractive, this type of volume representation has some pitfalls. Processing time is one of the most important down-sides due to the real-time nature of this project. As we will demonstrate in this thesis, a more efficient and visually compelling method of representing the same data-set is by using slice-based texture volumes.

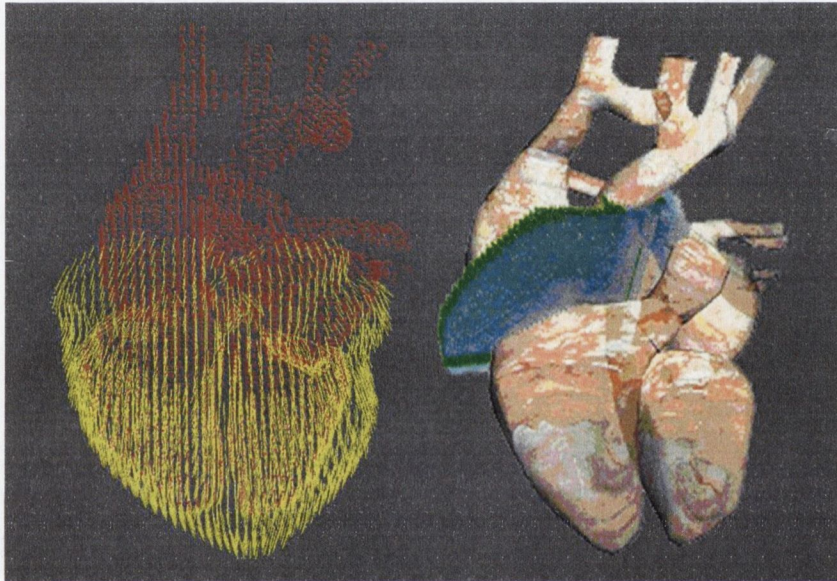


Figure 3.3: Previous Heart Model.

The electrical network was also constructed at this stage of the project. After some initial experiments with Greene's voxel space automata (Gre89), it was decided that this was not suitable for creating the ventricular network. This was mainly due to the large amount classification needed in the definition of the growth medium. Instead, the network creation was reduced to a 2D problem. Figure 3.4 demonstrates the process. A 2D reference image (a numbered grid for convenience) was created and mapped to the ventricle meshes. Then a commercial image editor was used to draw the bundle-branch network. The UV texture coordinate were computed by extracting the foreground pixels of the branch im-

age. Using the UV coordinates of each triangle's vertices, (u_1, v_1) , (u_2, v_2) , (u_3, v_3) , and the pixel's UV coordinates (u_0, v_0) , The barycentric coordinates b_1, b_2, b_3 were calculated as:

$$b_0 = (u_2 - u_1) * (v_3 - v_1) - (u_3 - u_1) * (v_2 - v_1)$$

$$b_1 = ((u_2 - u_0) * (v_3 - v_0) - (u_3 - u_0) * (v_2 - v_0)) / b_0$$

$$b_2 = ((u_3 - u_0) * (v_1 - v_0) - (u_1 - u_0) * (v_3 - v_0)) / b_0$$

$$b_3 = ((u_1 - u_0) * (v_2 - v_0) - (u_2 - u_0) * (v_1 - v_0)) / b_0$$

If the computed coordinates b_1, b_2, b_3 are positive, the foreground pixel is inside the triangle. If $b_i = 0$ and b_j, b_k are positive, the foreground pixel lies on the edge opposite vertex i . Also, if b_i and b_j are equal to zero, then the pixel lies on vertex k . If a pixel is found to be within the triangle the XYZ coordinates are found using the following equation:

$$(x, y, z)_{pixel} = (v_1 * b_1) + (v_2 * b_2) + (v_3 * b_3)$$

$(x, y, z)_{pixel}$ represents the Euclidean coordinates of the pixel and v_1, v_2, v_3 are the 3D coordinates of the triangle containing the pixel. In the volume, the closest surface voxel to the pixel's 3D coordinates is chosen for representation.

3.7 Simulation of Heart Electro-physiology

Interactivity is one of the most important features in a VR teaching tool. This, however, becomes more difficult for the developer when working with volumetric data, but this process is becoming increasingly easy with techniques such as slice-based volume rendering (KSH03). In the field of cardiac simulation, the cellular data-structures are normally vast and require very long processing times or supercomputers (KNWH03). CESLab (rC05) is a project based on commodity Apple Macintosh computers. This system is concerned with forward ECG

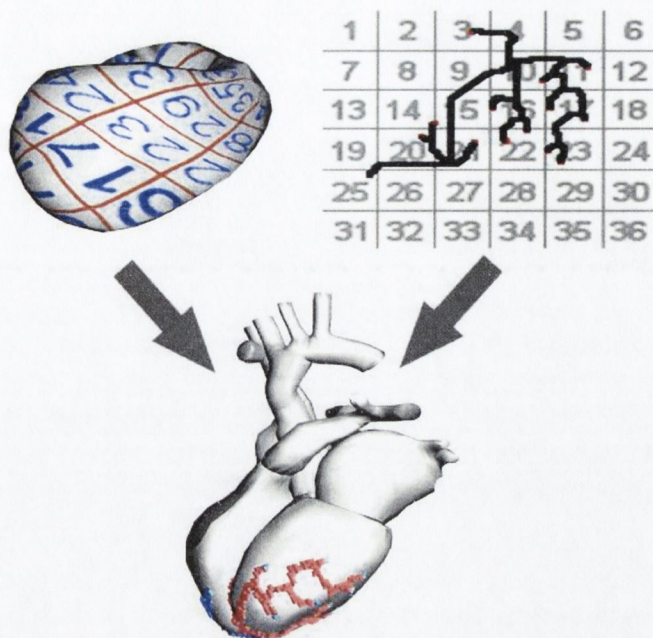


Figure 3.4: Electrical Network Construction.

simulation (*i.e.*, obtaining ECG from simulated cellular models), whereas we are generally interested in the inverse problem (*i.e.*, Representing ECG data with graphical models). At Washington University they have designed a fully ionic cardiac model which is used along with a multi-electrode (224 electrodes) vest and a CT heart-torso model to display cardiac electrophysiological and arrhythmia information (RGJR04). This project brings much more information than standard low-resolution 12-lead ECG simulations. However, to implement this kind of protocol in a clinical environment would be difficult both financially and practically. Although there is a myriad of papers such as that of Sermesant et al. (SFE⁺03) that deal with very detailed simulations of electrical propagation through the heart, we are more interested in simplified simulations suitable for real-time interaction.

3.8 Libraries for Interaction and Graphical User Interfaces

FLTK (Fast Light Toolkit) is a cross-platform open-source C++ graphical user interface (GUI) toolkit for Unix, Linux, Microsoft Windows and MacOS X operating systems. It also caters for 3D graphics with OpenGL and a GLUT emulation. GLUT (OpenGL Utility Library) is OpenGL's library of windowing and monitoring functions. FLTK's OpenGL implementation means that the user can use standard OpenGL commands and functions within the FLTK framework. This is very useful if converting from an initial GLUT implementation. Unlike FTLK, VTK is a toolkit specifically designed for scientific visualisation, but the graphics model is at a higher level of abstraction than OpenGL. This means that it is easier to create graphics but more difficult to have more specific control of the visualisation process. MFC (Microsoft Foundation Class) is a C++ GUI library specifically for Microsoft applications and can be ported to OpenGL to create 3D applications with GUIs. Unfortunately, a lot more work is required than when using FLTK and it is also platform-specific.

3.9 Increased Immersion Techniques

3.9.1 Stereoscopic Viewing Conditions

Stereopsis is an optical technique in which an image of a different location within a scene is shown to each separate eye, thus causing a stereo ocular 3D effect (Tid90). Due to easy-access of equipment within our laboratory, we experimented with two stereoscopic displays: a head mounted display with dual LCD screens (Figure 3.6) and also 3D shutter mechanism glasses (Figure 3.5). The head

3.9 Increased Immersion Techniques

mounted display operates by having two separate cameras within the scene and displaying the separate rendering on the separate LCDs. The 3D stereo glasses, however, require much less effort in implementation since all the work is done at driver level. This system operates by showing an image to one eye while a polarised shutter mechanism blocks off the opposite eye, and then switching back and forth. The shutter mechanism is synchronised with the monitor and operates at half the speed of the refresh rate frequency. Therefore, with a 100Hz monitor, the shutter on one eye would open at 50Hz.



Figure 3.5: 3D Stereoscopic Shutter-Mechanism Glasses.



Figure 3.6: Head Mounted Display - Inside View.

There are many other versions of stereoscopic displays available including

3.9 Increased Immersion Techniques

back or forward projected screens using dual projectors and polarised 3D glasses. Also there are commercial devices that are specifically designed for stereoscopic display such as the NuVision 21MX-SL Stereoscopic Monitor.

Chapter 4

Implementation

Now that the background and motivations behind this thesis have been discussed, the development of the myocardial infarction diagnostic and teaching tool will be described. Firstly, the acquisition and development of the cardiac model will be explained along with the volumisation techniques used. Then, an overview of the data-structures used as well as the overall design of the system will be presented. Thereafter, section the animation system will be described. ECG handling issues will then be discussed, including the design of the ECG window, the design of the SCP file reader/writer and also the classification and interpretation system. The MI simulation and representation techniques will be described, along with increased immersion techniques and the development the graphical user interface.

4.1 The Heart Model

4.1.1 Model Acquisition

The initial polygonal cardiac model used in the system was created in New York University's School of Medicine. Figure 4.1 is a diagram of this model. The

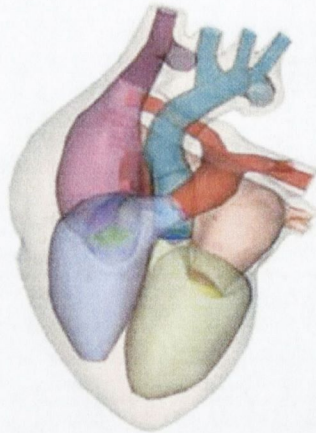


Figure 4.1: Initial heart model.

model was designed through collaboration between consultant cardiologists and graphical designers for the specific purposes of interactive learning and VR teaching aids and is freely available (NYU05). For our project, an *ideal* heart model was needed, since the heart would be used to represent data from many different heart types. Since only electrical abnormalities are represented on this heart dynamics or movement were not considered. The shape of MRI and CT-derived hearts may be that of a heart in mid-cycle or, in the case of a cadaver-derived model, doesn't reflect a normal living heart. MRI and CT-derived heart models may also have artefacts related to those particular imaging modalities. The NYU heart model suited our project the best because of its ease of integration into our system and its lack of deformities and abnormalities for use as a teaching tool. However, in its initial state it was unsuitable for use within our system since it lacked many of the important features in the heart's electrical network *i.e.*, SA node, AV node, left and right bundle branches. The SA node and AV node were added to the polygonal model using a commercial editor and were

each represented by a single spherical primitive. Surface representations for the bundle branches and Purkinje network were also added at this stage. However, the creation of a necessarily dense Purkinje network proved too cumbersome. Furthermore, volumization of such a fine-featured network is not possible on anything other than high-resolution volume lattices. Therefore, the bundle branches and Purkinje system were later replaced by translating texture maps into 3D. At the beginning of the project, initial test-ECGs were taken by monitoring a staff member in the department. These ECGs were free from any pathologies and were obtained using the standard 12 lead configuration.

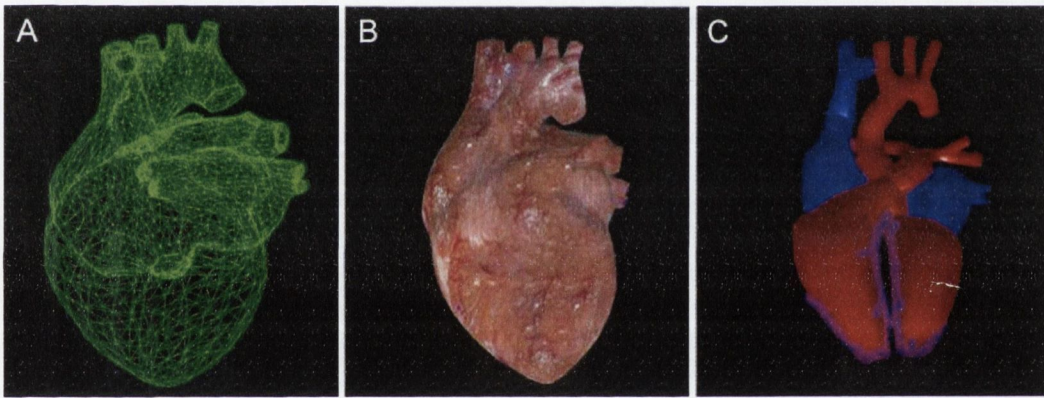


Figure 4.2: The final polygonal model.

4.1.2 Model Development

The model's outer mesh was textured to resemble the outside of a heart with a suitable texture (Figure 4.2 B). The inner-mesh was then coloured according to a well established colouring scheme. In medicine and medical education there are two colours that represent the circulation system: red and blue. At a glance, red represents arterial blood and blue represents venous blood. Within the heart, however, the colours mean oxygenated blood (red) and deoxygenated

blood (blue). So, for these reasons the superior and inferior *vena-cavas*, the right atrium, the right ventricle and the pulmonary arteries were coloured blue and the pulmonary veins, the left atrium, the left ventricle and the aorta were all coloured red. This colouration is useful as a teaching tool to remind students which section is which (Figure 4.2 C).

An extruded cylindrical polygonal mesh was initially used to demonstrate the bundle-branches extending down from the AV node (Figure 4.3). OpenGL points were used to represent the vertices. These points were then used in the animation by changing colour as the electrical activation propagated through this network. An algorithm was developed to reorder the vertex points so that the propagation was correct. This running order was saved out as an external file and reloaded on initialisation. As the project went on it became apparent that this bundle-branch network was more than was needed and the computation was quite expensive for a real-time system. Instead, the bundle-branches were now represented by a series of lines. A simple colour-changing mechanism was implemented where the initial activation of the *bundle of His* was synchronised with the onset of the QRS complex. This progression is only an informative tool and intended for the teaching tool application rather than a physiologically accurate portrayal.

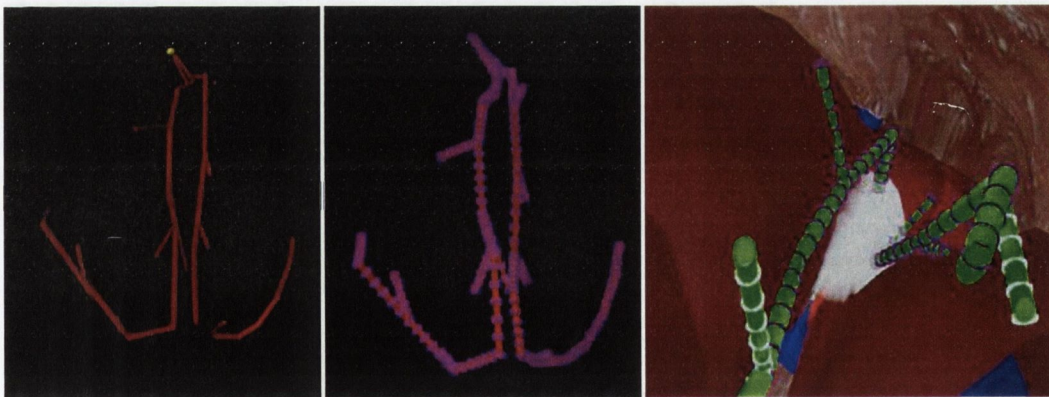


Figure 4.3: Screenshots of the initial representation of the bundle-branch network.

4.1.3 Voxelisation

Our initial model used points to represent each cell within the volume as discussed in the background section. However, at the drawing stage it was very obvious that this method was too slow for the system, so an alternative approach was needed. This method also had some aesthetic deficits as seen in figure 4.4. Volumes were created, in the first instance, by creating an octree for each mesh. The depth of the octree also represented the resolution of the volume buffer. Random rays were cast from the centre of each node and the number of triangular crossings were recorded. With this algorithm, any node that was inside the surface resulted in an odd number of crossings, whereas any nodes outside yielded an even number of crossings. To eliminate the possibility of error due to rays that were cast at vertices or edges, multiple rays were cast from each node. In order to produce the volume between the inner and outer meshes, boolean operations were applied to the voxel classifications of the mesh-set and the voxels representing the myocardium were extracted.

Texture-based volumization is becoming very popular recently because of its fast rendering advantages (WEE03) (KSH03). A method of taking slice data from the original model and altering each manually for cell assignment was developed. Therefore, instead of having a volume of separate points, we have 100 slices of 256×256 resolution. The slice data is attained using a very thin viewing field and an orthographic projection. The image information was outputted to .tga files. The myocardial cells were represented with an opaque value and the blank cells were represented as fully transparent values. Figures 4.5, 4.6 and 4.7 show this process of slice acquisition.

Using the resulting images from this process, the model's volume is displayed by reconstructing these slices along the same axis as the original viewing fields.



Figure 4.4: Initial volume represented with points.

Figure 4.8 shows firstly the reconstructed volume on its own and then with the inner mesh. This slice-based volume representation method is becoming widely accepted because of its speed advantages over other methods such as displaying cells as single points. The main reason for the speed advantages is because the graphics processing unit (GPU) is used to accelerate the texturing processing.

We chose not to use slice data from CT/MRI or freely available datasets such as the visible human project. The main reasoning behind this was that we should keep to the structure of the original *ideal* heart model and represent any abnormalities as regions within the volume.

4.1.4 Volume Artefacts

If a texture-volume is a stack of slices along one axis only, and if the camera becomes parallel or close to parallel with these slices, an artefact is produced. Figure 4.9 shows the artefact produced with the volumetric heart model. There

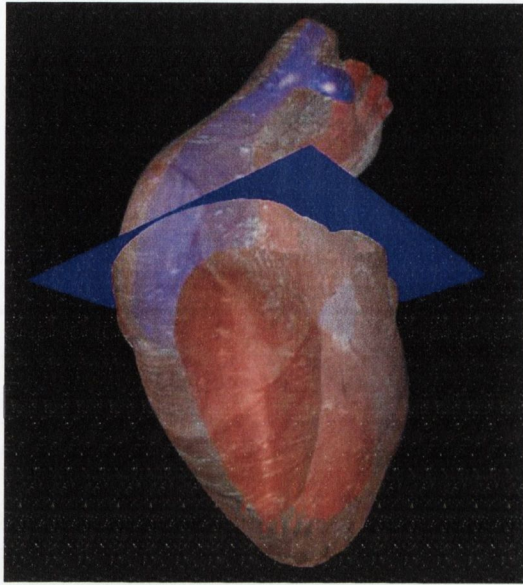


Figure 4.5: Slice Retrieval - location of viewing field.

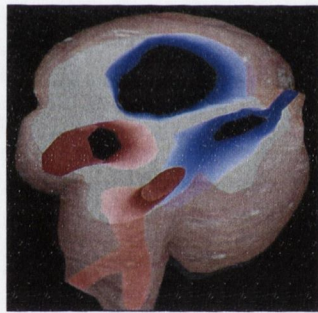


Figure 4.6: Slice Retrieval - slice as viewed in opengl window.

are a few methods of preventing this artefact. The slices could always be oriented close to perpendicular to the camera. This would involve texture swapping once the camera moves to a different location. The downside to this would obviously be processing time. Also, a lattice of textured slices could be produced with a stack of slices along each axis. With this heart model though, it was chosen to have two stacks of slices, one along the vertical axis and the second along the frontal or coronal axis. This was found to be sufficient because of the hybrid nature of the model, *i.e.*, an inner mesh was included, which masked any extra



Figure 4.7: Slice Retrieval - slice with dual colour representation.

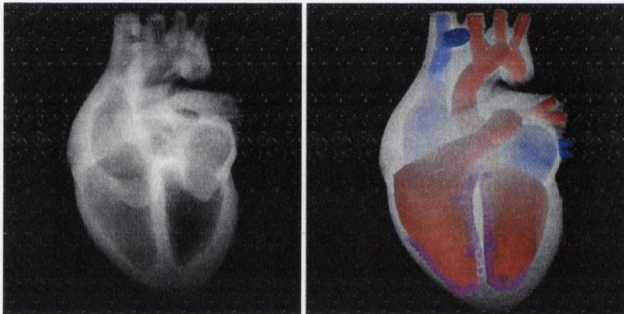


Figure 4.8: Reconstructed volume model - without and with inner mesh.

artefacts. We chose not to implement sagittal slices because the user would rarely need to look at the areas involved. There was also a texture memory limitation, which forced this decision.

4.1.5 Classification of Cells

There are five main types of cells within the volume: blank cells, atrial cells, ventricular cells, sino-atrial cells and atrio-ventricular cells. Bundle-branch injection cells were added to represent parts of the bundle branch. The classification of the heart cells was performed over several steps. Firstly, each slice was separately coloured within a commercial editor, each colour representing a different cell-type. Then, a set of functions within our software re-opened these slices and transferred this information into a general volume data-set that was outputted

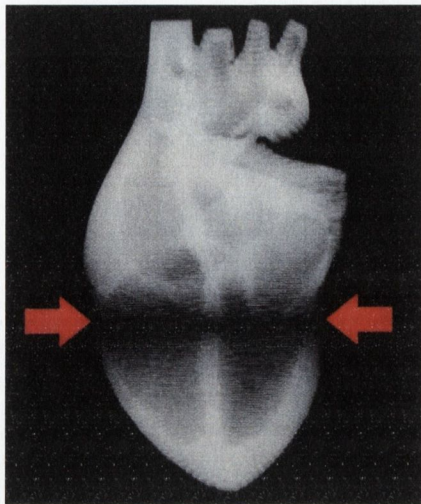


Figure 4.9: Artefact produced when camera was parallel to slice-stack.

to a file. Now, every time the MI software is started this volume information is used to allocate the cell-types to the volume model.

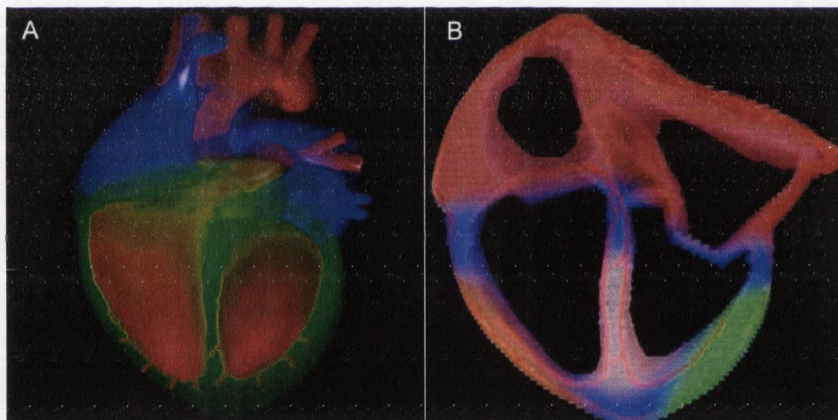


Figure 4.10: Classification of cell-types.

4.2 The Display Environment and the Graphical User Interface

4.2.1 Languages and Libraries

After starting the development of the system with GLUT it was decided that a graphical user interface (GUI) with buttons, sliders *etc.* would be useful. FLTK seemed to be the most obvious option. The programming languages used were C and C++, this was because of the suitability for OpenGL programming.

4.2.2 GUI Design and Layout

Several designs were considered. An initial design for the GUI incorporated 12 separate OpenGL ECG windows as well as the main OpenGL model window. This impacted negatively on interactivity since there were so many OpenGL contexts and also manipulating 13 different sub-windows all displaying graphics was very cumbersome. It was decided that it was sufficient to display only one ECG lead was sufficient to display at a time. All the other leads could be accessed separately and easily. This led to the next generation of the GUI which incorporated two different OpenGL sub-windows: the model window and the ECG window. After performing some speed profiling tests it was obvious that this configuration was still not optimal for a real-time interactive volumetric tool. To optimise for speed, we incorporated the ECG window as a separate viewport within the model window. This greatly improved the performance of the system and also eradicated several problems produced by having separate windows for the update of every frame. Interactive real-time volumetric tools are always processor-intensive especially if animation is also required. For this reason, any extra processing besides

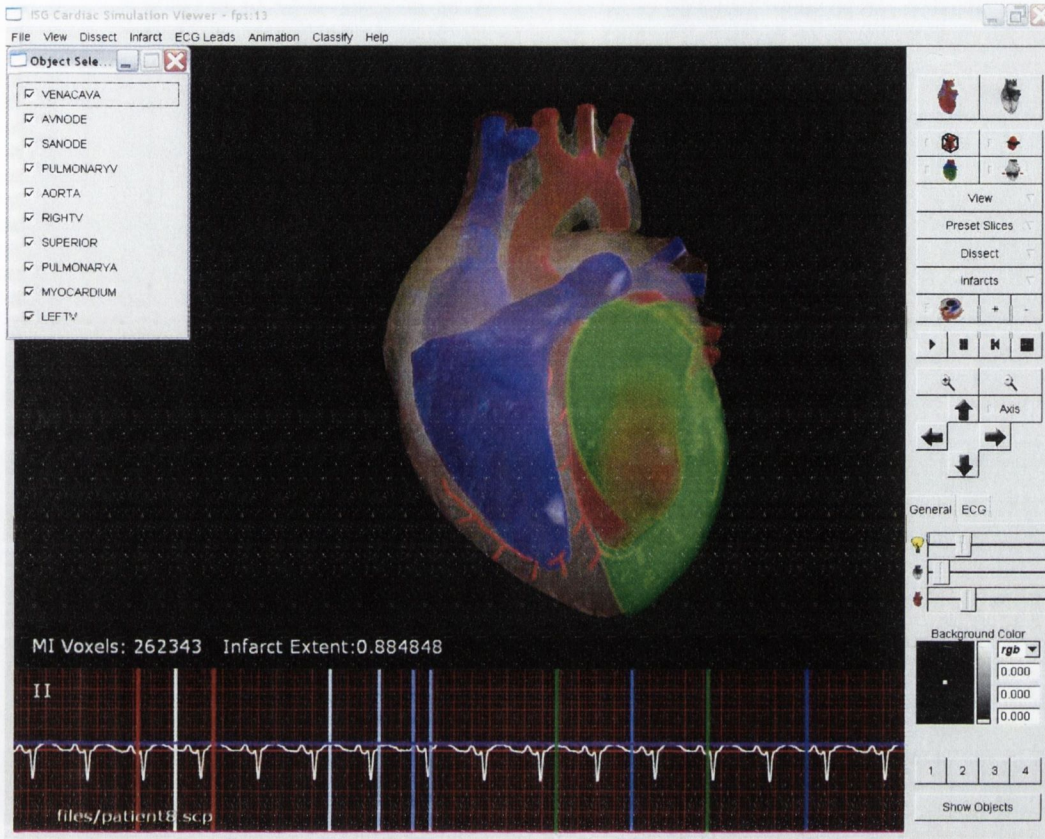


Figure 4.11: A screenshot of the visualisation toolkit at work with the final layout.

that involved with the model should be cut to a minimum.

4.2.3 Model Interaction

A set of features were incorporated to allow the user to navigate and alter the model and views. A tracker-ball model was implemented for rotation of the model while the viewing camera remains in a static location. When the mouse is clicked, the model rotates in whichever direction the user pulls. The zooming mechanism works by scaling the model. Zooming is normally implemented by altering the camera position, but for convenience we chose to scale the model instead. This meant that the camera model remained static and only the heart model would

move. The near and far clipping planes are brought as close to the model as possible so that, on scaling, the model does not cause put too much pressure on the processor. Various clipping procedures were incorporated so that the users can “dissect” the model. Mainly the clipping is performed by using the OpenGL clipping plane functions on the transverse, sagittal and frontal/coronal planes. Figure 4.12 demonstrates a screenshot of a frontal clipping plane approximately half way into the heart. This is particularly useful for the teaching tool when viewing the electrical progress through the bundle branches. Another viewing feature is that of slice-view. This feature uses a very thin viewing plane by bringing the near and far clipping planes very close together, thus leaving a very thin slice. The same method was originally used for retrieving the initial slice information for the volume model. Now, there are two predefined slice-views: a slice along the frontal plane that is aligned with and incorporates the bundle-branches, the SA node and AV node and also a slice along the transverse plane that incorporates the mid-section including the AV node. These were identified during the initial collaborations with the Physiology Department in Trinity College. Figure 4.13 shows a screenshot of the frontal slice-view technique.

4.3 Data-structures

4.3.1 Model Structure

The model is comprised mainly of an outer polygonal mesh skin, an inner polygonal mesh skin, a line-based bundle-branch network and a slice-based texture volume. For storage of the polygonal model, the OBJ format was chosen for convenience and the mesh model is broken into the following objects: SA node, AV node, vena-cava/right atrium, right ventricle, pulmonary arteries, pulmonary

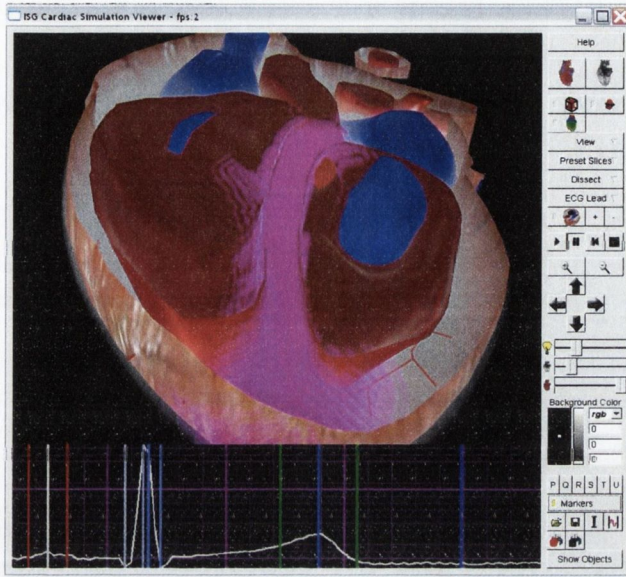


Figure 4.12: Screenshot of a model that is clipped along the frontal plane.

veins/left atrium, left ventricle and *Aorta*. These were separated for the ability to hide and colour individually. Although it was possible to use several pre-programmed OBJ loaders, an obj loader that catered for separate objects was needed. Figure 4.14 is a diagram demonstrating the data-structure that was used.

A visual dialogue box was incorporated that displays all the object names within the model's OBJ data-structure as tickable radio-buttons. As default, all the elements of the model are visible. However, the user can untick any of the objects. This calls a redraw which updates the model window. This feature would be of use in the teaching tool, but there would be no obvious advantage for the diagnostic tool.

4.3.2 Cell Data-structures

Each voxel within the volume has two main components: the cellular information and the pixel information. The pixel information tells the system about the color

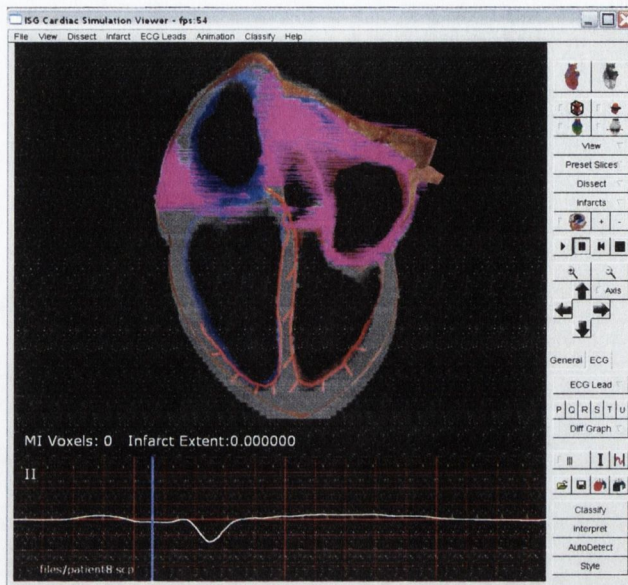


Figure 4.13: Screenshot of a model displayed with frontal slice-view during animation sequence.

values and transparency and basic information about the different tissues. On the other hand, the cellular data holds information about the specific cell types, timings and frame indices. The cell data-structure is currently open-ended to allow for more complex computations such as fully ionic modelling. Because this system is aimed at interactive tools, the cell structure has to be simple.

4.3.3 Animation Structures for Speed Optimization

Speed optimization is an important issue with this software because of the large amount of processing required by volumetric animation. The importance of speed optimization is reinforced by the need for real-time interactivity within the system. To provide for this, a frame indexing system was implemented to record the frame number where each cell is depolarized and repolarized. This information is collected during one iteration of the simulation and then reorganised into a speed-friendly structure and outputted to a file for every other time the same ECG file

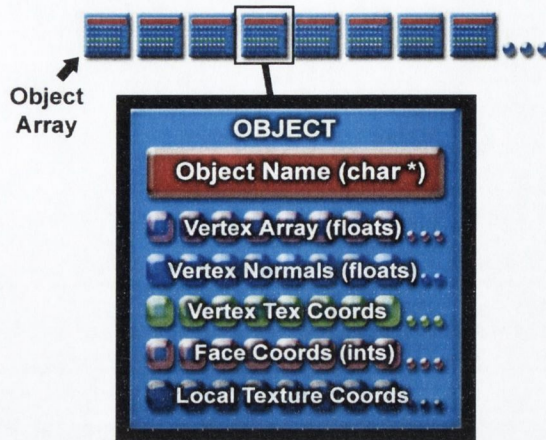


Figure 4.14: Datastructure for the handling of different model objects.

is used. This frame indexing system has increased the frame rate from approximately 1fps to 20 fps. One of the major advantages of this method is that the cell structure can become more complex without affecting the animation speed, as only the initial iteration is affected. The cellular progression algorithm is more accurate than previously yet, thanks to the frame indexing technique, running speed is not compromised, but has, in fact, improved drastically. The ECG synchronization system is effective in defining markers with which to determine the exact points within the animation.

4.3.4 ECG Handling - The SCP File Format and Huffman Decoding

Although initially we used straightforward ASCII data files of a normal heart with a time and voltage value for each step, once the ECG console was acquired it became apparent that the software would need to read in the SCP file format. The SCP-ECG file format is quite complex because it incorporates so many features. It is primarily a binary file format and most of the time the ECG is encoded with

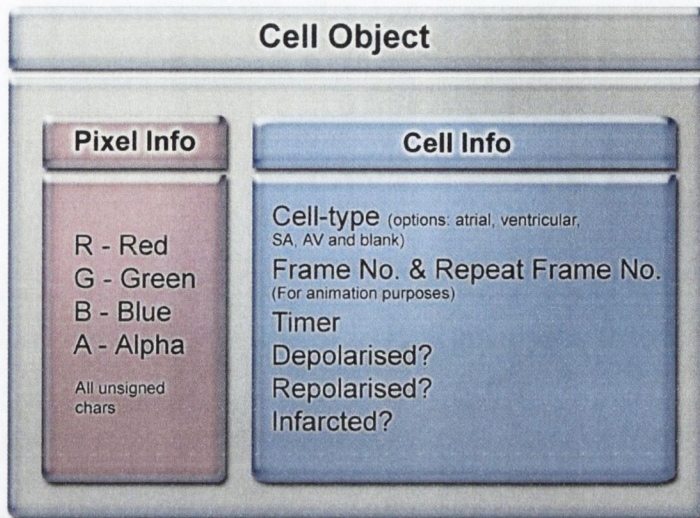


Figure 4.15: Structure of the cell object.

the default SCP-ECG Huffman table that can be seen in Appendix A. The file is mainly comprised of an initial CRC-checksum (size of file) and record length and then 12 sections. The first section holds the pointers to all other included sections and section two holds the main header information. Table 4.1 shows the structure of the SCP file format as defined by the SCP specifications (Eur00).

For the duration of the project we used a commercial ECG console that connects via serial cable to a laptop. Then, on the laptop, there is the manufacturer's software that records the ECG and then offers the feature of export to SCP file format. It emerged that the manufacturer's implementation of the SCP file writer was incorrect. This flaw was found by accident and our SCP reader was altered accordingly. The manufacturer's SCP file format never deviates from a particular path so we minimised our SCP reader to a certain protocol. Once the initial readings are made, section 0 gives information on the number of sections included in the file. Section 1 then includes the usual patient information. Section 2 specifies the type of Huffman table used (if any). The Huffman table used by

Table 4.1: Structure of SCP File

Section No.	Description
Prelim Info	CHECKSUM
Prelim Info	SIZE OF THE ENTIRE ECG RECORD (IN BYTES)
0	POINTERS TO DATA AREAS IN THE RECORD
1	HEADER - PATIENT DATA/ECG ACQUISITION DATA
2	HUFFMAN TABLES USED IN ENCODING
3	ECG LEAD DEFINITION
4	QRS LOCATIONS
5	ENCODED REFERENCE BEAT DATA
6	RHYTHM DATA
7	GLOBAL MEASUREMENTS
8	DIAGNOSIS FROM THE "INTERPRETIVE" DEVICE
9	MANUFACTURER SPECIFIC DATA
10	LEAD MEASUREMENT RESULTS
11	UNIVERSAL STATEMENT CODES

this manufacturers software is the default ECG Huffman table. This table was specifically designed and optimised for ECG compression (Eur00). Once the leads are defined in section 3, the next two sections are skipped since they do not apply to this project and the actual ECG data is read in as bytes to the raw data buffer of each lead object and then converted to bits and entered into the bit array of each lead object for decoding and processing. Figure 4.16 shows the SCP datastructure including the lead objects. The decoding process consists of traversing from bit to bit until a value is deciphered and then continuing through this bit buffer until the end. Each of these values are stored in the final data array of each particular lead object and some post-processing is required. Second difference (a type of encoding) post-processing is applied as well as an amplitude value multiplier (AVM) which finalizes the voltage value of each step.

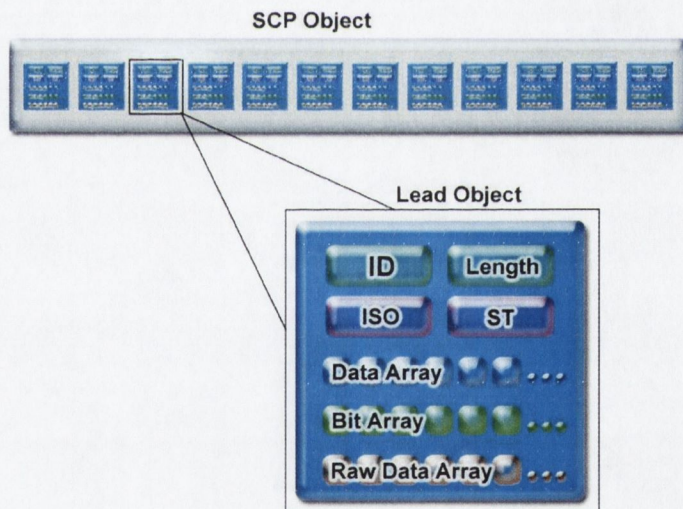


Figure 4.16: SCP object structure.

Our software has an SCP writer. Because most of our ECGs are only 10 seconds long the file sizes are relatively small. Therefore, compression was not a priority, so no Huffman encoding was required. The ECG raw data values are

stored in the SCP data file instead.

4.4 The ECG Window

The ECG window is a separate view-port within the main OpenGL window. Compared to the model window, the ECG window, which is situated below this, uses an orthographic projection. The back-plate is an OpenGL quad which is parallel to, in line with and the same size as the view-plane. Superimposed onto this are the grid-lines that make the ECG window look like a conventional tracing. There is an option that the default colour settings (the ECG tracing as white, the grid-lines as red and the back-plate as black), can be changed to the conventional paper-tracing colours (black for the ECG tracing and white for the back-plate). Once the grid-lines are drawn, the next layer is added: the ECG tracing. This is represented by a series of white OpenGL lines. Both the grid and ECG lines are anti-aliased. Figure 4.17 demonstrates the layered structure of the ECG window.

Once the marker allocation tool is switched on, a vertical line-marker follows the mouse's x value until the intended wave has been allocated. For the ST and *iso-electric* line-markers, a horizontal line-marker follows the mouse's y value until the appropriate level is selected. On the mouse's release, each time a selection is made a marker file is created using the same name as the SCP file but with a ".mf" extension. Each marker file stores the markers as the integer coordinates of the ECG window rather than the actual ECG values. Within each marker file the following information is stored: the P,Q,R,S,T and U waveform markers and the ISO and ST values for all 12 leads. In total there are 30 separate integer values within each marker file. The ECG is scaled horizontally to the time-size of the ECG record. The vertical scaling is more approximate by scaling to four

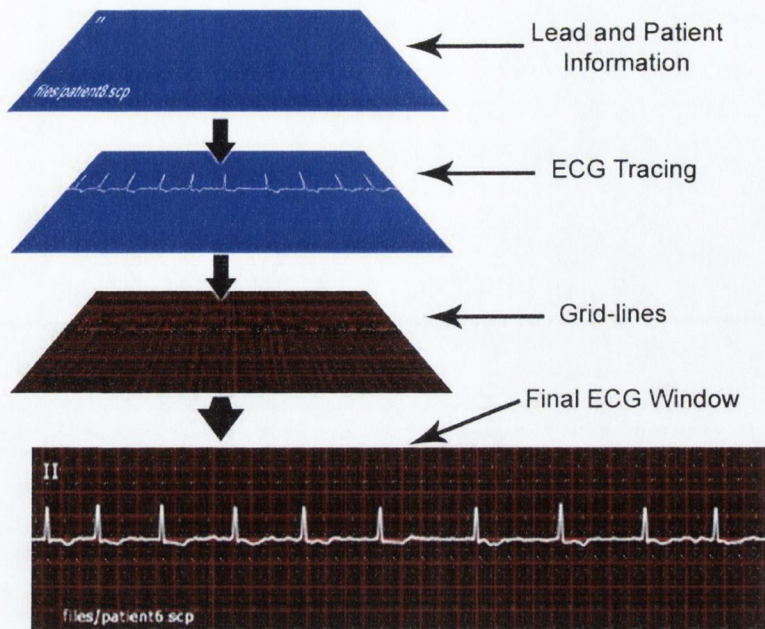


Figure 4.17: ECG window structure.

millivolts. This means that there are 2 millivolts to the top and bottom of the iso-electric line. If the ECG tracing goes above or below these limits the values are rounded-off to the upper and lower limits. Of course, this rarely happens, as most ECGs rarely go above 1 millivolt or below -1 millivolt. A cropping function was incorporated that allows the user to select a section of the ECG record and then crop the entire record so that just this section is present. This cropping mechanism is spread through all four leads and the scaling values are changed accordingly.

4.5 The Animation System

A key feature with the system is that the representation of the electrical excitation of cells on the volumetric model runs in synchrony with the featured ECG. A set of pre-defined ECG markers is the basis of the animation. These markers may be

defined either manually or automatically. The automatic wave classifier uses the So and Chan QRS detection algorithm (SC97). Tan et al (TCC00) found that this algorithm had a greater sensitivity than that of Pan and Tompkins (SC97). So and Chan's method was also aimed at ambulatory ECG monitors for real-time detection. This quality is in keeping with our system's real-time specifications. There are many other suitable QRS detection algorithms, but the So and Chan algorithm was the easiest method to implement since it operates on a simple slope detection method with simple filters and threshold mechanisms as defined in the medical principles chapter (SC97).

The electrical cycle begins with the SA node, which is represented in the polygonal mesh as a sphere and also in the volume as a single voxel. The SA node sphere flashes along with the preliminary firing of the cells in the vicinity of the SA node. With every iteration each cell's status is identified. If a certain cell is depolarized then its neighbouring cells are depolarized, thus causing a spread of the electrical excitation. To direct a nearest-neighbour algorithm, a shape is needed. We initially used a cross-shape (Figure 4.18) but found that a spherical shape (Figure 4.19) with a defined radius produced more credible results.

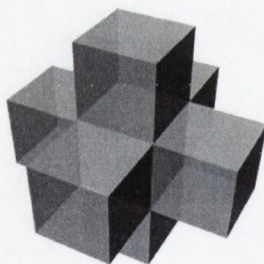


Figure 4.18: Initial propagation shape.

There are many conditions in the decision for electrical propagation. Apart from the depolarized/repolarized condition, the cell-type is another large consid-

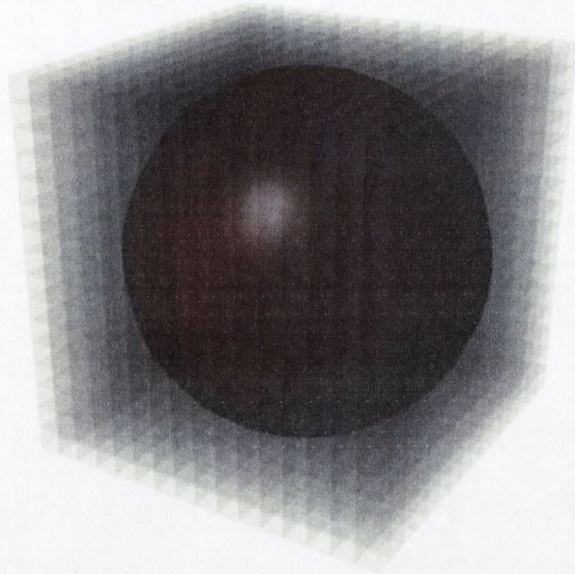


Figure 4.19: Final propagation shape.

eration. For example, when the progressing ECG marker is within the P wave, the atrial cells should be the only cells being activated. For this reason, it was necessary to categorize the volume into cell-types. This was done by differentiating each cell-type with a different color. We did this by manually editing each slice with a commercial editor. Currently we have 5 main cell-types which include blank, atrial, ventricular, sino-atrial and atrio-ventricular cells. Figure 4.20 shows an example of this. Blue represents atrial cells and green represents ventricular cells.

The bundle-branches are displayed as a series of lines with insertion points within the septum and on the inferior borders of the ventricles. There have been many different generations of this animation system. The initial version used a pre-computed database of circles to display the isotropic spread on each slice. Although this ran quickly, it had several disadvantages regarding anatomical phenomena. This cellular spread ignored anatomical structures and spread right

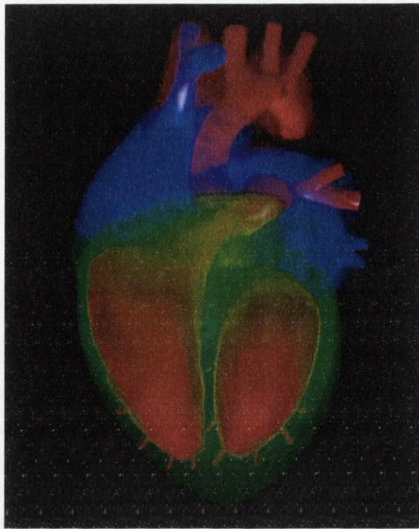


Figure 4.20: Diagram of different cell types.

through the whole volume. The current spread, however, only spreads where there are other cells. It was decided from the outset that muscle/tissue dynamics (*i.e.*, contraction of the tissue on electrical activation) would not be implemented within this animation system. Although, this would be interesting for students as a teaching tool feature, it would not be of use diagnostically.

4.6 The ECG Classification and Interpretation System

The ECG window was designed in such a way as to allow the user to assign manually allocated markers. Figure 4.21 shows a screenshot of a marker-assigned window of lead II. The white vertical line is marking the P wave with the red P_{in} and P_{out} markers at either side of the waveform. The middle three blue-coloured markers define the Q, R and S waveforms and the T wave is defined and surrounded by the two green markers referring to T_{in} and T_{out} . The U waveform is

also selected but is not relevant in the animation and is rarely used in cardiology.

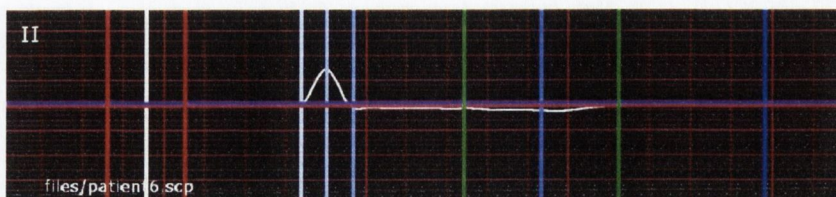


Figure 4.21: ECG window with classified wave markers.

Figure 4.22 shows a screenshot of the ECG window with the ST segment marker. A horizontal line was chosen as the best manual selection tool since it can traverse several ECG waveforms, thus acting as an averaging feature.

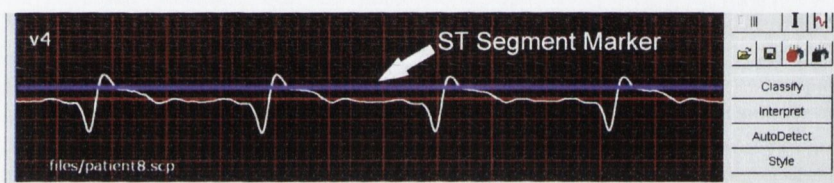


Figure 4.22: ECG window with average ST segment marker.

4.6.1 Automatic Representation of Myocardial Infarctions

Myocardial infarctions are represented within our system as areas around central voxels that correspond to the lead vectors. We introduced voxels within our model by aligning them to axes representing the lead vectors. The voxels are inputted into the volume where the axes intersect with the model. The electrical propagation animation recognizes the infarcted cells and cannot pass these cells, thus spreading around them. The MI detection system measures the parameters as found by either the automatic or manual markers system. Currently the system measures the difference between the ST segment and the iso-electric line for each lead, thus giving the extent, if any, of infarction. These measurements are then

used as references for the radius around that specific lead's model-representation voxel. The T waves are also checked for inversion. The animation of the electrical propagation is automatically choreographed with markers that are selected by the user or automatically selected using the automatic wave classifier. This wave classifier uses the So and Chan QRS detection algorithm (SC97), which was the most suitable detection algorithm because of its suitability to real-time systems. Once the QRS complex is found, the other waveforms are found by traversing backwards and forwards from that point. This is not always accurate, so a manual human-guided wave classification tool is incorporated into the software. We incorporate a standard metric for MI into our system. The purpose of a metric within our system would be to see if the bio-chemical measurements correlate with our measurements. At the moment we use a voxel counter that counts the number of infarcted voxels once the interpretation process is complete. This is of key importance to the next stage of the project which is to compare this voxel count with the blood chemical measurements.

4.6.1.1 Wave Abnormalities

The wave abnormalities considered in the system include ST segment elevation or depression, T wave inversion or acute elevation and Q wave pathologies. Even though T and Q wave abnormalities are considered, the area of most relevance is ST segment deviation. The ECG axis is often used by cardiologists to diagnose deviation from the normal path of electrical propagation. This kind of deviation can sometimes be seen in non-pathological cases. For this reason, and also because the scope of this project could not include these kinds of pathologies, the ECG axis was not considered for this toolkit.

Table 4.2: MI Changes

Location of the Infarct Site	Corresponding Leads
Anterior	V3 and V4
Antero-lateral	V5, V6, I and AVL
Septal	V1 and V2
Inferior	II, III and AVF

4.6.1.2 MI Location

An initial MI location and extent algorithm operated as follows: (i) first find out which leads were abnormal, (ii) then check these results against a reference and (iii) represent them as previously allocated infarctions introduced to the volume. This reference is a well established method of locating infarctions (Pha96). However, it was decided, with the input of a cardiologist and a physiologist, that a more intuitive and informative tool would be helpful to display exactly what the leads are showing.

The MI localization algorithm operates on the assumption that a particular lead acts as a view to a particular region of the heart. The orientation and location of the heart itself is assumed to be normal. Rare abnormalities such as dextrocardia, which means the displacement of the heart to the right, are ignored. Even though these phenomena are normally quite obvious to trained cardiology workers, yet another advantage of a “human in the loop” process. The software also assumes that the user has accurately placed all the ECG leads in the correct positions. All 12 of the ECG axes converge at a central area. The location of this area has been chosen to be the centre of the heart, *i.e.*, above the ventricles but below the atria. This is an approximation, but is considered to be sufficient for the inherently ambiguous nature of ECG. There are always assumptions with

4.6 The ECG Classification and Interpretation System

the use of ECG, and also the ECG is never used alone. The ECG is seen in clinical practice as an informative tool to be used along with other modalities and indicators, not as a 100% reliable diagnosis.

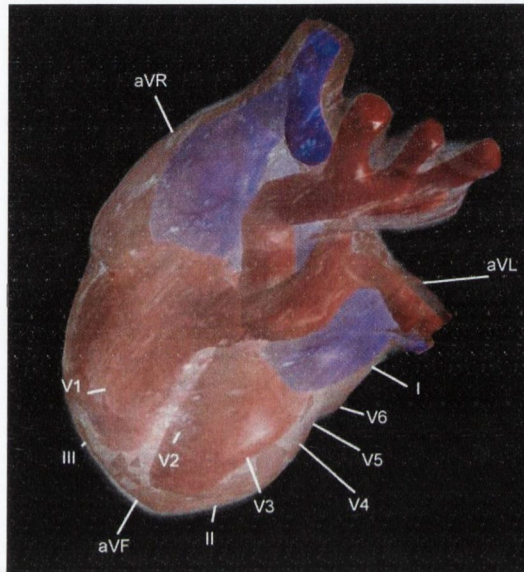


Figure 4.23: ECG lead axes in relation to the model.

The ECG axes (Figure 4.23) were introduced to the system and allowed for allocation of central lead voxels. These voxels were added to the volume and located at the intersection points of the volume and the ECG axes. These voxels are then used as central locators for each lead and, once an extent has been retrieved from each abnormally detected lead, the extents are illustrated around these voxels of each corresponding lead. There are several ways to represent the extent around the lead. The easiest way is to colour the cells with a certain radius around each particular central voxel. Another method would be to translate a surface map of electrical conduction onto the volume. Both of these methods are similar.

4.6.1.3 MI Extent

Figure 4.24 shows a typical measurement, where i refers to the level of ST segment deviation from the base-line or iso-electric line. The default iso-electric line is a voltage of 0.0 millivolts. There is an option, however, if there is shift from 0.0 mV, to manually set the iso-electric line. This feature enhances the portability of the software, because clinically acquired ECGs are not always perfect. Figure 4.25 demonstrates two different MI extents from the same lead (v2). The first screenshot has an extent of 181696 voxels, whereas the second screenshot has an extent of 101333 voxels.

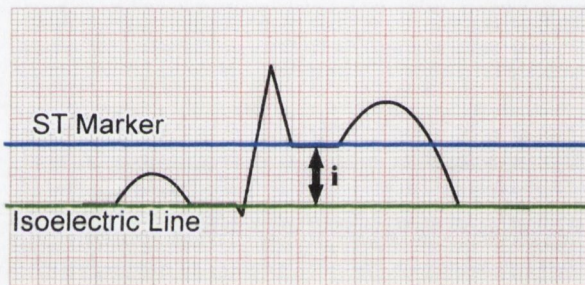


Figure 4.24: Measuring the ST segment.

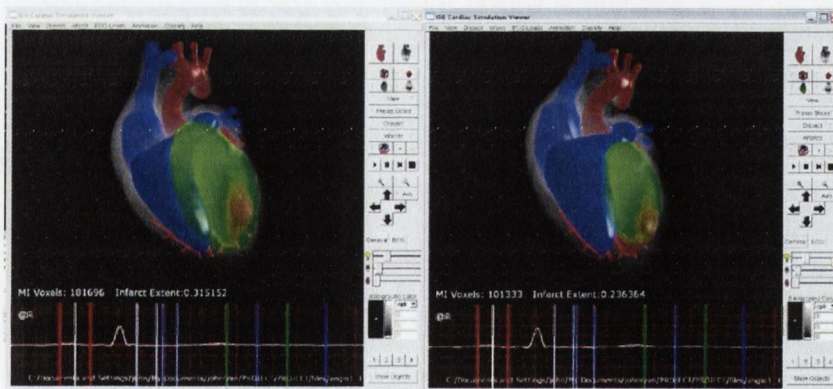


Figure 4.25: Two different extents.

The representation of the MI or stress region around a certain central lead

voxel involves the multiplication of i (*i.e.*, the level of ST segment deviation) with a set radius as defined by our cardiology collaborators as proportional to what they thought was an accurate representation of the ECG tracings. An extra MI sensitivity weighting can also be applied, which is alterable using a slider.

4.6.1.4 The MI Sensitivity Slider

The method of assigning the sizes of the infarct areas on the heart volume model is approximate so, to provide a method of varying the sizes, an extent weighting or sensitivity feature was incorporated. This allows the user to decrease an area of infarction that may be too big to make sense of. It was decided that the best GUI component for this was a slider. It is important for the user to understand that this tool should not be used to definitively monitor the progress of an MI from the graphical tool alone. This is why the ST accumulator is an important metric. The only way to assign an accurate weighting for the volumetric representation of MI would be to perform an in-depth evaluation of the actual physical MI extents with corresponding ECGs. This would not be possible within the scope of this project.

4.6.1.5 The Voxel-Count as a Metric

It was highly advisable to incorporate some kind of standard metric for MI into our system. Currently, cardiologists use chemical measurements from blood analysis to determine the extent and progress of infarction within the myocardium. Although ECG is used to firstly diagnose an infarct, chemical measurements are the standard for monitoring the progress. The purpose of a metric within our system would be to see if these chemical measurements correlate with the measurements within our system. A voxel-counter is currently used that counts the

number of infarcted voxels once the interpretation process is complete. This is of key importance when comparing this voxel-count with the blood chemical measurements. There are some problems with this method. An infarction is represented by an elongated section of tissue within a certain radius from a central lead voxel. This, of course, is an approximation with several assumptions and would require evaluation to prove whether or not this metric is in correlation with other standard metrics like CK and troponin levels in blood.

4.6.1.6 The ST Accumulator as a Metric

Unlike the voxel-count, the ST accumulator gives a value directly derived from the ECG data. This value is a cumulative value of ST segment deviation. This ST accumulator is based on voltage and is measured in millivolts (mVs) by referencing the actual ECG data and adding each abnormal lead's deviations from the iso-electric line. When the infarction regions within the volume overlap, the voxel-count is not affected because it is computed for every cell within the specified radius. However, the voxel-count increases exponentially as the radius increases. This is an obvious fault with using a voxel count as a metric. The total radii of all infarction regions are in direct correlation with the ST accumulator value.

4.6.1.7 The MI Report Dialogue Window

Once all the classifications and interpretations were performed, rather than just displaying the results as visuals on the model or MI voxel counters, it was decided that a more informative secondary report window should be developed. Figure 4.26 displays a screen-shot of such a window. The information displayed within this window is collated during the interpretation period. Within the "ECG-

Interpreter” class the ECG is firstly checked for changes. If there are any changes, a “Diagnosis” class is scrutinised. Firstly, all the ST changes are checked and any of the abnormal leads are added to the report. Then the same is done with T-wave inversions and flat T waves and finally an approximate interpretation is performed giving possible diagnoses such as “Possible Anterior Infarction”. These diagnoses are based on common MI recognition and localization criteria (Pha96).

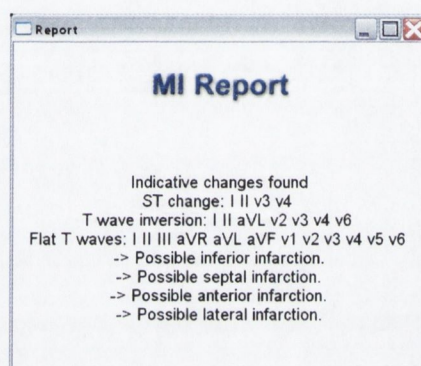


Figure 4.26: Screenshot of a sample MI report dialog window.

4.7 The Surface Representation Experiment

We experimented with a method of displaying the electric potential on the outer surface of the heart in real-time. A similar approach to the central voxel allocation was used to classify the outer texture of the heart mesh. We used the axes of the lead vectors in relation to the texture. A reference texture with obvious landmarks was used so that pixels could be assigned different leads. Then, during each frame of the ECG progression, the electrical values on the texture would be altered to directly correspond with the actual values as read from the ECG file. Figure 4.27 demonstrates the results of this process. A Gaussian spread

was used at each central pixel. There were several problems with this method of visualisation. Firstly, and most importantly, there was no obvious advantage to either a clinician, student or patient. Secondly, because of the texture-mapping, a lot of effort would be needed to correctly represent the separate areas of the heart. In the end it was decided to not continue down this route.

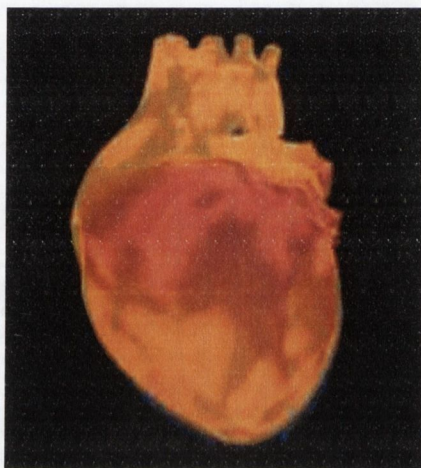


Figure 4.27: Direct surface representation of lead voltages.

4.8 Enhancing the VR Environment

4.8.1 Stereoscopic Viewing Conditions

In order to give the user a greater sense of immersion, we implemented a simple stereoscopic vision system. We chose not to use the dual screen goggles (Figure 4.28 B) because it was easier to implement with polarized 3D glasses (Figure 4.28 A). These glasses are very cost effective and do all the computations at driver level, so are very easy to implement. The glasses are synchronized with the CRT monitor to act as a shutter system. A different image is interleaved every second frame and shown to alternate eyes. The software had to be converted to a GLUT

(OpenGL windowing library) program instead of FLTK (graphical user interface library that caters for OpenGL rendering). FLTK did not support stereoscopic vision. Even though a full implementation would have been useful, we decided to concentrate more on the fundamental concepts of the project (*i.e.*, the MI visualisation). This is an area very suitable for further research.

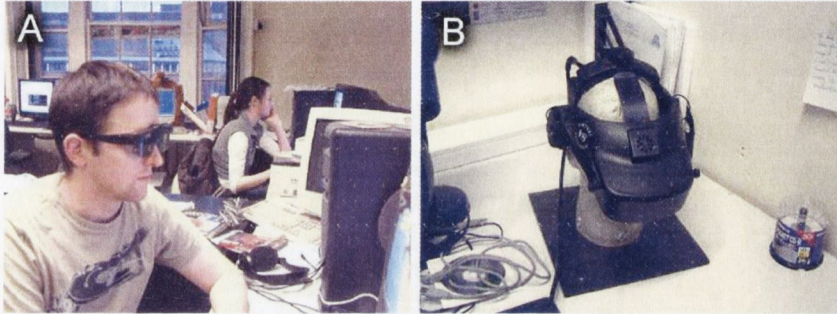


Figure 4.28: Stereoscopic apparatus.

Chapter 5

Clinical Trials and Evaluation Methodologies

The previous chapters described the initial considerations and motivations for developing a system to visualise myocardial infarctions, followed by the software development itself. This chapter discusses the process of evaluating the software in different phases. Firstly, the logistics of recording the ECGs, getting training for this task and gaining access to patients and their records will be described. The first phase of our software evaluation was the monitoring of the ECGs of patients with STEMI and NSTEMI in the coronary care unit (CCU) in St James' Hospital. The second phase of evaluation was the experimental technique for monitoring the ECGs of patients during percutaneous transluminal coronary angioplasties.

5.1 Evaluating Diagnostic and Teaching Tools

5.1.1 Case Studies

Although case studies do not have a well-understood theoretical basis compared to formal experiments and surveys, they can provide excellent and cost-effective evaluation (KPP95). In the field of medical software development, case studies are especially useful. Not only is it easy to see the potential applications of such tools, a comprehensive description of the process is also described. This kind of evaluation is commonplace in the medical research field. Case studies are more practical for certain applications that require more time and more information. For example, in this project, although a quantitative study of the ECGs monitored in synchrony with PTCAs would be useful, a few strong case studies would be more practical and produce sufficient results.

5.1.2 Quantitative Validation

When dealing with a well established condition where in-depth knowledge of each case is not needed when evaluating a certain tool, quantitative validation is ideal (TSYM99). This kind of validation technique is especially useful when performing a mass audit of how a certain tool is performing on a large scale and is normally more useful for a well established technology rather than an initial prototype (EMS⁺02). In the field of automatic ECG interpretation, the developed algorithms are often evaluated quantitatively (TRB03). This method gives strong sensitivity and specificity values since the bigger the population, the stronger the results.

5.1.3 Experimental Techniques

Sometimes it is particularly beneficial to evaluate a certain system experimentally. This involves an initial *educated guess* as to how it would perform under certain circumstances and then testing this theory. These kinds of validation techniques raise some important safety and ethical issues if a patient's safety or confidentiality is at risk, however small this risk (Jos01). Experimental research, however, does have its merits. Some of the most important drugs such as penicillin have been "stumbled upon" through this form of research. Nonetheless it is of paramount importance to have an excellent theoretical basis for each experiment performed and a justification for why the benefits outweigh any risks to the patient, no matter how small. For this type of research, an ethics committee is normally consulted before starting.

5.1.4 Qualitative Validation

Qualitative evaluation has several sub-categories and each has advantages and disadvantages for different scenarios. Structured interviews are similar to user-surveys because they incorporate specific questions and do not deviate from the main design. On the other hand, semi-structured interviews are particularly useful when feedback or open-discussion is required (EWC⁺99). These kinds of interviews are well suited for the evaluation of medical tools, because the questions would allow the doctors or clinical workers to give critical feedback with a view to future improvements. This also gives an approximate idea of how the tool would be accepted in the related field.

A user feedback survey or questionnaire is an effective way of gauging the application's acceptance, especially if it is anonymous. In cardiology, however,

and especially in countries like Ireland that have limited numbers of cardiologists and a very busy health service, these surveys are not too attractive. This is because the cardiologists or cardiology workers generally do not have the time or patience to fill out questionnaires.

5.1.5 Combined Evaluation

Rather than adhering to only one of the above techniques, a robust evaluation should include several techniques. This is especially applicable to our project where there are several layers of acceptance involved. Firstly, the basic detection algorithm would need to be evaluated quantitatively by having a large number of abnormal ECGs. To get more informative feedback as to how the interpreter would be working, a series of case studies would be very helpful. To measure how such a diagnostic and teaching tool would be accepted in the practitioner / student population, a series of structured or semi-structured interviews would need to be performed as well as a user feedback questionnaire.

5.2 Initial Considerations for ECG Retrieval

There are several repositories that hold freely available recordings of ECG and other biological signal data. One of the largest of these repositories is that of physionet (<http://physionet.org>), which includes an archive of several biological signal categories. Within the ECG category there are links to several external archives, mainly the MIT-BIH, ANSI and European ST-T databases. Along with the ECG signals, there are annotations and references relevant to each of the ECGs. One of the main disadvantages with these databases is that the ECGs are mainly only holter (long-term ECG) or single lead recordings. The problem with

this is that localizing and finding the extent of MIs depends on more than a few leads. Ideally, 12 synchronous leads should be used in the standard configuration. At the beginning of the project it was decided that, in order to attain the best selection of ECGs and also to have thorough accompanying case information, we should perform the ECGs ourselves. After a few meetings with our collaborators in St James' Hospital Dublin, it became apparent that this would be possible.

5.3 Recording the Electrocardiogram

Figure 5.1 shows the 12 lead ECG console that we used for the duration of this project (Cardioline Delta 3 Plus). It is connected via serial cable to a laptop, where the ECG is recorded using the manufacturer's software. This software allows us to export the ECG in the SCP file format. This ECG is encoded with the default Huffman table (See Appendix A). For the coronary care unit cases, the ward sister was telephoned every day and asked if there were new patients admitted that presented with MIs. If so, we travelled to the hospital and acquired the ECG using the standard 12 lead configuration. The patient was either in the supine or sitting position and ECG was recorded for ten seconds. In the angioplasty cases, we were resident in the catheter laboratory for one day per week during the angioplasty clinic and if the patient's angiogram revealed obstructions in the coronary arteries we applied the standard 12 lead ECG configuration. After 60 seconds of balloon inflation, we recorded 10 seconds of ECG. These two evaluation strategies will be discussed in more detail in the coming sections.

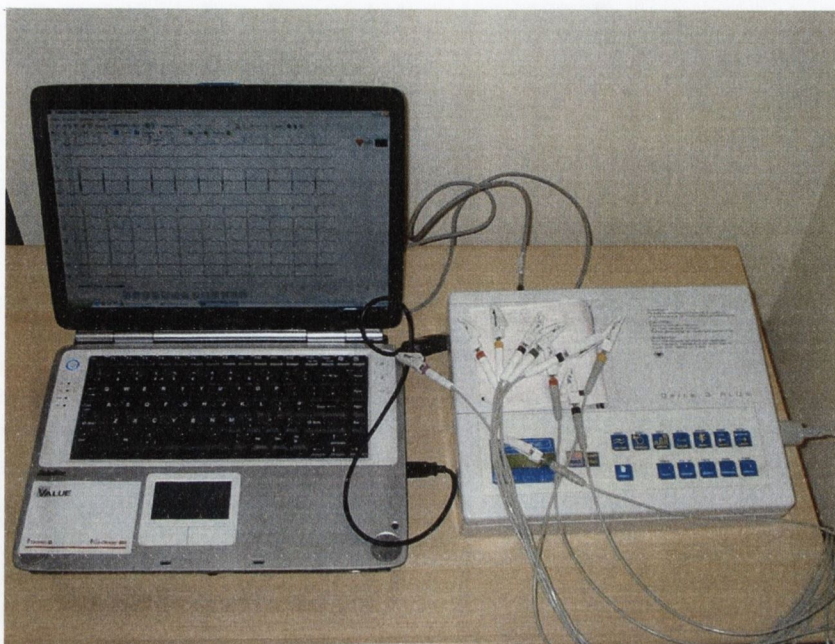


Figure 5.1: Our 12 lead ECG console connected via serial cable to a laptop.

5.4 Ethical Considerations and Proposals

In St James' hospital, it is standard procedure, if a research project will be using confidential information or accessing patients as external collaborators, that ethical permission is required. The ethics committee reviews research ethics proposals and grants them permission if they are confident that the research parties are competent in maintaining confidentiality and the patient's best interests are sustained. Storage and disposal of information, as well as the type of information itself, are important considerations. Throughout this project no information was recorded that was not needed or relevant to the MI software. All information was stored in one place and remained secure for the duration of the project. Once the project is finished all the information will be deleted. At the beginning of the evaluation stage, we applied for and were granted ethical clearance. Since it was not in the scope of the project to employ a cardiac technician for the

acquisition of ECG data, it was of key importance to be qualified and registered in a medical discipline. There were several reasons for this. Firstly, from an insurance perspective, a regular computer scientist would not be insured to access and monitor patients, even on a joint department of physiology / department of computer science project. There were also reasons on a patient-care and coping level. Because of the critical nature of most MI patients, it was important to have experience in dealing and coping with these kinds of patients.

5.5 The Training Period

It was necessary to gain skills in the area of ECG acquisition for the data collection section of the project. A training period of 3 days was spent in the cardiology department acquiring standard 12 lead ECGs and stress-test ECGs. Once this training period was completed it was possible to gain access to MI patients in the coronary care unit, the catheter laboratory (angiography suite) and the accident and emergency department. It was very important to learn the exact positions of the ECG leads so that all the ECGs taken during the project were verifiably correct. Common artefacts and problems were identified such as muscle noise, electrical interference and loose leads so that should this happen during acquisition these problems were rectifiable.

5.6 The Coronary Care Unit

The coronary care unit in St James' hospital is one of the largest in the country and provides access to a large selection of coronary diseases and abnormalities. Once ethical permission was attained it was possible to perform ECGs on suitable

patients.

5.6.1 Patient Selection

Since this was the first evaluation step and also overlapped with some of the development, there was an evolution of prerequisites for ECG monitoring. When this phase began it was decided to only monitor patients presenting with ST segment elevation MIs (STEMIs). However, as time went on, it became apparent that NSTEMIs (Non ST segment elevation MIs) were more common. At one stage, one of our cardiologist collaborators referred to this lack of STEMIs as a growing trend since a lot of the patients ST segments become closer to the iso-electric line once they receive thrombolytic treatment. After this, some of the more acute and extreme NSTEMI patients were considered for input to our database. T wave abnormalities then became of interest in the development of the software. After several months of monitoring we had acquired enough variations of different MI locations in CCU from adequate representation of this area of the patients process.

5.6.2 Recorded Information

The following is a list of parameters that were recorded on each CCU patient. This list was collated with some advice from a cardiologist collaborator. Not all the information was necessary, but it was important to record all relevant data. It was decided to record this information directly from the patient's notes at the same time as the acquisition of the ECG data. Not all fields were completed on all patients because of incomplete patient notes.

Patient Identification Information This was recorded for future reference,

should a revisiting of the notes/records or subsequent examinations such as angiograms and echo-cardiograms be needed.

Date of Birth and Age To calculate the mean age of MI and retrieve any information relevant to the age or D.O.B.

Sex Necessary to find the gender distribution of MI patients and evaluate any relationships between gender and any other parameters.

ECG File Identifier Important for the cross referencing of this data and the ECG data.

Diagnosis as Recorded on Notes Imperative for the comparison of the softwares findings compared to those of trained and expert cardiologists and clinicians.

History - General This is a general history including information about predisposing factors to MI *e.g.* family history and lifestyles such as high-stress jobs, obesity etc.

History of MI Re-stenosis or re-infarction is quite common and is relevant to this project.

History of CABG/PTCA Coronary artery bypass grafts (CABGs) and percutaneous transluminal coronary angioplasties (PTCAs) are directly related to MIs and therefore previous exams of this type were recorded.

Smoking Status Smoking has been proven to cause various coronary disorders. The smoking status was recorded for an approximate indication of how many MI patients in our study were in this category.

Blood Pressure The blood pressure levels throughout the patient's stay is relevant because high blood pressure is an indicator of a patient's susceptibility to MI (LRR⁺⁹⁴).

Diabetes Status Diabetes is well established as a predisposing factor for cardiac disorders (EWM02), and was therefore relevant to this project.

Time of Onset of MI Symptoms MI signs on the ECG progress through time. Therefore, it was important to understand the full time-line of each patient's conditions.

Time of Presentation at Accident and Emergency Department This is important because this is also the time that the patients treatment may have begun and also the acquisition of preliminary ECGs.

Time of ECG This is essential because it shows how long along the time-line of MI for this patient is.

White Blood Cell Count (WCC) WCC is a bio-chemical marker of myocardial Infarction and also for the prediction of recurrence of MI (LMK⁺⁸⁵).

Haemoglobin concentration (Hb) The haemoglobin concentration in blood correlates with coronary artery disease (TMN⁺⁹⁸).

Creatine Kinase (CK) CK is a bio-chemical marker of myocardial necrosis, although troponin I and T are preferred as they are more specific and reliable (GR03).

Troponin Troponin I and T bio-chemical markers are highly specific and sensitive for myocardial damage (MSRA00).

Did the patient go for echo-cardiogram? This was useful for a possible cross reference.

Did the patient have an angiogram? This was useful to see an outcome and verify a location

5.6.3 General Findings in the CCU

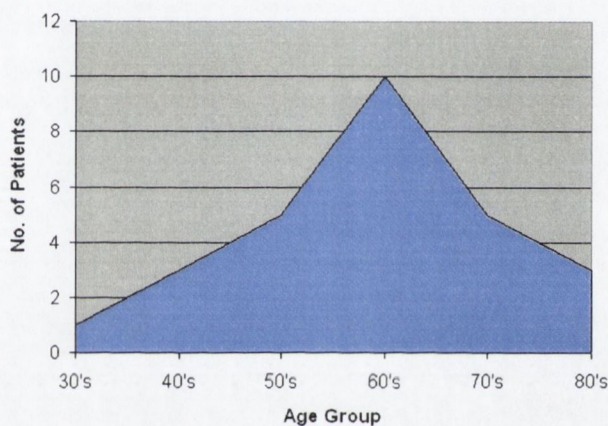


Figure 5.2: Age Distribution.

Out of the 27 patients monitored during this phase the mean age was 63. This compares favourably with previous studies (FBC+02), with similar mean ages. Out of the 27 patients, 74% were male. This distribution is comparable with previous studies (FWH+96).

Out of the initial 27 patients with MI, the smoking status was retrieved for 19 cases. Out of these, 42% of patients were smokers, 47% were non-smokers and 11% were ex-smokers. Figure 5.4 demonstrates this distribution.

Although it was aimed to retrieve the blood-pressure, diabetes and cholesterol values, this became more difficult in practice due to incomplete patient notes. Of the 19 blood-pressure measurements we acquired, 58%(11) had high

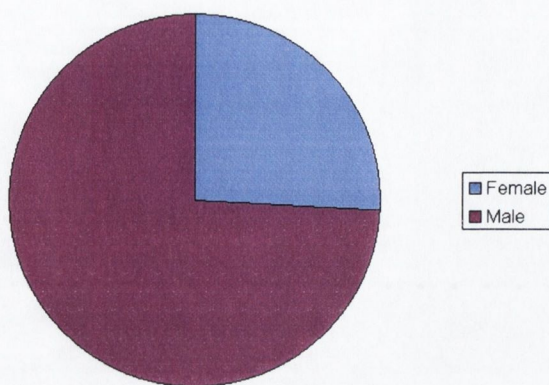


Figure 5.3: Gender Distribution.

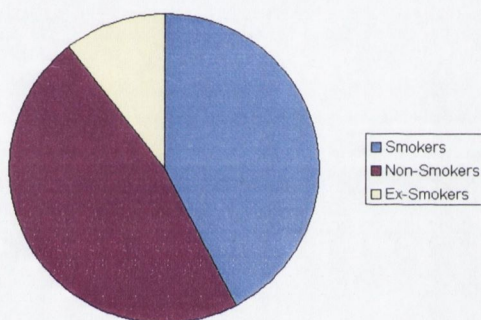


Figure 5.4: Smoking Status Distribution.

blood-pressure. Other pre-disposing factors were more ambiguous. Of the two patients we retrieved diabetes status on, one was diabetic and of the three patients we received cholesterol measurements on, all three had high cholesterol. Eight patients had a previous history of cardiac problems and seven patients had a family history of MI. One patient suffered from clinical depression.



Figure 5.5: Angiography Sequence of Coronary Arteries.

5.7 The Angioplasty Limb

5.7.1 Experiment Design

The original idea for this phase of evaluation was conceived at a meeting with our clinical collaborators. After the acquisition of the coronary care unit ECGs, extra evaluation techniques were being considered. An evaluation of the localising algorithm was needed and the best idea was that of recording an ECG at the same time as the balloon being inflated during a percutaneous transluminal coronary angioplasty (PTCA) procedure. On inflation, the coronary artery becomes blocked temporarily and causes a temporary ischemia which results in ST change. This is an ideal method for testing the localization feature of our software since there are recorded angiography videos that can be cross-referenced for the confirmation of location. It was decided to work with our cardiologist collaborator once a week in the catheter laboratory until enough ECGs were taken. The amount of PTCA procedures performed varied from none to four in one day.

5.7.2 Lead Placement and Displacement

During an angioplasty the angiography x-ray C-arm pivots around an iso-centre, in this case the heart, giving various different views of the heart and coronary arteries. It was important, in placing the leads, that none of them would run under the patient and overlay the x-ray image. It was also very important to inform the

patient not to move during the procedure, because during the first set of angioplasties several problems emerged. Firstly, if the patient moved, the leads might have moved into the path of the x-ray image and also the electrodes may have become loose or fallen off. Pre-planning was a crucial point for this phase because, once the sterile coverings were placed, it was important not to have to change the leads, just in case the sterile area was infiltrated and the patient's safety thereby jeopardised. The leads also could not obscure the movement of the angiography equipment, so they had to be tucked close to the patient, but not close enough to occlude the relevant anatomical structures on the angiograph. Generally, the leads all led to the left of the angiography table since the cardiologists and other staff were working from the right side. The standard configuration of the 12 lead ECG was sometimes altered because the chest leads obscured the cardiologists view on the angiograph. Although our cardiologist collaborator often made some of the views more oblique to allow for the leads, this was sometimes not enough. In some of the cases the chest leads were lowered to the next intercostal space. Although this is not ideal for localisation, it was considered sufficient for this project and this displacement did not impact on the results (*i.e.*, the regions on the heart model were approximately the same as non-displaced chest ECGs).

5.7.3 Acquisition of ECGs and Video Fluoroscopy Footage

Preliminary ECGs were taken at the start of every procedure. These ECGs provided a base-line from which to compare the ST change, if any. Also, the finishing ECG may have some resulting ST segment deviation due to the earlier blockage. Once the balloon was inflated we waited for between 40 and 60 seconds to allow a reasonable amount of ischaemia to occur, thus producing ST segment deviation. Then an ECG was recorded for 10 seconds. If the procedure involved

multiple angioplasties for more than one vessel, an ECG was taken each time during inflation. After the procedure, once the cardiologist had completed all necessary tasks, a final ECG was taken for each patient. This was to see if there was still some ST segment deviation or if it had decreased.

Video fluoroscopic sequences were recorded during every angioplasty procedure. These video sequences are very helpful in confirming the location of the balloon catheter on inflation. It was possible to get copies of these recordings for some of the patients that had angioplasties on recordable CDs. The file format for these recordings were in DICOM file format. This format has become the standard throughout the medical equipment world. Therefore, it was not difficult to find freely available software for the viewing of such recordings. We used a free-ware application called "ezDicom" for the reviewing of these files. This software allows the output of stills from the recorded angiography footage.

Chapter 6

Results

In the previous chapter, we described our evaluation strategy and the related logistics. In this chapter, we will show the results of these evaluations and discuss the findings in detail. Firstly, we will illustrate the findings of the CCU phase of our evaluations. Then, the angioplasty validation results will be discussed and finally, other results including graphical issues, clinical feedback and T wave abnormalities will be discussed.

6.1 The CCU Findings

6.1.1 Refining the Patient List

A noticeable trend in this phase of the project was that, by the time the patient got to the CCU ward, either their ST segments became less elevated or their waveforms changed into NSTEMIs. Although these are still of interest in this project, the patient list was filtered to just STEMIs for the validation of the software. Of these 17 filtered patients, the software produced representations that were compatible with the cardiologist's diagnoses.

6.2 CCU - Case Studies

Of the 17 STEMI patients, we will present the case studies and results of patients with six representative locations of MI. We have presented the results in a clinical format by presenting a clinical history and ECG demonstrating a myocardial infarct in specific anatomical locations in the 6 patient histories described in the next six sub-sections.

All six patient's ECGs were interpreted correctly by our software and represented within the model's volume as green areas. Patient 1's ECG showed ST segment elevations on leads I and aVL. Clinically this is seen as a lateral MI (*i.e.*, an area of infarction on the lateral wall or left side of the heart). Therefore, our model's representation is correct (Figure 6.1). Patient 2's ECG had ST segment elevations on leads v2 and v3, which is seen clinically as an antero-septal infarction (*i.e.*, an area of infarction within the septal wall or the anterior myocardium). The model's representation is an accurate portrayal of this phenomenon (Figure 6.2). Patient 3's ECG demonstrated ST segment elevation on leads I, II, v4, v5 and v6. This infarction is more extensive than the previous two. All the leads are in agreement of the area and there are no conflicts. Clinically this is seen as an antero-lateral infarction and our software's representation of this data is anatomically correct (Figure 6.3). Patient 4's ECG diagnoses clinically as an infero-lateral MI (*i.e.*, on the bottom and left side of the heart) with ST segment elevations on leads I, II, aVF and v6. Again, our software interpretation is correct (Figure 6.4). Patient 5's ECG demonstrates a *true* inferior MI (*i.e.*, purely on the bottom of the heart). The software represents these ST elevations on leads III and aVF correctly (Figure 6.5). Interestingly our software has picked up on patient 6's left bundle branch block (LBBB) correctly (Figure 6.6).

6.2.1 Patient 1: Lateral MI

48 year old male presented with chest pain which started 12 hours previously while driving. He was a recently diagnosed type II diabetic and was a current smoker with *hypertension* and *hyperlipidaemia*. Presenting ECG revealed *sinus rhythm* with 1mm ST segment elevation in the lateral leads. He was treated with aspirin, clopidogrel, betablocker, statin and low molecular weight heparin. The peak troponin T = 0.71 mg/L. Diagnostic angiography demonstrated a critical stenosis in a high obtuse marginal branch of the left circumflex. He was treated directly with angioplasty and stenting with a *drug eluting stent*. His post procedure course was uncomplicated. Figure 6.1 demonstrates the results of this case study.

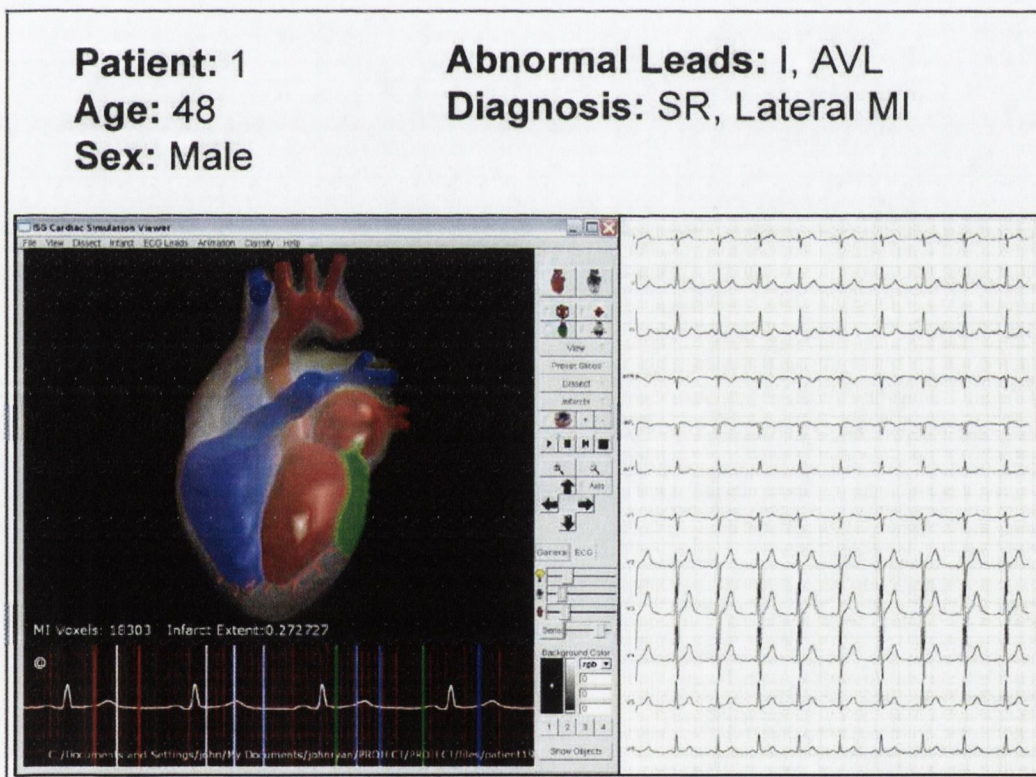


Figure 6.1: Patient 1 - Lateral MI (Green represents area of infarcted tissue). Clinically, lateral refers to the left side of the heart, thus our software's interpretation is correct.

6.2.2 Patient 2: Antero-Septal MI

81 year old male presented with a 2 day history of intermittent episodes of severe central chest discomfort. He had documented coronary artery disease on an angiogram performed 6 weeks earlier and was awaiting elective *percutaneous coronary intervention (PCI)* to the left anterior descending (LAD) coronary artery. The ECG was taken 12 hours after presentation. Peak troponin was 0.38 mg/L. He was stabilised on medical therapy and then underwent PCI to the LAD the day after admission. Figure 6.2 demonstrates the results of this case study.

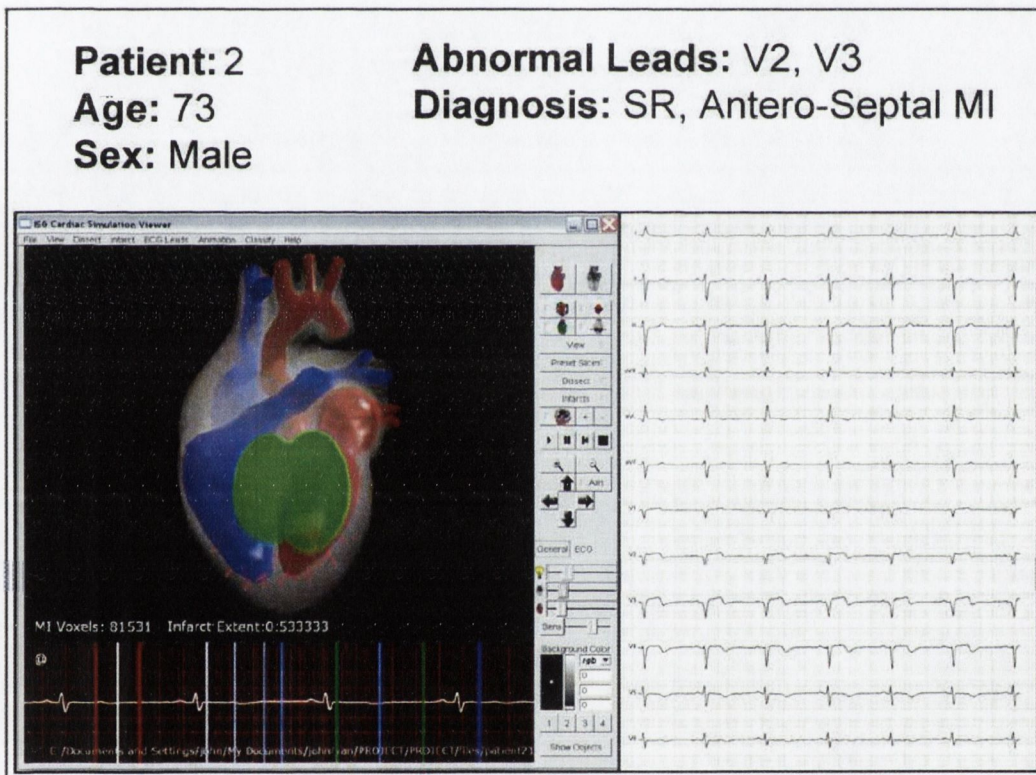


Figure 6.2: Patient 2 - Antero-Septal MI. A stress area in the anterior region of the septal wall. Our software's interpretation is anatomically correct.

6.2.3 Patient 3: Antero-Lateral MI

65 year old female presented with a 2 day history of *epigastric* pain. The ECG demonstrated *sinus tachycardia* with ST elevation in leads V2 - V5 and Q waves in the same leads. The peak CK was 4460 IU/L and peak troponin was 5.21 mg/L. The patient developed symptomatic left ventricular failure which responded to medical therapy with *diuretics*, *betablockers* and *ACE inhibitors*. Figure 6.3 demonstrates the results of this case study.

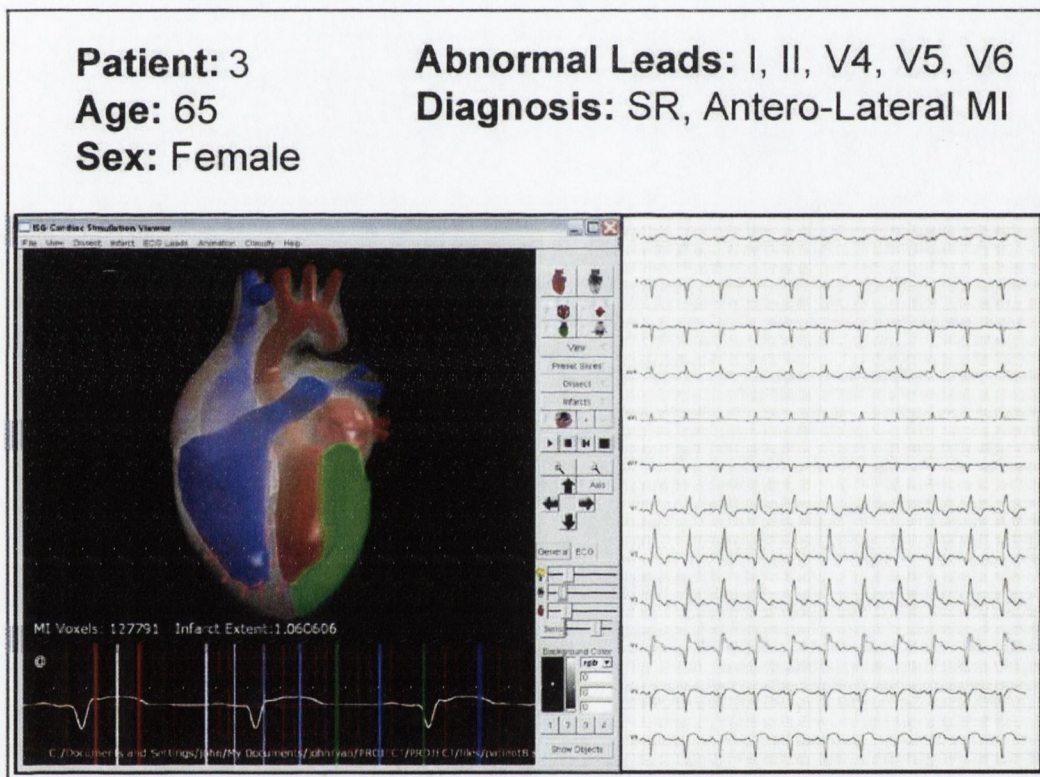


Figure 6.3: Patient 3 - Antero-Lateral MI. Again, our software's interpretation is correct.

6.2.4 Patient 4: Infero-Lateral MI

58 year old male presented to a district hospital with an acute inferolateral MI. He received *thrombolysis* within 3 hours of the onset of symptoms but failed to reperfuse. He was transferred to our hospital for rescue angioplasty. He had a VF (*ventricular fibrillation*) arrest during the diagnostic angiogram and following successful resuscitation he underwent PCI to the dominant left circumflex/obtuse marginal bifurcation (arteries). The ECG was recorded 16 hours after successful PCI. Peak CK was 3769 IU/l and peak troponin was 6.05mg/L. He made an excellent recovery after the coronary intervention. Figure 6.4 demonstrates the results of this case study.

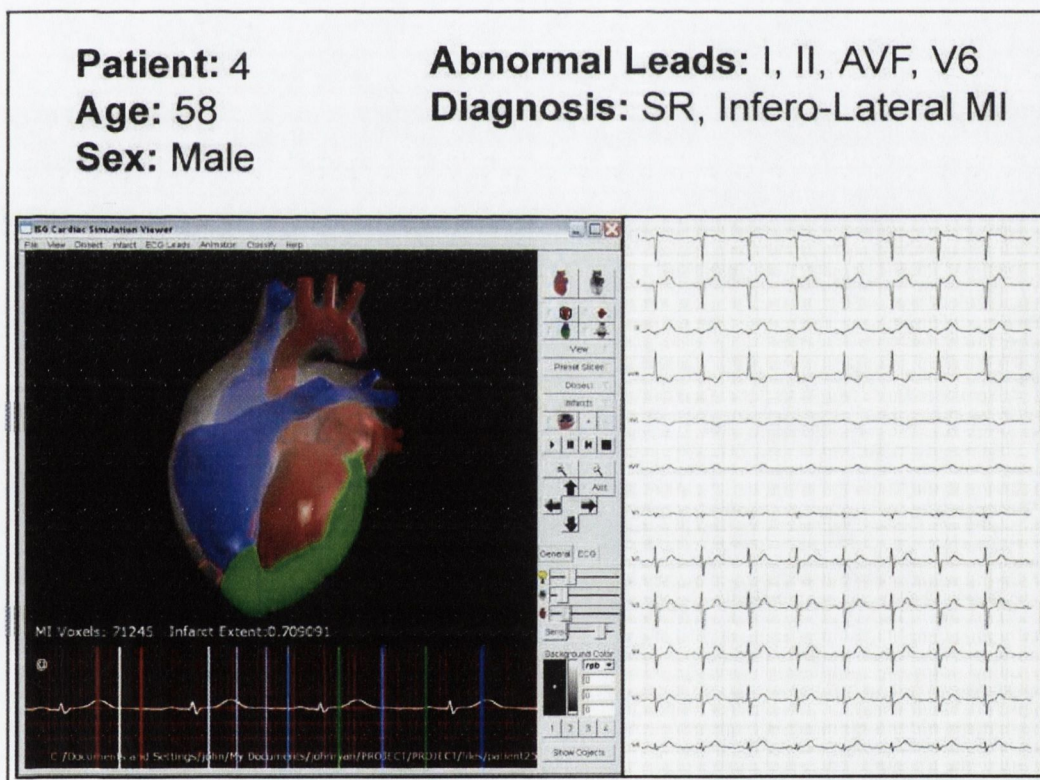


Figure 6.4: Patient 4 - Infero-Lateral MI. Green region on inferior and lateral aspects of the heart model. This verifies the softwares interpretation.

6.2.5 Patient 5: Inferior MI

56 year old female presented with an inferior STEMI of three hour's duration. She was randomised in the CLARITY (TIMI 28) trial and was treated with intravenous rapilylin (a new drug). The ECG was recorded 16 hours after presentation. Peak troponin was 1.08mg/L. This patient's hospital course was complicated by a urinary tract infection which required intravenous antibiotic treatment. She was discharged home on day 8. Figure 6.5 demonstrates the results of this case study.

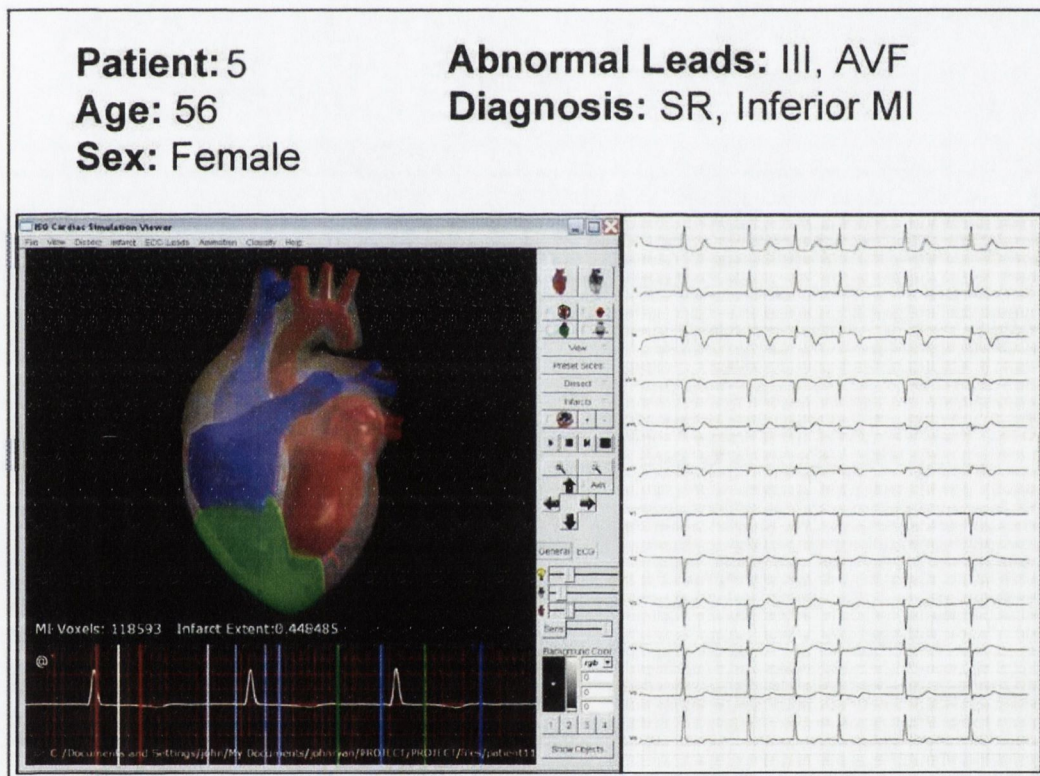


Figure 6.5: Patient 5 - Inferior MI. Green region on the inferior aspect of the heart. Our software's interpretation is correct.

6.2.6 Patient 6: LBBB

70 year old male who had an acute coronary syndrome after a *femoral endarterectomy*. He had a past history of ischaemic heart disease and had a previous MI in 1988 and underwent *CABG* at that time. The ECG was recorded 24 hours post operatively and the peak troponin was 0.53mg/L. The clinical course was complicated by the development of cardiac failure which required intravenous therapy. He eventually settled and was discharged on medical therapy. Figure 6.6 demonstrates the results of this case study.

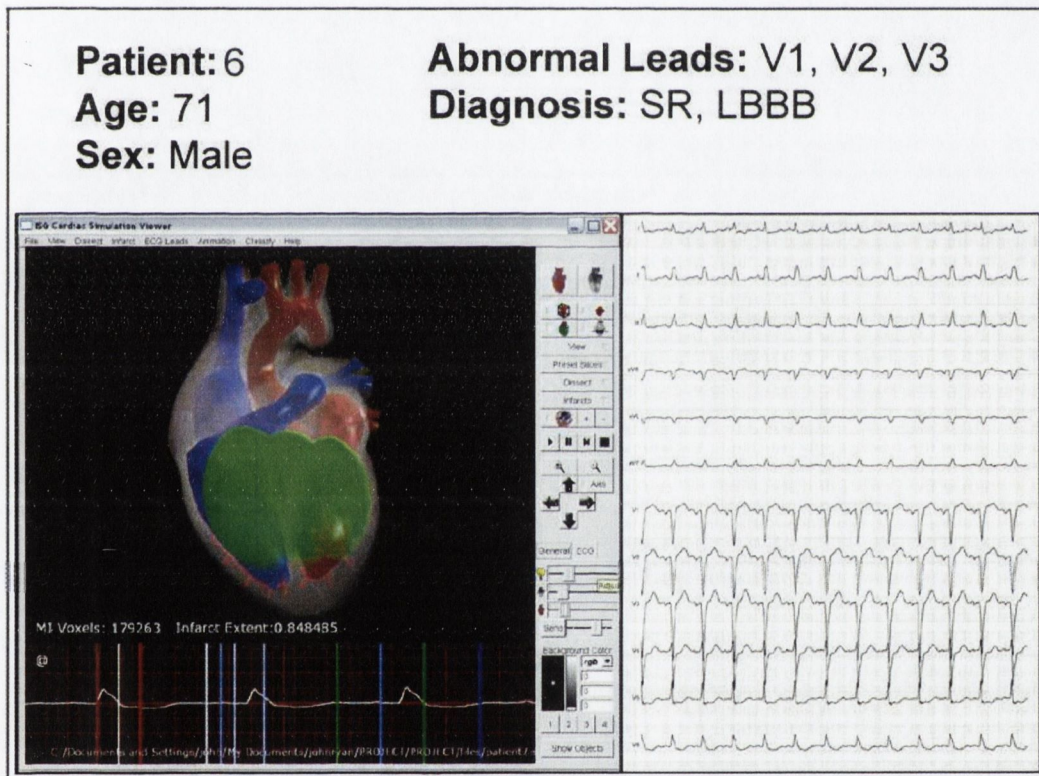


Figure 6.6: Patient 6 - with left bundle-branch block. The software picks up on the region of stress.

6.2.7 The Metrics - A Comparison

Figure 6.7 shows a graph that compares the above six patients' MI extent measurements. The values of all six measurements are percentages of the total and the ST accumulator (pink) is chosen as the ascending value to compare the voxel count (navy) against. The ST accumulator was chosen as the stronger metric because it correlates directly with the actual electrical values of the ECG data. This comparison was basically a test to see how the voxel count metric correlates with the ST accumulator. From the graph, we can see that the voxel count metric is unpredictable. Before doing this test the spherical nature of the infarct areas meant that there would be a problem of the count increasing exponentially. However, after testing, it appears that the problem is more complex. These offsets are probably due to the placement of the central lead voxels, *i.e.*, infarct areas might run out of the myocardial areas into some sections more than others. Another reason for these offsets could be that, even though some of the infarct regions overlap, the voxels are counted for both full regions. Further research would be needed in this area to develop a more solid metric.

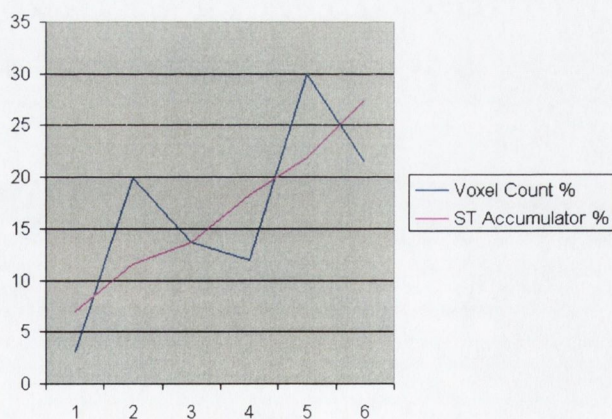


Figure 6.7: Comparison of metrics, with the ST accumulator ascending.

6.3 Validating the System in the Catheter Laboratory

Over a period of three months we monitored patients in the catheter laboratory in St James' Hospital Dublin. Patients undergoing angioplasties were selected and asked to participate in our study. The main aim of this phase of evaluation was to validate the locations of MI that our system detects. As discussed in the previous chapters, during an angioplasty procedure a balloon catheter is inserted into the vessel that is occluded. This balloon is then inflated and causes a temporary elevation of the ST segment on the ECG leads concerned. By recording a 12 lead ECG while a patient is undergoing an angioplasty, we can prove whether or not the location demonstrated within our system is correct. We found that, if the patient demonstrated an elevation in the ST segment due to balloon inflation, our software accurately represented the location involved. In each case, a ten second ECG was taken after 60 seconds of balloon inflation.

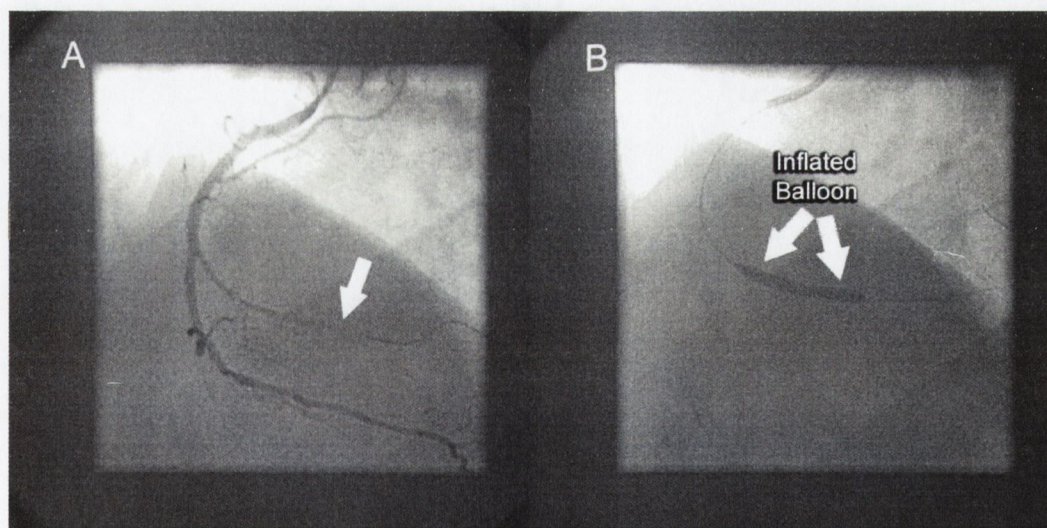


Figure 6.8: Initial Angiograms

6.3.1 Patients with Minor ST Elevation

Some of the patients experienced more ST change on balloon inflation than others. This patient demonstrated very little ST change and has a more localised stress-area than other patients. A coronary angioplasty was performed on the right marginal branch of this patient's right coronary artery. Figure 6.8 A shows an angiogram capture with an arrow pointing at the offending artery. Figure 6.8 B shows an angiogram capture without contrast agent demonstrating the guide-wire and inflated balloon in the same artery.

Figure 6.9 A shows an angiogram with an arrow pointing at the stent that was placed after the balloon was inflated and Figure 6.9 B shows an angiogram with contrast agent post inflation and stenting. Note the difference in vessel diameter between Figures 6.8 B and 6.9B.

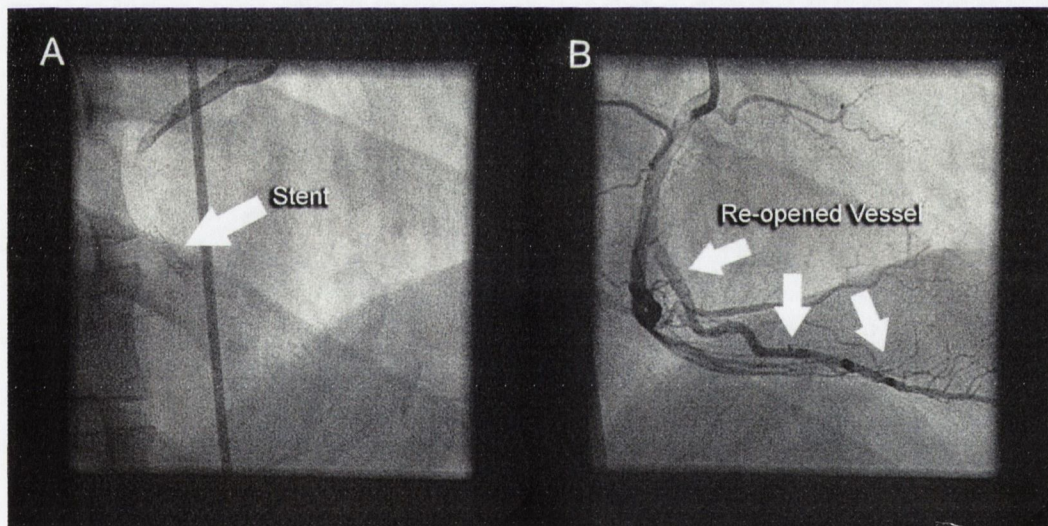


Figure 6.9: Angiograms After vessels were re-opened

Figure 6.10 shows a screenshot of our system's results and also the corresponding ECG. Although, the MI or stress area is quite small, this is an accurate representation of the area that is normally supplied by the marginal branch of

the right coronary artery.

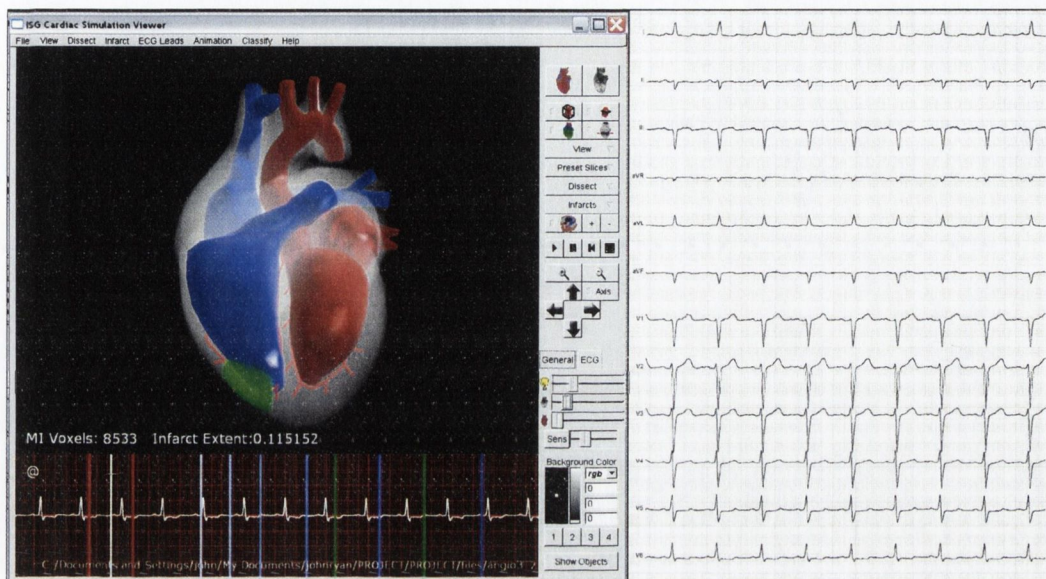


Figure 6.10: The software's interpretation and corresponding ECG

Patient 8 also showed minor ST changes. In Figure 6.11, there is a small region of stress at the lateral side of the heart. This is due to a small ST segment elevation on v6.

6.3.2 Patients with More Extensive ST Elevation

After a preliminary ECG with no ST segment elevation, patient 1's ECG showed the predicted abnormalities in leads II, III and aVF. On Figure 6.12 the ST segments on both the II and III leads are raised in the post-inflation ECGs. These elevations are then reflected in the software's interpretation (Figure 6.13). Figure 6.14 demonstrates the results from patient 7's ECGs.

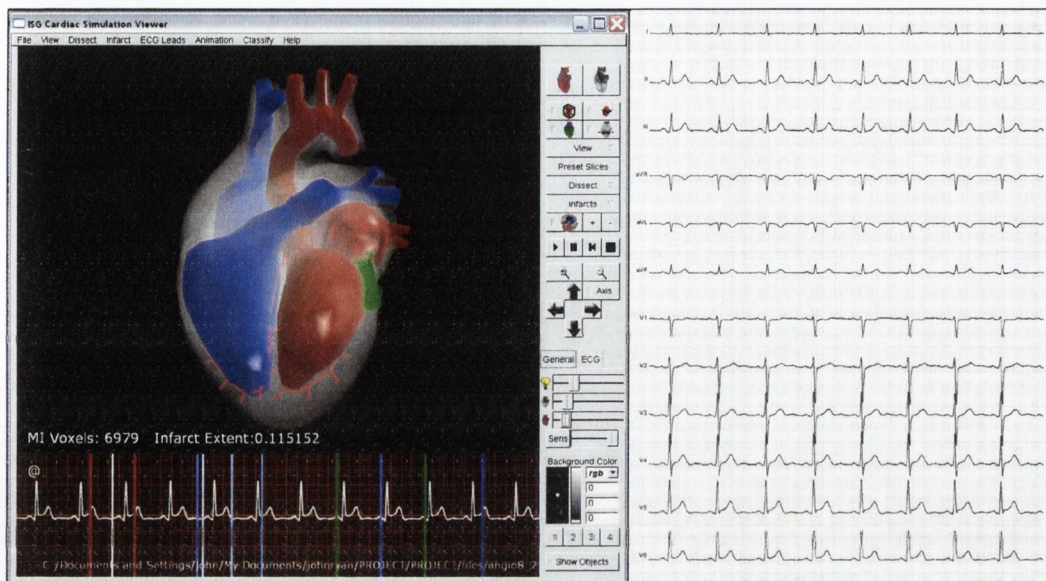


Figure 6.11: Patient 8's interpretation and ECG

6.3.3 The Standard Progression

The standard progression of the patients ECGs during these procedures was to be normal or slightly elevated before the procedure, then, on balloon inflation the ST segment would be elevated temporarily. After the procedure, the ECG would typically return to normal again. Patient 6 was a good example of this progression. The ECG acquired prior to the exam (Figure 6.15 A) demonstrated no ST elevation. Then, on inflation, the ECG demonstrated ST changes on the anterior and inferior aspects of the myocardium (Figure 6.15 B). Finally, on deflation of the balloon, the ECG corrects itself and becomes normal again (Figure 6.15 C).

6.3.4 Patients with Initial ECG Abnormalities

Because PTCA is a treatment for abnormal blood-flow in the coronary arteries, it is quite common to see abnormal ECGs at the beginning of the procedure.

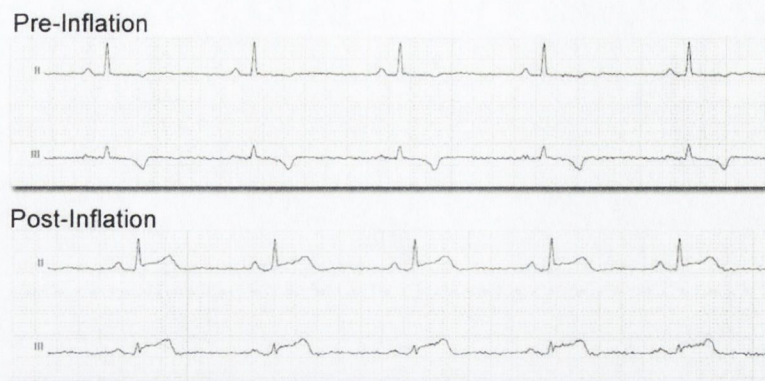


Figure 6.12: Comparison of ECGs, leads II and III.

Patient 9 appears to have the most abnormalities and had undergone a multi-vessel angioplasty. In the first three angiograms of patient 9's procedure, the crocodile-clips of the ECG leads are visible. For some of the patients, these leads had to be moved lower on the patients chest if the cardiologist could not see the arteries of interest. In this case, the abnormal arteries were visible just over the leads. The occluded artery appears as an indentation from the bottom (Figure 6.16). The inflated balloon is then visible in Figure 6.17. In Figure 6.18 the same vessel (left anterior descending coronary artery) is re-opened without an occlusion.

Figure 6.19 demonstrates the progression of patient 9's ECGs throughout the procedure. Figure 6.19 A corresponds with the ECG taken when the balloon was inflated in the mid left anterior descending artery and Figure 6.19 B corresponds to the ECG taken when the stent was being placed with the balloon still inflated in the same vessel. Figure 6.19 C's ECG was taken during the balloon inflation in the second artery (the left main, trifurcation marginal). Figure 6.19 D corresponds with the final ECG. This progression shows a gradual improvement while the patient is undergoing the procedure.

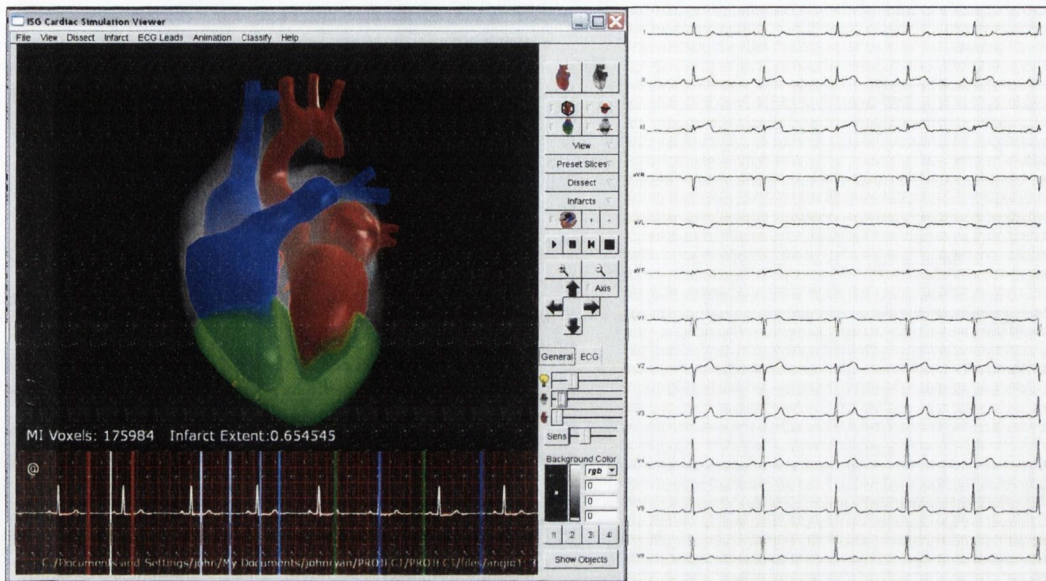


Figure 6.13: Patient 1: Inferior stress-area.

6.3.5 Summary of the Angioplasty Phase Findings

Overall, the software was accurate in representing all of the induced abnormalities seen in this section of the evaluation. One of the limitations of this phase was that some types of infarctions were not explored. A typical example is that of posterior infarction. However, it is very rare for an angioplasty to be performed for posterior coronary arteries. For this reason, it was outside the time-line of this project to wait until we covered all possible infarctions. We chose to finish acquiring ECGs after the eighth week of angioplasties. Some of the days yielded no cases. A total of nine cases were considered to be adequate for the needs of this project. This is based on the criteria that we had covered all the common vessels that are treated in angioplasties.

Patients 3 and 8 demonstrated minor ST segment changes during the balloon inflation process. Our software accurately represented these minor stress areas as smaller regions and the locations were anatomically correct (Figures 6.10

6.3 Validating the System in the Catheter Laboratory



Figure 6.14: Patient 7: Inferior and anterior stress-areas.

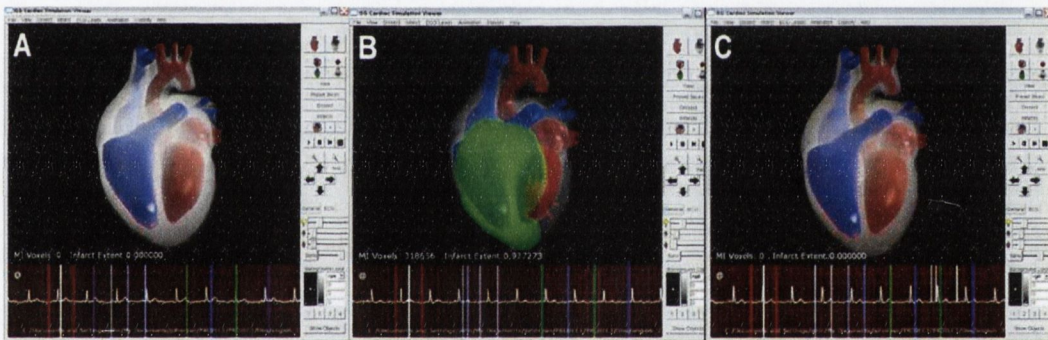


Figure 6.15: Standard Progression of Angioplasty ECGs.

and 6.11). Patient 1's ECG demonstrated more ST change than these previous examples. The raised leads of II, III and aVF are normally indicative of inferior MI because these regions are supplied by the same vessel that was blocked temporarily by the balloon catheter. This is a good example of the software's capability to accurately diagnose the extent and location of MI (Figure 6.13). Patient 7's ECG had raised leads on II, III, aVF and v1. This is indicative of stress in both the anterior and inferior regions. Our software demonstrates these

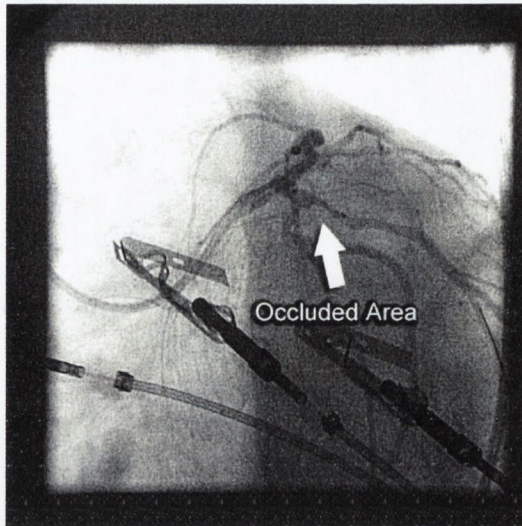


Figure 6.16: Angiogram demonstrating initial views of the occluded artery.

phenomena accurately (Figure 6.14). Patient 6's three ECGs show the standard progression from no ST segment elevation (Figure ??) to an elevated ST segment (Figure ??), and finally, back to no ST segment elevation (Figure ??). Patient 9 was a complex case and needed multiple angioplasties. Nonetheless, our software accurately showed the progression from abnormal ECGs to more normal ECGs (Figure 6.19). The recorded angiograms were helpful in verifying that the locations were correct. There is ample scope for future work in this area and our angioplasty evaluation strategy has been shown to be successful.

6.4 Clinical Feedback

Throughout the duration of this project we have collaborated closely with several medical experts and cardiologists. Both of the previous evaluation phases were closely monitored by our main cardiologist collaborators and advice was given throughout. This is one of the reasons why an in-depth feedback survey was not performed. Another reason for this was that, by the time we had finished all

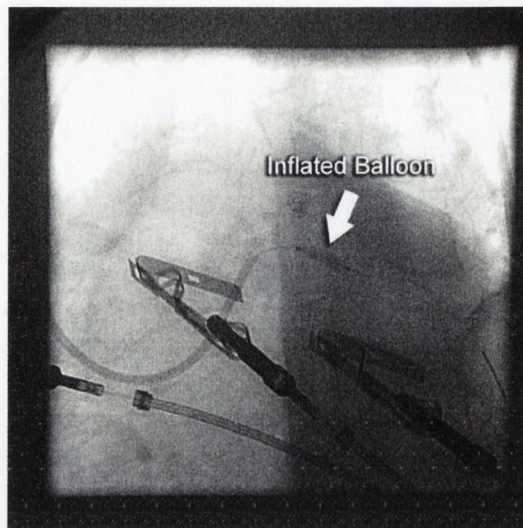


Figure 6.17: Angiogram demonstrating the same artery with inflated balloon.

the clinical trials and evaluations, it was considered that these results provided sufficient proof that our software worked. It is important to consider that, when seeking feedback from medical professionals such as cardiologists, they may not have the time to give detailed feedback. This is especially true in Ireland, where there is already an under-staffed and over-worked health-service.

Our project was presented and demonstrated at a forum that is held every few months within St James' hospital. Among the attendees were cardiologists, accident and emergency consultants, registrars, nurses and other staff. This was a good opportunity to get feedback. Our system was recognised as having several merits. Firstly, as a diagnostic and monitoring tool, our tool helps to solidify the quantitative diagnosis of MI extent and location by providing a visualisation of both factors. One feature that was seen as particularly useful was that of the ST accumulator metric. This was seen to give a good indication of MI extent. Another recognised merit of this system was that of an educational tool. It is often difficult to grasp the concept of three-dimensionality for 2D ECG tracings.

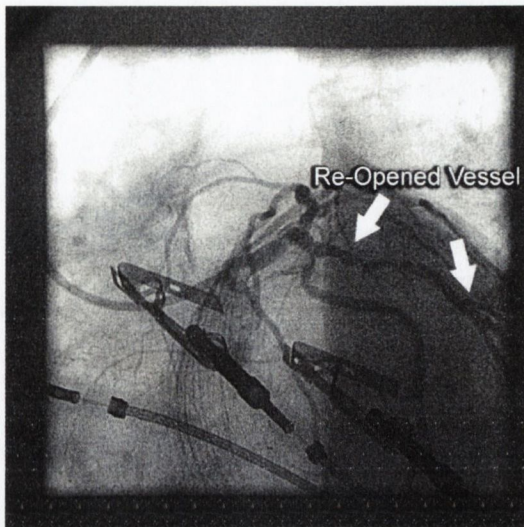


Figure 6.18: Angiogram post-reperfusion.

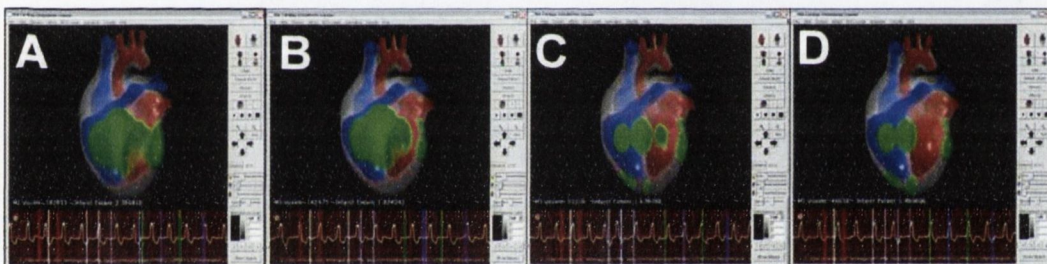


Figure 6.19: Progression for Patient 9.

This software was recognised as giving the user both the standard ECG tracings and the corresponding visualisations of this data. Another merit was that of a patient information tool. A patient could see his/her abnormality on a heart rather than cryptic ECG tracings. Although not tested within this project, a patient evaluation would be useful to gauge the level of usefulness in this area.

6.4.1 An Interview with a Consultant Cardiologist

Our main clinical collaborator, Dr Niall Mulvihill, is a Consultant Cardiologist and lecturer in Physiology and Cardiology at St James's Hospital and Trinity

College Dublin. We interviewed him about his thoughts on our project. The following is the transcript of the audio recording of the interview:

Question 1. In the fields of diagnosis and monitoring, what do you think are the merits of our application?

“In terms of diagnosing ST segment infarction, it aids the 12 lead ECG and the clinical assessment in the correct diagnosis of this condition. And it also aids in diagnosing the location and extent of the myocardial infarct. Having aided in the diagnosis, it can also help in the dynamic management of the patient, by allowing you to assess the response to reperfusion strategies such as thrombolysis or infarct angioplasty.”

Question 2. In the field of medical education, how do you feel our application would contribute?

“This is one of its greatest potential benefits because, teaching medical students, nursing colleagues and doctors to interpret ECGs is very difficult and complicated, and having an application that would generate a 3D image from a 12 lead ECG has huge educational implications because it allows an ECG to be interpreted in the setting of a 3D image, which allows the assimilation of knowledge much easier for trainees.”

Question 3. How appropriately do you feel the model represents the heart (Colours, aesthetics, accuracy)?

“I think it represents theoretically what would be known as a normal sized heart, a non-diseased heart. It is also important to differentiate between the right-sided cardiac structures from the left-sided cardiac structures. And then representing the infarct in green to separate it from the right and left

sided structures is very important. So in practical terms I think it's a good model and the fact that it can be utilised by the user and rotated around to show the three-dimensional structures is very useful."

Question 4. The single ECG window was designed for working on one lead at a time. Is this a factor?

"It is a factor, because it is more time-consuming to interpret each lead separately. But ultimately, in the same way as software has been developed to automatically interpret 12 lead ECGs, I'm sure there are applications that can be developed to automatically interpret the ST segments within this model. As a teaching tool though, it is useful for people to be able to use the software themselves, and, if they want to override the machines interpretation to be able to identify the deviations from the iso-electric lines themselves."

Question 5. You have previously seen our animations of the electrical propagation of the heart. How do you feel these animations perform?

"Whether it is useful in the setting of assessing myocardial infarctions, I'm not sure. But in terms of educating people about electrical propagation in the myocardium, it's very useful. There are already some of these programs available, but they are specifically designed with therapeutics in mind and we use them in cardiac cath labs in performing electro-physiology procedures, but they are not widely available as a teaching tool because they are part of fixed systems within a cath lab."

Question 6. One of the features of the animation system is that a slice

of the volume can be viewed as the electrical cycle progresses.

What do you think about this?

“That has fantastic potential educational applications because again, like 12 lead ECG, educating people about cardiac electrics can be difficult and, to aid the education with images would be very useful.”

Question 7. Do you feel that the CCU evaluations were successful?

“I think, as a first attempt at a clinical evaluation, it has been highly successful in that we’ve been able to use the software to correctly demonstrate anatomical locations of myocardial infarcts. We’ve also come up with a rather vague assessment of infarct size. When I say vague, I mean it’s vague because, we haven’t specified in advance, the timing of the ECG in relative terms to the clinical presentation. So I would see that the future projects that we can undertake, with this software, will be to assess its ability to determine a myocardial infarct size, location and response to treatment at each stage after acute clinical presentation. But, for a first assessment of the software, I think it has been very successful in the CCU evaluation.”

Question 8. Do you feel that the angioplasty evaluations were successful?

“This part of the project was very clever because it allows us to assess the software’s sensitivity at detecting very early ST segment deviations which occur when we inflate a balloon inside a coronary artery. The fact that we’ve been able to successfully identify a very rapid onset of ST segment deviation with this software, indicates that it is very useful at detecting early onset of acute coronary occlusion. Also, we demonstrated that we can rapidly resolve the ST segment resolution and this is, again, demonstrated within

the system. So, it certainly supports the case that we can use this software over a temporal phase of the assessment and management of patients with ST segment elevation in the CCU for future studies.”

Question 9. We used a human-guided algorithm for the estimation of MI extents. Do you feel more or less confident that you, as a user, are detecting the ST segment rather than a computer algorithm?

“I think, the fact that one can identify each of the components of the entire ECG waveform for each lead and then be able to define the iso-electric line and mark out yourself where the deviations are, takes out any potential flaws in the software. But, with software developments, there are no doubts that we can design programs to do this. We still have the human model that allows the individual operator to override the computer-based approach in the detection.”

Question 10. What do you think of the layout (i.e., the graphical window on top, the ECG below and the controls to the side), of the software application?

“Yes. It works very well. It’s a very user-friendly window. The images are very clear. The ECG controls are easy to use.”

Question 11. Do you think that the software is easy to use?

“Yes. In terms of estimating cardiac size, it’s a hell of a lot easier to derive a model like this from a 12 lead ECG than it is to do a trans-thoracic echo, which is going to take 20 minutes of a technician’s time plus the movement of a big machine around the hospital. So, this has huge potential implications for CCU applications.”

Question 12. Within the immediate future, what improvements do you think the software would benefit from?

“I’m not sure there are any improvements to be made initially. I think, what we need to do is define more extensively what the clinical benefits of the software are and have a fixed system within our coronary care unit, so that we can train the nurses to use the system and to collect the data. Therefore, we could utilise these patients by having serial ECGs of each patient and have it very well defined with the time of the ECG recording, the onset of symptoms, the initiation of treatment and the response to treatment.”

Question 13. Do you believe that there are commercial possibilities with this project?

“Undoubtedly!”

6.5 Other Results

As well as the aforementioned evaluations of our software, there were several other outcomes of the project.

6.5.1 Graphical Issues

The ECG recognition and interpretation needs of our system benefit from the extra scope made available by using the slice-based technique. Another advantage of this method is aesthetics. This style of volume representation seems to be more uniform and, generally, looks better than its counterparts. Graphics hardware may be exploited to alter textures. This is yet another advantage of using this technique. Our earlier systems (MORB03) (ROBM04) depended on

either 20 minutes of pre-computations and displayed at a rate as slow as 2 fps (frames per second) or ignored anatomical boundaries. The newer slice-based system displays a larger volume at between 10-20 fps with real-time computations. Speed optimization is an important issue with this software because of the large amount of processing required by volumetric animation. The importance of speed optimization is reinforced by the need for real-time interactivity within the system. To provide for this, a frame indexing system was implemented to record the frame number where each cell is depolarized and repolarized. This information is collected during one iteration of the simulation and then reorganised into a speed friendly structure and outputted to a file for every other time the same ECG file is used. This frame indexing system has increased the frame rate from approximately 1fps to 20 fps. One of the major advantages of this method is that the cell structure can become more complex without affecting the animation speed, as just the initial iteration takes longer. The cellular progression algorithm is more accurate than previously, yet using the frame indexing technique, running speed is not compromised. In fact, the running speed has improved drastically. The ECG synchronization system is effective in defining markers with which to determine the exact points within the animation. Figure 6.20 demonstrates the electrical progression of a normal non-pathological ECG within our system.

6.5.2 The “Human in the Loop” Approach

Human in the loop algorithms can have many benefits over conventional *fully automatic* algorithms. We found that using this approach had several advantages for our project. Firstly, there was a time benefit. Rather than spending weeks or months researching and developing an ST segment detection algorithm, we simply used one of the best established methods of recognising such a waveform, *i.e.*, the

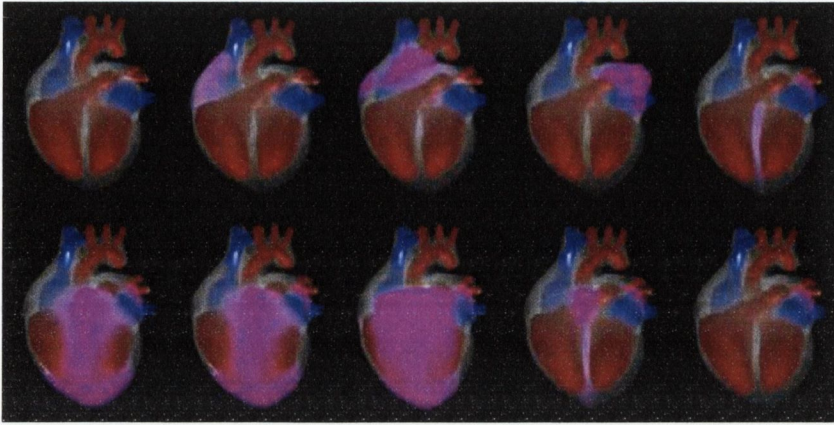


Figure 6.20: Animation Strip of Cardiac Electrical Cycle.

user / cardiologist. The ease of use of the system's GUI also brings the advantage of user acceptance. Clinical acceptance is a major factor in the development of medical tools. This factor depends on the clinical effectiveness *i.e.*, the sensitivity of the algorithm and also the ease of use or integration into a clinical setting. The GUI was designed with this in mind. Our collaborators favored the human-guided technique over automatic algorithms that were ineffective with common ECG pitfalls such as electrical or muscular noise. We confirm that this branch of interactive optimisation is very useful for these types of medical tools.

6.5.3 T Wave Inversion

We experimented with interpreting T wave abnormalities by using the classified wave-markers to acquire the actual electrical value from the ECG data. All T wave abnormalities were interpreted and diagnosed correctly. Most of the NSTEMIs had at least one T wave inversion. However, this is an area that is quite ambiguous and abides by the principle of "rubbish in - rubbish out". The problem is that, although T wave inversions may represent MI in the later stages, this not the only reason for this phenomenon and even in some cases this may not

even be an abnormality. This T wave inversion system can only be reliable if the clinician knows these limitations and the patient has an already diagnosed MI. This area would require further research. Figure 6.21 demonstrates an example where the system produced this kind of conflicting information.

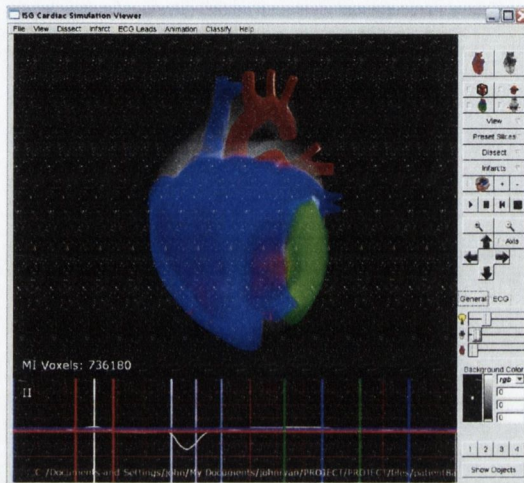


Figure 6.21: Example of conflict between T wave inversion and ST change, blue represents T wave inversion and green ST change.

Chapter 7

Conclusions and Future Work

In this thesis, we presented several new techniques for the diagnosis and management of myocardial infarctions. We described the development of a computer graphics toolkit that aids the cardiologist or clinician in this field. This tool is also valuable for both student and patient education. This thesis provides contributions to the domains of computer graphics, ECG detection algorithms, cardiology and medical education. These contributions are as follows:

1 For the Cardiologist / Medical Practitioner

In the field of electrocardiography, visual feedback tools are rare and normally limited to 2D tracings. This thesis has described a **novel ECG visualisation application for use in the diagnosis and monitoring of myocardial infarctions**. The standard 12 lead ECG configuration is used and the user has a large input in the detection phase. We also offer a **new metric** that is a **cumulative indicator of ST segment deviation**. There is a need for future validation of this metric by a concurrent comparison with blood analyses. ECG measurements are established as more accurate than blood-chemical markers, so a common metric like this is very useful in the credibility of such a tool. Very positive feedback has been

received from consultant cardiologists and several other medical workers.

2 For the Medical Student / Patient

This tool provides the student with a **3D volumetric representation of the cardiac electrical cycle**. Our system also provides **representation of myocardial infarctions** and any ECG SCP file can be read and represented both within the volume and the animation system. When learning electrocardiography, the abstract concept of 3D localisation is difficult to visualise. This tool provides the student with a greater spatial awareness of the heart's functions and abnormalities, allowing the student to see both the relevant ECG and the corresponding visualisation. After an interview with a lecturer of medicine and cardiology, he confirmed that this is one of the main benefits of this system. Even though a medical lecturer can immediately recognise the benefits, an in-depth validation study would be needed to reinforce the educational benefits over conventional teaching methods. This tool also provides the patient with a visual representation of his/her condition. Rather than seeing cryptic ECG tracings, the patient can see an actual heart with MI regions.

3 In the Field of ECG Detection Algorithms

The **approach to evaluating our ECG detection algorithm is novel**. The ECGs and corresponding angiographs were recorded while a patient's coronary arteries are being operated on during an angioplasty procedure. This provides definitive feedback about the MI extent and location and is more credible than a random ECG file from an online repository. This is mainly because the experiment was designed purely for the validation of the algorithm and also, a more detailed case study could be performed.

Human in the loop algorithms are becoming more popular as proof of the benefits emerge (AAL+00). Our MI detection system uses such an algorithm in the classification of the ST segments within our toolkit. This approach has saved development time and also improved the accuracy of the system. We found this feature to be very attractive to cardiology workers, since they trust their own judgements more than those of an automatic ST segment detection algorithm.

4 In the Domain of Computer Graphics

We have presented a **novel application of real-time interactive volumetric animation techniques** in the representation of the electrical depolarisation and repolarisation of cardiac cells. This visual representation is automatically **synchronised with the electrocardiogram** (ECG) input data. Other projects in this field have used high performance computing techniques or vastly complex cellular structures (SFE+03). This project, however, was more concerned with simplifying this process for **real-time optimisation**. We use **texture-based slices** in the representation of the myocardial volume to improve speed. Our system has been accepted within cardiology circles as a useful diagnostic and monitoring tool as well as a medical education and patient information tool. Our current collaborators are currently writing papers in cardiology and other medical journals about the results of our system.

5 The ECG File Format Domain

The **standard communications protocol** (SCP) ECG file format is relatively new. We provide a visualisation toolkit that uses this *new* file format. By using this file format, we are promoting its integration into a

clinical or educational setting.

7.1 Future Directions

The scope of this project and the sheer magnitude of this area of research meant that a lot subjects were left open for future work and even though some topics would require a whole research team, there are others that are achievable in the short term.

In our software, the areas of infarction are represented as spherical regions around central lead voxels. Although this has been proven to be visually useful it may not be as accurate as possible. If there are two or more regions of infarction, a blending algorithm may further strengthen this toolkits representation. Also, experimenting with translating surface maps of infarction areas into the volumetric data would be interesting. The only way to assign an accurate weighting for the volumetric representation of MI would be to perform an in-depth evaluation of actual physical MI extents with corresponding ECGs.

Both clinically and commercially, the area of automatic ST segment detection has many applications and is a richly researched area (SLMM95) (MOL00) (JSH+98) (GSOL00) (JMM98). The integration of an automatic detection algorithm within our system would probably speed up the process of MI representation. Further research in this area would be very beneficial. Both methods could be compared quantitatively in a thorough study.

We mainly addressed in this thesis the problem of visually representing ST wave abnormalities. Other abnormalities such as T and Q wave pathologies should be researched further. We discussed in the previous chapter that our software displayed conflicting information when representing T wave inversions.

The reason for this is because, even though this may be seen as an abnormality, in some cases T wave inversions occur normally. An improved technique would include the incorporation of more specific information and maybe even previous ECGs that could be used to see if T wave inversion is normal in that particular patient's case. Q wave pathologies are also indicative of MI and normally occur after the ST segment had normalised. The inclusion of these abnormalities would be useful.

The current animation system is quite crude and was developed as an approximate representation of the electrical cycle for use as a teaching tool. A possible future direction of this project would be to incorporate a more detailed animation by including fibre orientations and full ionic modelling of cells.

Speed optimisation is another area that could be improved on. Graphics hardware could be exploited to improve the speeds of animation. Shaders are currently available for speed optimisation in real-time graphics and could provide an upgrade for the animation system. High performance computing would be another way of improving speed.

In the field of cardiology, in order to give our software more credibility, an analysis of how our metrics correlate with blood-chemical markers would be very helpful. In order to do this, we would have to take ECGs at different stages of the patient's stay in hospital and compare them with the Troponin and CK levels at the same stages. We already know that the ECG is generally the better solution because it gives information about the location of MI, but we would need to test how the metrics perform regarding extent. The ST accumulator metric would be chosen because of its previously discussed benefits. *Stress-testing*, commonly used as a diagnostic technique for heart abnormalities, is another area within cardiology that could be used for the evaluation of this tool.

A more recent addition to the project was the evaluation of the tool within an animal testing laboratory. One month previous to our visit, as part of an external study, 15 pigs were induced with MIs. This was performed by injecting alcohol into the specific coronary arteries. During our visit, we acquired the ECGs of all 15 pigs. The ECG leads were obviously placed in different locations compared to the 12 lead configuration of human ECG. This configuration was previously developed by one of our cardiologist collaborators. Preliminary results suggest that our software can be extended into the animal realm and because blood samples were taken for all the pigs, we aim to validate the ST-accumulator metric.

We are currently in discussions regarding the commercialisation of this project. This route is the best if the software is to become available for clinical use.

Appendix A

The SCP File Format

SCP is an ECG file format that was developed with the aim of creating a standard format for the transfer of ECG data between equipment made by different manufacturers. Its initial rationale was the same as that of the DICOM medical image file format. Now, the DICOM file format now incorporates handling for SCP. The SCP file format has an initial and then several different sections. Each section has the same structure, as seen in Figure A.1. It is a binary file format and incorporates a compression feature. The compression is based on huffman encoding. The manufacturer or programmer can specify their own huffman table or they can make use of a standard default huffman table as seen in Figure A.2. ECG data can also be recorded as raw values. The compression is very valuable when dealing with large amounts of ECG information such as the domain of Holter ECG recording. Other features of the SCP file format include the recording of notes, annotations, beat references *etc.*

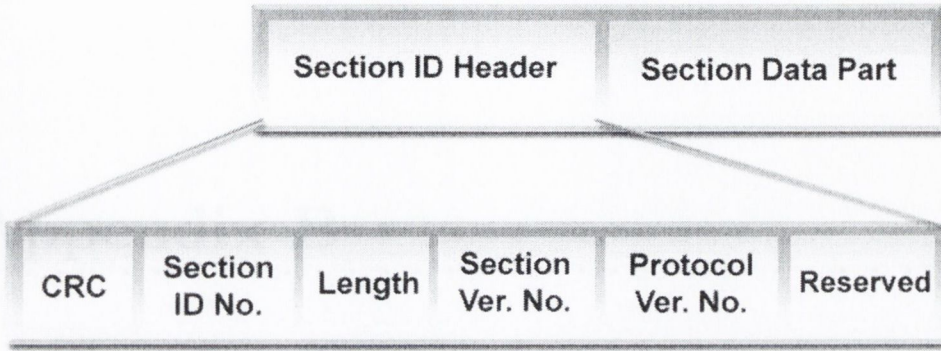


Figure A.1: SCP Section Header Structure.

No.	number of bits		table mode	base value	prefix code (in bits)	store binary as
	entire code	prefix				
1	1	1	1	0	0	0d
2	3	3	1	1	100	1d
3	3	3	1	-1	101	5d
4	4	4	1	2	1100	3d
5	4	4	1	-2	1101	11d
6	5	5	1	3	11100	7d
7	5	5	1	-3	11101	23d
8	6	6	1	4	111100	15d
9	6	6	1	-4	111101	47d
10	7	7	1	5	1111100	31d
11	7	7	1	-5	1111101	95d
12	8	8	1	6	11111100	63d
13	8	8	1	-6	11111101	191d
14	9	9	1	7	111111100	127d
15	9	9	1	-7	111111101	383d
16	10	10	1	8	1111111100	255d
17	10	10	1	-8	1111111101	767d
18	18	10	1	8 bit orig.	1111111110	511d
19	26	10	1	16 bit orig.	1111111111	1023d

Figure A.2: Default Huffman Table.

Appendix B

The OBJ File Format

The OBJ file format was firstly developed for the WaveFront 3D package by Silicon Graphics. The file format is open source, therefore is very popular among many 3D packages like Maya and 3D Studio Max. The key feature that made it ideal for this project was its object definitions. This allows multiple objects with the file with all their characteristics such as vertices, faces, normals, texture coordinates etc. Mostly it is ASCII based so it is quite easy to implement. This characteristic also means that the OBJ file can be edited in a text editor. This made it very useful when reordering and deleting certain objects such as the bundle-branches.

Each line within the OBJ file begins with a command. For example, the command `#` means that the line is commented out. The following table (B.1) describes the actions of each command instruction.

The following is some sample instructions from the heart model's OBJ file.

```
# object VENACAVA  
g VENACAVA
```


Table B.1: OBJ Instructions

Instruction	Description
v	This command specifies a vertex and is followed by three coordinates: x, y and z
vt	This command specifies the vertex coordinate of the associated vertex and are grouped by the face command. The following coordinates include U, V and optional W
vn	This command specifies the vertex normal. These are also grouped by the face command.
f	This command specifies a polygonal made from indexing the vertex list. If the texture or normal information is included the indices are separated by “//”.
g	Specifies an object name.
#	Instructs that this line is commented out.
usemtl	Specifies the name of the material to use.

```

v -0.64871 -2.80456 -4.06704
v -0.867482 -3.77842 -2.87575
v -0.614586 -2.98606 -4.01476
v -0.847655 -4.49586 -2.94996
v -0.590756 -3.09794 -3.98395
v -0.811549 -1.72977 -4.39639
v -1.04407 -2.9968 -2.72899
.
.
.
vn 0.206465 -0.589691 0.780792
vn 0.280385 -0.426326 0.860018
vn 0.343528 -0.246573 0.906196

```

vn 0.393472 -0.057347 0.917546

vn 0.428296 0.134079 0.893636

vn 0.446656 0.32036 0.835385

vn 0.447855 0.494325 0.74503

.

.

.

vt 0.530248 0.223513

vt 0.508659 0.241467

vt 0.412959 0.237206

vt 0.482309 0.231049

vt 0.425436 0.240799

vt 0.435608 0.255098

.

.

.

usemtl (null)

f 8492/1664/8483 8493/1665/8484 8494/1666/8485

f 8495/1667/8486 8492/1664/8483 8496/1668/8487

f 8496/1668/8487 8492/1664/8483 8494/1666/8485

f 8496/1668/8487 8497/1669/8488 8495/1667/8486

f 8498/1670/8489 8495/1667/8486 8497/1669/8488

f 8499/1671/8490 8500/1672/8491 8501/1673/8492

f 8502/1674/8493 8503/1675/8494 8500/1672/8491

Appendix C

Sample ECGs

Three 12 lead ECG printouts from this project are included.

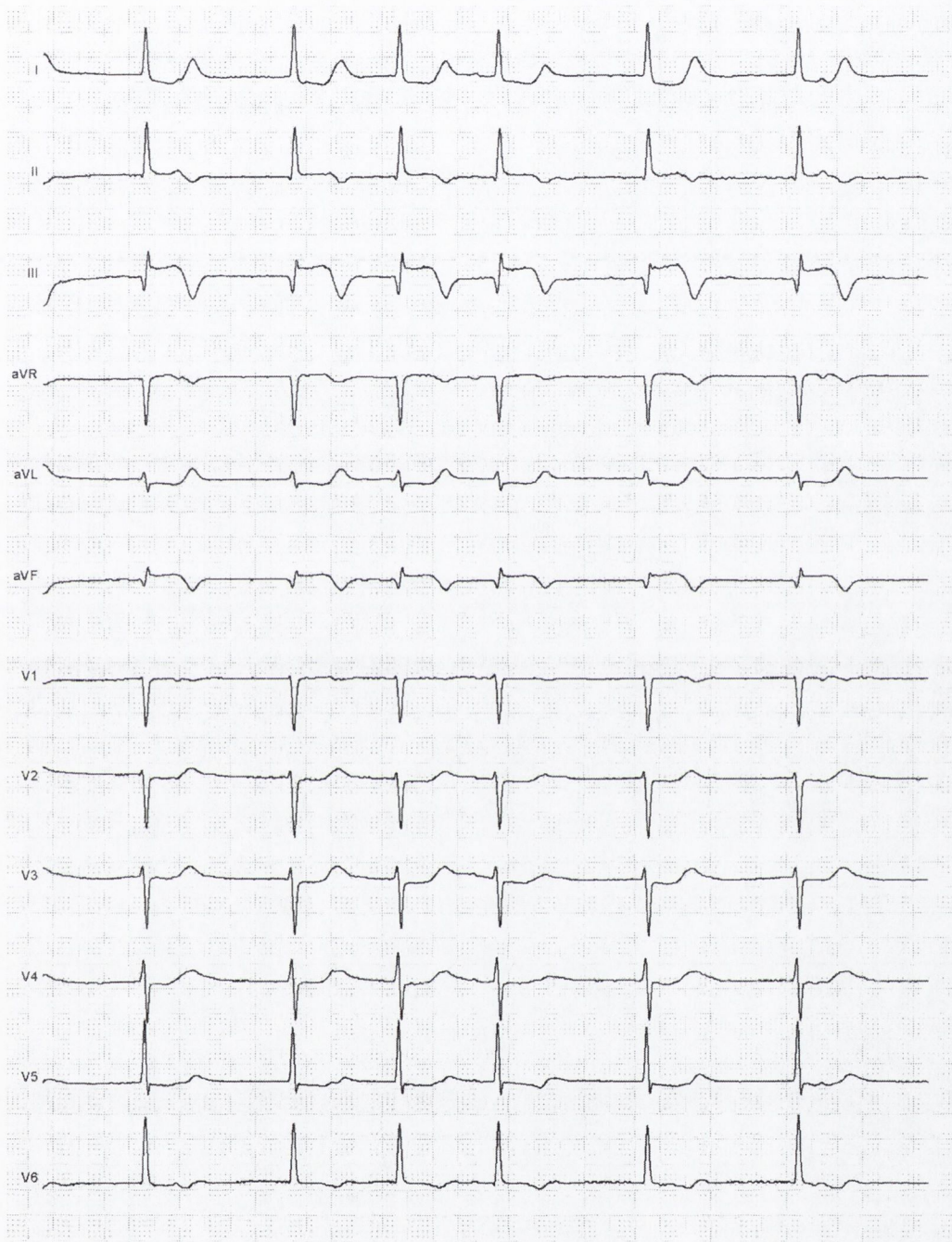


Figure C.1: ECG taken during the CCU evaluation phase. There is noticeable ST segment elevation on leads III and aVF. There is also ST depression in I, aVL, v2, v3 and v4

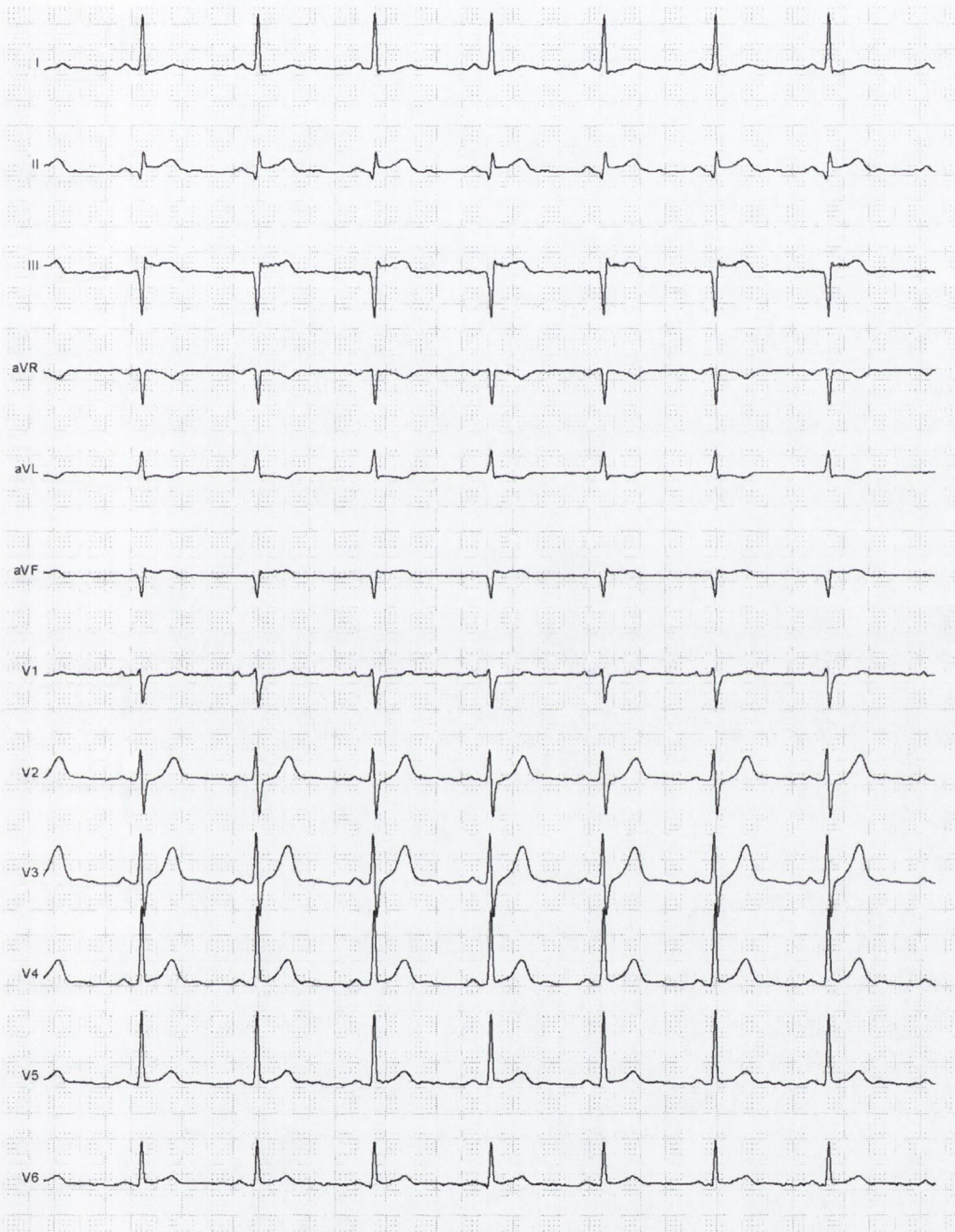


Figure C.2: ECG taken during the CCU evaluation phase. There is noticeable ST segment elevation on leads II, III and aVF.

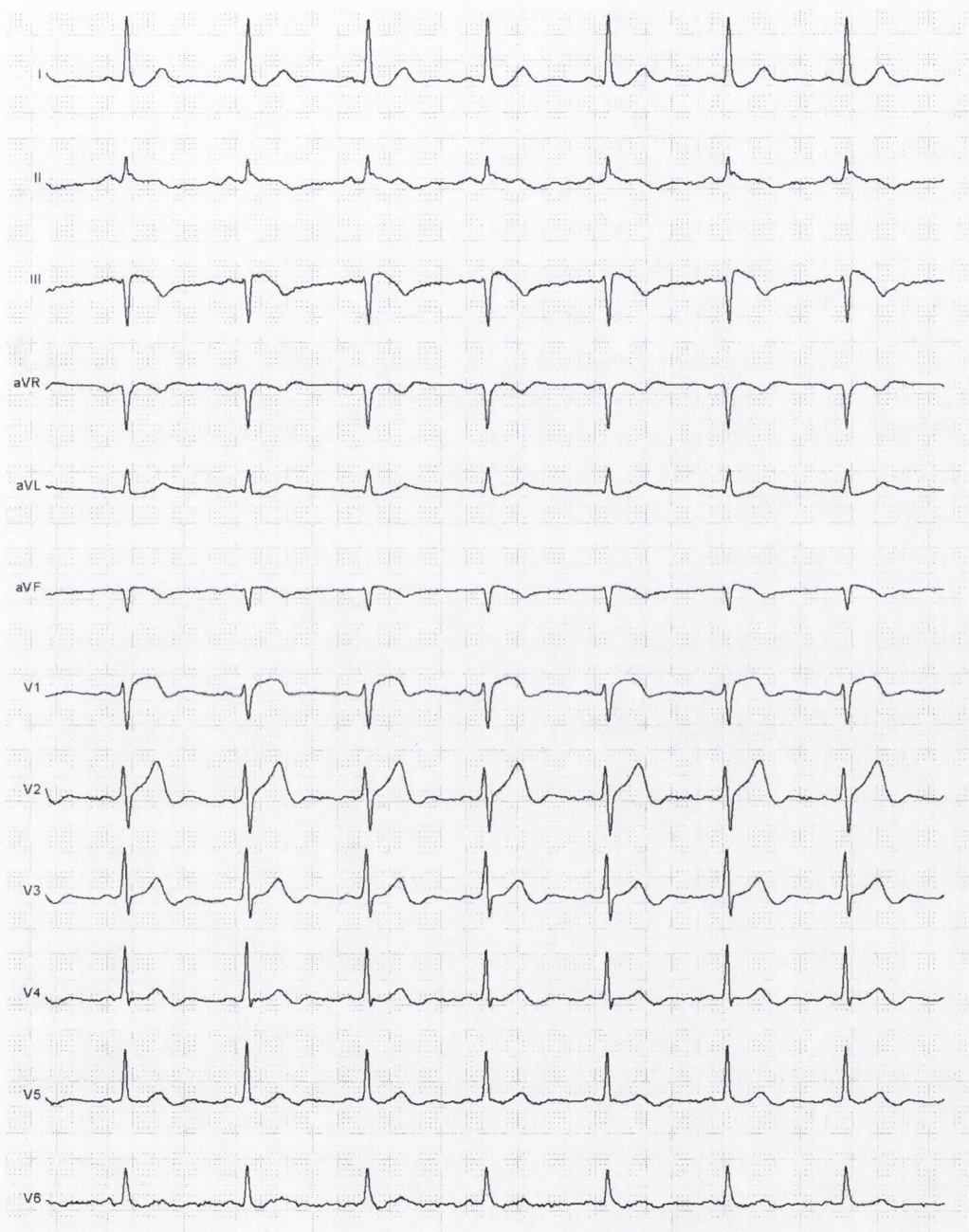


Figure C.3: ECG taken during the angioplasty evaluation phase. There is noticeable ST segment elevation on leads III, aVF, v1 and v2.

Appendix D

Glossary

ACE Inhibitors Drugs used in the treatment of high blood pressure.

Angiography The branch of x-ray imaging concerned with the imaging of arteries. Normally a contrast agent / dye is administered to highlight the arteries.

Angioplasty The opening of an obstructed artery using a mechanical device such as a balloon catheter. The obstruction is generally due to *atheroma*.

Aorta The largest artery in the body and runs directly from the heart.

Atria The atria are the upper two chambers of the heart. (*Atrium - singular*)

Atrio-Ventricular (AV) Node The AV node is part of the heart's nerve system and is the pathway between the atria and ventricles.

Atheroma An abnormal growth of tissue within an artery.

Atherosclerosis A build up of cholesterol and other deposits on the inner wall of an artery.

Betablockers Drugs commonly used in the treatment of coronary diseases that help calm the heart.

Bundle of His The upper part of the bundle-branch nerve network within the heart.

Coronal Plane Also called the frontal plane, this refers to the plane directly parallel to the view-plane if the human model was facing the camera. This is normally parallel to the XY plane.

Coronary artery bypass graft (CABG) A surgical procedure that uses parts of other vessels to bypass a diseased vessel.

Depolarisation The reduction or process of neutralising the polarity in cells.

Diuretics Drugs that increase the flow of urine and decrease the extracellular volume.

Drug Eluting Stent A stent that gives off a drug from treatment during and after stenting.

Endarterectomy A surgical procedure that excises the inner wall of an artery to get rid of atherosclerosis.

Femoral Referring to the femoral artery of femur bone.

Epigastric Referring to the upper middle region of the abdomen.

Holter Holter ECG refers to a process of monitoring a patient over 24 hours or more.

Hypertension The medical term for high blood pressure.

Hyperlipidaemia The medical term for high cholesterol.

Infarction The process of death within cells or tissue. Normally referring to the heart or brain.

Ischemia / Ischaemia The lack of oxygen to a particular region of tissue/cells, normally caused by a blockage within the supplying blood-vessels.

Isoelectric line This ECG term is the line that corresponds to zero electrical activity within the heart.

Isosurface An isosurface is a surface mesh made of polygons that is drawn in the volume.

Morbidity The incidence or prevalence rate of a specific disease.

Mortality A ratio that compares the number of people who die from a specific disease from a population.

Myocardial Infarction The *infarction* of an area of the *myocardium*.

Myocardium The muscular tissue within the heart (the heart mainly comprises of this tissue).

Necrosis The process of cell-death or death of tissue.

NSTEMI Non ST segment elevation myocardial infarction.

Octree An octree is a data structure used in the organisation of three-dimensional space. This has a hierarchical tree architecture with each node being split into 8 children.

Percutaneous Transluminal Coronary Angioplasty (PTCA) Percutaneous

refers to gaining access to an organ via a needle-puncture rather than conventional surgery. Transluminal refers to passing through a vessel. PTCA is the full medical term for conventional angioplasty.

Pixel A single unit of a 2D image, typically represented by colour and transparency information.

Polygon A closed plane shape with three or more sides.

Primitive In computer graphics this refers to a basic, building block shape.

QRS Complex This is the part of the ECG wave that starts at the Q waveform and ends at the S waveform.

Reperfusion The restoration of blood-flow to tissue or organ.

Repolarisation This occurs after *depolarisation* and means that the cells are regaining their polarity.

Sagittal Plane This describes the plane that is perpendicular to the coronal plane and cuts the human model straight down the middle. This is normally parallel to the YZ plane.

Sensitivity When used in medical papers, this term normally refers to the proportion of positive test results out of all positive cases.

Septum The internal separation of the two ventricles, a common area of infarction.

Sino-atrial (SA) node This node is a nerve-node that begins the cardiac cycle and is located at the top-rear of the right atrium.

Sinus Rhythm The normal electrical conductance of the heart. Normal PQRST elements and no arrhythmia.

Sinus Tachycardia An abnormally fast cardiac rhythm originating from the sino-atrial node.

Specificity When used in medical papers, this term normally refers to the proportion of true negatives of all the negative samples.

STEMI ST segment elevation myocardial infarction.

ST Segment The segment of the ECG between the S and T waveforms. See Chapter 2 - Medical Principles.

Stenosis Blockage

Stress Testing A stress test is a common technique used in the assessment of coronary artery abnormalities. The patient is asked to run on a treadmill until they feel pressure within their chest. At this stage, an ECG is acquired. The ECG demonstrates areas of stress (*i.e.*, ST elevation).

Texel The texture coordinate version of the *pixel*.

Thrombolysis The treatment of thromboses by lysing or breaking it down.

Thrombosis Blood clot.

Transverse Plane The same as the plane normally recorded by a CT scanner. This is normally parallel to the XZ plane.

Ventricular Fibrillation An abnormal coordination of the contraction of the ventricular muscles.

Video Fluoroscopy The recording of moving picture x-rays, commonly used in angiography.

Voxel A single unit of volume. The 3D version of the 2D *pixel*.

Bibliography

- [AAL⁺00] David Anderson, Emily Anderson, Neal Lesh, Joe Marks, Brian Mirtich, David Ratajczak, and Kathy Ryall. Human-guided simple search. In *Proceedings of the Seventeenth National Conference on Artificial Intelligence and Twelfth Conference on Innovative Applications of Artificial Intelligence*, pages 209–216. AAAI Press / The MIT Press, 2000. 2.6.4, 7
- [AGM⁺02] A Andresen, M.D Gasperina, R Myers, G.S Wagner, R.A Warner, and R.H.S Selvester. An improved automated ecg algorithm for detecting acute and prior myocardial infarction. *Journal of Electrocardiography*, 35:105–110, 2002. 2.6.4
- [APFR04] P Ammann, M Pfisterer, T Fehr, and H Rickli. Raised cardiac troponins. *British Medical Journal*, 328:1028–1029, 2004. 2.4.3
- [Azu97] R Azuma. A survey of augmented reality. In *presence: teleoperators and virtual environments 6*, pages 355–385, 1997. 3.5.1
- [BL05] D Bartz and S Lakare. Scaffolding-based segmentation of coronary vascular structures. In *Proceedings of Volume Graphics 2005*, pages 47–54, 2005. 3.5

- [BMF⁺03] D Bartz, D Mayer, J Fischer, S Ley, A DelRio, S Thust, C Heussel, H Kauczor, and W Strasser. Hybrid segmentation and exploration of the human lungs. In *Proceedings of IEEE Visualization 2003*, pages 177–184, 2003. 3.5
- [BNC96] M Bro-Nielsen and S Cotin. Real-time volumetric deformable models for surgery simulation using finite elements and condensation. In *Proceedings of Eurographics*, pages 57–66, 1996. 3.3
- [BS05] T Becker and R Simon. Dicom and waveform data. <http://www.uni-kiel.de/Kardiologie/dicom/1999/waveforms.html>, 2005. 2.7
- [CCF94] B Cabral, N Cam, and J Foran. Accelerated volume rendering and tomographic reconstruction using texture mapping hardware. In *VVS '94: Proceedings of the 1994 symposium on Volume visualization*, pages 91–98, New York, NY, USA, 1994. ACM Press. 3.2.3
- [CCW94] J M Cruickshank, J Cooper, and T S Warrender. Blood pressure and myocardial infarction Low blood pressure can be hazardous. *BMJ*, 308(6939):1301a–1302, 1994. 2.4.2
- [CKY00] M Chen, A.E Kaufman, and Roni Yagel. *Volume Graphics*. Springer, 2000. 3.2
- [CM98] E Chen and B Marcus. Force feedback for surgical simulation. *Proceedings of the IEEE*, 86(3):524–530, 1998. 3.5
- [CQHKM98] Y Chen, Z Qing-Hong, A Kaufman, and S Muraki. Physically-

based animation of volumetric objects. In *Proceedings of Computer Animation*, pages 154–160, 1998. 3.3

[CWP⁺03] J Curtis, Y Wang, E Portnay, F Masoudi, E Havranek, and H Krumholz. Aspirin, ibuprofen, and mortality after myocardial infarction: retrospective cohort study. *BMJ*, 327(7427):1322–1323, 2003. 2.5.1

[CZG04] C Chang, Y Zhang, and Y Gdong. Cellular automata for edge detection of images. In *Proceedings of 2004 International Conference on Machine Learning and Cybernetics*, pages 3830–3834, 2004. 3.4

[DPO⁺03] H.D Dobson, R.K Pearl, C.P Orsay, M Rasmussen, R Evenhouse, Z Ai, G Blew, F Dech, M.I Edison, J.C Silverstein, and H Abcarian. Virtual reality: New method of teaching anorectal and pelvic floor anatomy. *Diseases of the Colon and Rectum*, 46(3):349–352, 2003. 3.1

[dWAB⁺03] F Van de Werf, D Ardissino, A Betriu, D Cokkinos, E Falk, K Fox, D Julian, M Lengyel, F Neumann, W Ruzyllo, C Thygesen, S Underwood, A Vahanian, F Verheugt, and W Wijns. Management of acute myocardial infarction in patients presenting with st-segment elevation. *European Heart Journal*, 24:28–66, 2003. 2.5.5

[EMS⁺02] M Eccles, E McColl, N Steen, N Rousseau, J Grimshaw, D Parkin, and I Purves. Effect of computerised evidence based guidelines on management of asthma and angina in adults in primary care: cluster randomised controlled trial. *BMJ*, 325(7370):941–, 2002. 5.1.2

- [Eur00] European Committee for Standardization. *Standard Communications Protocol for Computer-Assisted Electrocardiography*, October 2000. 2.7, 4.3.4, 4.3.4
- [EWC⁺99] J Emery, R Walton, A Coulson, D Glasspool, S Ziebland, and J Fox. Computer support for recording and interpreting family histories of breast and ovarian cancer in primary care (RAGs): qualitative evaluation with simulated patients. *BMJ*, 319(7201):32–36, 1999. 5.1.4
- [EWM02] J Evans, J Wang, and A Morris. Comparison of cardiovascular risk between patients with type 2 diabetes and those who had had a myocardial infarction: cross sectional and cohort studies. *BMJ*, 324(7343):939–, 2002. 2.4.2, 5.6.2
- [FBC⁺02] B.J Foley, M Barry, P Crean, R Curtin, R.T Murphy, G.E Pate, A Talbot, M.J Walsh, and D Ward. Audit of acute myocardial infarctions at saint james' hospital, dublin, 1996 to 1999. *Irish Medical Journal*, 95(9), 2002. 1.1, 2.3, 2.5.3, 2.5.6, 5.6.3
- [FHM05] Jos Fernandez, Matthew Harris, and Carsten Meyer. Combining algorithms in automatic detection of r-peaks in ecg signals. In *Proceedings of IEEE Symposium on Computer-Based Medical Systems*, pages 297–302, Los Alamitos, CA, USA, 2005. IEEE Computer Society Press. 2.6.1
- [FWH⁺96] J French, B Williams, H Hart, S Wyatt, J Poole, C Ingram, C Ellis, M Williams, and H White. Prospective evaluation of eligibility

- for thrombolytic therapy in acute myocardial infarction. *BMJ*, 312(7047):1637–1641, 1996. 5.6.3
- [Gal91] L Galvani. About luigi galvani’s first experiments de viribus electricitatis in motu musculari commentarius. <http://www.columbia.edu/cu/lweb/eresources/exhibitions/treasures/html/152.htm>, 1791. 2.2.1
- [GBKA04] M Gelautz, M Brandejski, F Kilzer, and F Amelung. Web-based visualization and animation of geospatial data using x3d. In *Geoscience and Remote Sensing Symposium, 2004. IGARSS '04. Proceedings. 2004 IEEE International*, pages 4773–4775, 2004. 3.1.1
- [Ger00] B.J Gersh. *The ultimate guide to heart health: Mayo clinic heart book*. William Morrow, 2000. 2.4.1
- [GM98] A.H Gershlick and R.S More. Recent advances: Treatment of myocardial infarction. *British Medical Journal*, 316:280–284, 1998. 2.5.5
- [GR03] E Grech and D Ramsdale. Acute coronary syndrome: unstable angina and non-ST segment elevation myocardial infarction. *BMJ*, 326(7401):1259–1261, 2003. 2.4.3, 5.6.2
- [Gre89] N Greene. Voxel space automata: Modeling with stochastic growth processes in voxel space. *ACM Siggraph*, 23(3), 1989. 3.6
- [GSOL00] J Garcia, L Sornmo, S Olmos, and P Laguna. Automatic detection of st-t complex changes on the ecg using filtered rms difference se-

ries: application to ambulatory ischemia monitoring. *IEEE Transactions on Biomedical Engineering*, 47(9):1195–1201, 2000. 2.6.2, 7.1

[GWGS02] S Guthe, M Wand, J Gonser, and W Strasser. Interactive rendering of large volume data sets. In *Proceedings of IEEE Visualization*, pages 53–60, 2002. 3.2.3

[HBAN04] S Huang, R Baimouratov, A Ananthasubramaniam, and W Nowinski. A medical imaging and visualization toolkit in java. In *Proceedings of SPIE*, pages 48–58, Bellingham, WA, USA, 2004. SPIE. 3.1.1

[HCFP98] Julia Hippisley-Cox, Katherine Fielding, and Mike Pringle. Depression as a risk factor for ischaemic heart disease in men: population based case-control study. *BMJ*, 316(7146):1714–1719, 1998. 2.4.2

[HCL⁺05] D Hartwell, J Colquitt, E Loveman, A Clegg, H Brodin, N Waugh, P Royle, P Davidson, L Vale, and L MacKenzie. Clinical effectiveness and cost-effectiveness of immediate angioplasty for acute myocardial infarction: systematic review and economic evaluation. *Health Technology Assessment*, 9(17):1–128, 2005. 2.5.6

[HMK⁺97] L Hong, S Muraki, A Kaufman, D Bartz, and T He. Virtual voyage: interactive navigation in the human colon. In *Proceedings of Siggraph*, pages 27–34, 1997. 3.5

[JESMM⁺97] II J. Edward Swan, Klaus Mueller, Torsten Moller, Naeem Shaareef, Roger Crawfis, and Roni Yagel. An anti-aliasing technique

- for splatting. In *VIS '97: Proceedings of the 8th conference on Visualization '97*, pages 197–ff., Los Alamitos, CA, USA, 1997. IEEE Computer Society Press. 3.2
- [JMM98] F Jager, G Moody, and R Mark. Detection of transient st segment episodes during ambulatory ecg monitoring. *Computers and Biomedical Research*, 31(5):305–322, 1998. 2.6.2, 7.1
- [JN02] D.G Julian and R.M Norris. Myocardial infarction: is evidence-based medicine the best? *The Lancet*, 359(9316):1515–1516, 2002. 2.5.2
- [Joh03] N John. High performance visualization in a hospital operating theatre. In *Proceedings of the Theory and Practice of Computer Graphics*, pages 170–175, 2003. 3.5
- [Jos01] D Josefson. Healthy woman dies in research experiment. *BMJ*, 322(7302):1565a–, 2001. 5.1.3
- [JPVP99] N John, N Phillips, R Vawda, and J Perrin. A vrml simulator for ventricular catheterisation. In *Proceedings of Eurographics UK*, pages 1–6, 1999. 3.1.1
- [JRSB00] N John, M Riding, A Sadarjoen, and L Blumrozen. Bringing 3d to teleradiology. In *IV '00: Proceedings of the International Conference on Information Visualisation*, pages 4–8, Washington, DC, USA, 2000. IEEE Computer Society. 3.1.1
- [JSH⁺98] T Joo, P Schmitt, D Hampton, K Briscoe, T Valenzuela, and L Clark. Enhanced acute myocardial infarction detection algo-

- rithm using local and global signal morphology. In *Computers in Cardiology*, pages 285–288. IEEE, 1998. 2.6.2, 2.6.3, 7.1
- [KHO02] B.U Kohler, C Hennig, and R Orglmeister. The principles of qrs detection. *IEEE Engineering in Medicine and Biology*, pages 42–57, january/february 2002. 2.6.1
- [KKPW03] A.M Kelly, D Kerr, I Patrick, and T Walker. Call-to-needle times for thrombolysis in acute myocardial infarction in victoria. *The Medical Journal of Australia*, 178(8):381–385, 2003. 2.5.2
- [KMBB99] S Kadambe, R Murray, and G.F Boudreaux-Bartels. Wavelet transform-based qrs complex detector. *IEEE Transactions on Biomedical Engineering*, (46):838–848, 1999. 2.6.1
- [KMM⁺01] J Kniss, P McCormick, A McPherson, J Ahrens, J Painter, A Keahey, and C Hansen. Interactive texture-based volume rendering for large data sets. *Computer Graphics and Applications*, 21(4):52–61, 2001. 3.2.3
- [KNWH03] P Kohl, D Noble, R.L Winslow, and P Hunter. *The making of the virtual heart*. Cambridge University Press, 2003. 3.7
- [KPP95] B Kitchenham, L Pickard, and S Pflieger. Case studies for method and tool evaluation. *Software*, 12(4):52–62, 1995. 5.1.1
- [KS03] S Kimmel and B Strom. Giving aspirin and ibuprofen after myocardial infarction. *BMJ*, 327(7427):1298–1299, 2003. 2.5.1
- [KSH03] R Kahler, M Simon, and H.C Hege. Interactive volume rendering of large sparse data sets using adaptive mesh refinement hierar-

- chies. *IEEE Transactions on Visualization and Computer Graphics*, 9(3):341–351, 2003. 3.7, 4.1.3
- [LC87] W.E Lorensen and H.E Cline. Marching cubes: a high resolution 3d surface construction algorithm. In *Proceedings SIGGRAPH 1987*, pages 163–169. ACM, ACM, 1987. 3.2
- [LCP02] G Lip, B Chin, and N Prasad. ABC of antithrombotic therapy: Antithrombotic therapy in myocardial infarction and stable angina. *BMJ*, 325(7375):1287–1289, 2002. 2.1.3
- [LDB95] Z Lee, P Diaz, and E Bellon. Manipulation of volume and graphics objects for the visualization of medical data under opengl. In *Proceedings of IEEE Symposium on Computer-Based Medical Systems*, pages 89–93, Los Alamitos, CA, USA, 1995. IEEE Computer Society Press. 3.1.1
- [Lei03] J.W Leitch. Changing times in the treatment of myocardial infarction. *The Medical Journal of Australia*, 178:367–368, 2003. 2.4.4.1, 2.5.3
- [Lev88] M Levoy. Display of surfaces from volume data. *IEEE Computer Graphics and Applications*, 8(3):29–37, 1988. 3.2
- [LMK⁺85] G Lowe, S Machado, W Krol, B Barton, and C Forbes. White blood cell count and haematocrit as predictors of coronary recurrence after myocardial infarction. *Thromb Haemost*, 54(3):700–703, 1985. 5.6.2
- [LRR⁺94] U Lindblad, L Ramstam, L Ryden, J Ranstam, S Isacson, and

- G Berglund. Control of blood pressure and risk of first acute myocardial infarction: Skaraborg hypertension project. *British Medical Journal*, 308:681–685, 1994. 5.6.2
- [Mac05] Jan Macek. Incremental learning of ensemble classifiers on ecg data. In *Proceedings of IEEE Symposium on Computer-Based Medical Systems*, pages 315–320, Los Alamitos, CA, USA, 2005. IEEE Computer Society Press. 2.6.1
- [MB02a] I Malik and A Berger. Science commentary: Coronary angioplasty and stenting. *BMJ*, 325(7363):519–520, 2002. 2.5.5
- [MB02b] F Morris and W.J Brady. Abc of clinical electrocardiography, acute myocardial infarction - part i. *British Medical Journal*, 324:831–834, 2002. 2.4.4.2
- [MGSH97] J Meyer, S Gelder, T Schneider, and H Hagen. Invis - interactive visualization of medical data sets. In *Scientific Visualization Conference*, pages 233–233, 1997. 3.2.4
- [MHL98] R. M. H. McMinn, R. T. Hutchings, and B. M. Logan. *The Concise Handbook of Human Anatomy*. Manson Publishing, 1998. 2.1.1
- [MM02] S Meek and F Morris. ABC of clinical electrocardiography: Introduction. I—Leads, rate, rhythm, and cardiac axis. *BMJ*, 324(7334):415–418, 2002. 2.4.4.5
- [MMC99] Klaus Mueller, Torsten Moller, and Roger Crawfis. Splatting without the blur. In *VIS '99: Proceedings of the conference on Visualization '99*, pages 363–370, Los Alamitos, CA, USA, 1999. IEEE Computer Society Press. 3.2

- [MNK⁺04] H Mayer, I Nagy, A Knoll, E Schirmbeck, and R Bauernschmitt. The endo[pa]r system for minimally invasive robotic surgery. In *Proceedings of IEEE RSJ International Conference*, pages 3637–3642, 2004. 3.5
- [MOL00] J Martinez, S Olmos, and P Laguna. T wave alternans detection: A simulation study and analysis of european st-t database. In *Computers in Cardiology*, pages 155–158. IEEE, 2000. 2.6.2, 7.1
- [MORB03] Robert Mooney, Carol O’Sullivan, John Thomas Ryan, and Christopher Bell. The construction of a volumetric cardiac model for real-time ecg simulation. In *Poster proceedings of the 11th International Conference in Central Europe on Computer Graphics, Visualization and Interactive Digital Media*, pages 97–100. WSCG, WSCG, 2003. 3.2.1, 3.6, 6.5.1
- [MSRA00] S Maynard, G Scott, J Riddell, and A Adgey. Regular review: Management of acute coronary syndromes. *BMJ*, 321(7255):220–223, 2000. 5.6.2
- [MY96] K Mueller and R Yagel. Fast perspective volume rendering with splatting by utilizing a ray-driven approach. In *Proceedings of Visualization*, pages 65–72. IEEE, 1996. 3.2.2
- [NM05] Neophytos Neophytou and Klaus Mueller. Gpu accelerated image aligned splatting. In *Volume Graphics 2005 Proceedings*, pages 197–205, Aire-la-Ville, Switzerland, 2005. Eurographics Association. 3.2.2

- [NYU05] NYU. Vmrl heart model. <http://education.med.nyu.edu/courses/old/embryology/courseware/vheart/>, 2005. 4.1.1
- [O'S01] B O'Shea. A study of the use of aspirin by general practitioners in suspected myocardial infarction. *Irish Medical Journal*, 94(2), 2001. 2.5.1
- [PCV95] R Poli, S Cagnoni, and G Valli. Genetic design of optimum linear and non-linear qrs detectors. *IEEE Transactions on Biomedical Engineering*, (42):1137–1141, 1995. 2.6.1
- [Pha96] Tim Phalen. *The 12-Lead ECG in Acute Myocardial Infarction*. Mosby Lifeline, 1996. 2.1.3, 2.4.4, 2.4.4.2, 2.4.4.3, 2.4.4.4, 2.5.3, 4.6.1.2, 4.6.1.7
- [PHS+98] E Prescott, M Hippe, P Schnohr, H Hein, and J Vestbo. Smoking and risk of myocardial infarction in women and men: longitudinal population study. *BMJ*, 316(7137):1043–1047, 1998. 2.4.2
- [PS03] S Pierce and T Skalak. Cellular automata model of microvascular remodeling. In *Proceedings of 2003 Summer Bioengineering Conference*, pages 225–226, 2003. 3.4
- [PT85] J Pan and W.J Tompkins. A real-time qrs detection algorithm. *IEEE Transactions on Biomedical Engineering*, 32(3):230–236, 1985. 2.6.1
- [rC05] Web ref. Ceslab. cardiac electrophysiological simulation package. <http://www.cesinst.com>, 2005. 3.7

- [RGJR04] C Ramanathan, R Ghanem, P Jia, and Y Rudy. Noninvasive electrocardiographic imaging for cardiac electrophysiology and arrhythmia. *Nature Medicine*, 10:422–428, 2004. 1.4, 3.7
- [ROBM04] John Ryan, Carol O’Sullivan, Christopher Bell, and Robert Mooney. A virtual reality electrocardiography teaching tool. In *Proceedings - 2nd International Conference, Biomedical Engineering*, pages 250–253. IASTED, IASTED, 2004. 3.2.1, 6.5.1
- [SC97] H.H So and K.L Chan. Development of qrs detection method for real-time ambulatory cardiac monitor. In *Proceedings - 19th International Conference - IEEE/EMBS*, pages 289–292. IEEE, IEEE, 1997. 1.2, 2.6.1, 4.5, 4.6.1
- [SCC⁺04] SK Semwal, K Chandrasheker, D Carroll, A Deshmukh, and N Bastian. Global share system and haptic-imprints. In *Proceedings of The 3rd IEEE International Workshop on Haptic, Audio and Visual Environments and Their Applications*, pages 31–36, 2004. 3.1.1
- [SFE⁺03] M Sermesant, O Faris, F Evans, E McVeigh, Y Coudire, H Delingette, and N Avache. Preliminary validation using in vivo measures of a macroscopic electrical model of the heart. *International Symposium on Surgery Simulation and Soft Tissue Modelling Lecture Notes*, 2673:230–243, 2003. 1.5, 3.7, 7
- [SGB⁺95] Gregg W. Stone, Cindy L. Grines, Kevin F. Browne, Jean Marco, Donald Rothbaum, James O’Keefe, Geoffrey O. Hartzle, Paul Overlie, Bryan Donohue, Noah Chelliah, Gerald C. Timmis,

- Ronald Vlietstra, Michelle Strzelecki, S Puchrowicz-Ochocki, and W.W O'Neill. Predictors of in-hospital and 6-month outcome after acute myocardial infarction in the reperfusion era: The primary angioplasty in myocardial infarction (pami) trial. *Journal of the American College of Cardiology*, 25(2):370–377, 1995. 2.5.5
- [SGJ94] H Shen, P Gharpure, and C Johnson. Visualization of 3-d wave propagation in the heart - a new technique. In *Engineering in Medicine and Biology Society. Engineering advances: New opportunities for biomedical engineers. Proceedings of 16th Annual International Conference of the IEEE*, pages 684–685, 1994. 3.3, 3.4
- [SHS+00] N Suzuki, A Hattori, S Suzuki, Y Adachi, T Kumano, A Ikemoto, and A Takatsu. Virtual surgery system with haptic sensation for both hands. In *Proceedings of EMBS International Conference*, pages 2419–2422, 2000. 3.5
- [SLG+96] A State, M Livingston, W Garrett, G Hirota, M Whitton, and E Pisano. Technologies for augmented reality systems: realizing ultrasound-guided needle biopsies. In *Proceedings of Siggraph 96*, pages 439–446, 1996. 3.5.1
- [SLMM95] R Silipo, P Laguna, C Marchesi, and R Mark. St-t segment change recognition using artificial neural networks and principal component analysis. In *Computers in Cardiology*, pages 213–216. IEEE, 1995. 2.6.2, 7.1
- [TA00] K Thygesen and J.S Alpert. Myocardial infarction redefined a consensus document of the joint european society of cardiol-

- ogy/american college of cardiology committee for the redefinition of myocardial infarction. *Journal of the American College of Cardiology*, 36(3):959–969, 2000. 2.4.3
- [TC02] E Tatara and A Cinar. Interpreting ecg data by integrating statistical and artificial intelligence tools. *IEEE Engineering in Medicine and Biology*, pages 42–57, january/february 2002. 2.6.1
- [TCC00] K.F Tan, K.L Chan, and K Choi. Detection of the qrs complex, p wave and t wave in electrocardiogram. In *Proceedings of International Conference on Advances in Medical Signal and Information Processing*, pages 41–47, 2000. 4.5
- [TD05] J Townsend and S Doshi. Reducing mortality in myocardial infarction. *British Medical Journal*, 330:856–857, 2005. 2.5.5
- [THE93] THE COUNCIL OF THE EUROPEAN UNION. *Council Directive 93/104/EC of 23 November 1993 concerning certain aspects of the organization of working time*, November 1993. 3.5
- [Tho97] G Thompson. Grand Rounds–Hammersmith Hospital: Hazards of running a marathon. *BMJ*, 314(7086):1023–, 1997. 2.4.3
- [Tid90] R Tidwell. Stereopsis takes off in flight simulation. In *Proceedings of IEEE Southeast Conference*, pages 578–582, 1990. 3.9.1
- [TMN⁺98] R Turner, H Millns, H Neil, I Stratton, S Manley, D Matthews, and R Holman. Risk factors for coronary artery disease in non-insulin dependent diabetes mellitus: United Kingdom prospective diabetes study (UKPDS: 23). *BMJ*, 316(7134):823–828, 1998. 5.6.2

- [TRB03] B Tighiouart, P Rubel, and M Bedda. Improvement of qrs boundary recognition by means of unsupervised learning. In *Proceedings of Computers in Cardiology*, pages 49–52, 2003. 5.1.2
- [TS90] P Trahanias and E Skordalakis. Syntactic pattern recognition of the ecg. *IEEE Transactions on Pattern Analysis and Machine Intelligence*, 12(7):648–657, 1990. 2.6.1
- [TSYM99] M Tsuruoka, R Shibasaki, Y Yasuoka, and S Murai. Spectral analysis of human movement stability using time series data in medicine. In *Proceedings of 12th IEEE Symposium on Computer-Based Medical Systems*, pages 190–195, 1999. 5.1.2
- [WEE03] D Weiskopf, K Engel, and T Ertl. Interactive clipping techniques for texture-based volume visualisation and volume shading. *IEEE Transactions on Visualization and Computer Graphics*, 9(3):298–312, 2003. 3.2.3, 4.1.3
- [Wes89] Lee Westover. Interactive volume rendering. In *VVS '89: Proceedings of the 1989 Chapel Hill workshop on Volume visualization*, pages 9–16, New York, NY, USA, 1989. ACM Press. 3.2.2
- [WKLM02] B Wilson, M Kwan-Liu, and P McCormick. A hardware-assisted hybrid rendering technique for interactive volume visualization. In *Volume Visualization and Graphics*, pages 123–130, 2002. 3.2.4
- [WW96] Kathleen J. W. Wilson and Anne Waugh. *Anatomy and Physiology in Health and Illness*. Churchill Livingstone, 1996. 2.1.3, 2.3
- [WWE04] D Weiskopf, M Weiler, and T Ertl. Maintaining constant frame rates in 3d texture-based volume rendering. In *Proceedings of*

- Computer Graphics International (CGI) 2004*, pages 604–607, 2004. 3.2.3
- [XHT92] Q Xue, Y.H Hu, and W.J Tompkins. Neural network-based adaptive matched filtering for qrs detection. *IEEE Transactions on Biomedical Engineering*, (39):317–329, 1992. 2.6.1
- [Zyw05] C Zywiets. Scp-ecg. <http://www.openecg.net/>, 2005. 2.2.1, 2.7